SYNTHESIS AND CHARACTERIZATION OF HIGHLY STABLE FUNCTIONAL SILICA NANOPARTICLES FOR LBL ASSEMBLY

by Melike Barak

Submitted to the Graduate School of Engineering and Natural Sciences
in partial fulfillment of
the requirements for the degree of
Master of Science

Sabanci University
July 2018

SYNTHESIS AND CHARACTERIZATION OF HIGHLY STABLE FUNCTIONAL SILICA NANOPARTICLES FOR LBL ASSENIBLY

APPROVED BY

Assoc. Prof. Dr. Tevzi Çakmak Cebeci
.....
(Thesis Supervisor)

Asst. Prof. Dr. Serkan Ünal
.....

Asst. Prof. Dr. Burcu Dedeoğlu
.....

DATE OF APPROVAL: 31/07/2018

ABSTRACT

SYNTHESIS AND CHARACTERIZATION OF HIGHLY STABLE FUNCTIONAL SILICA NANOPARTICLES FOR LBL ASSEMBLY

Melike Barak

Master Dissertation, July 2018

Supervisor: Assoc. Prof. Dr. Fevzi Çakmak Cebeci

Keywords: silica nanoparticles, microemulsion, surface modification, functional groups, crosslinking, LbL, electrostatic interaction, robustness

Layer by Layer (LbL) assembly is a superior method to create thin films with aqueous based dispersions which include polyelectrolytes and nanoparticles. LbL presents exceptional advantages like conformal coatings with controlled structure and composition by using electrostatic interactions of oppositely charged materials. Nevertheless, these interactions may cause weaker mechanical properties on the thin films. In order to eliminate the drawback, the covalent bond between oppositely charged materials can establish by crosslinking of functional groups.

Silica nanoparticles are mostly used in the LbL process due to enhance adhesion of films by creating roughness on the surface. They are also suitable for surface modification which provides surface charge manipulation, stable dispersibility and good mechanical property. Silane alkoxy groups are one of the best choices for functionalization process. These coupling agents promote mechanical robustness of the surface via the formation of physically and chemically stable covalent bonds.

In this study, silica nanoparticle was synthesized by hydrolysis and condensation of tetraethyl orthosilicate (TEOS) in surfactant/cyclohexane/ammonia media by microemulsion method. Monodisperse and having around 50 nm diameter silica nanoparticles were achieved to use in further steps. Amino and poly (ethylene glycol)-

terminated alkoxy silanes were performed to ensure positive and negative surface charges on the silica nanoparticles surface by crosslinking. The functionalized silica nanoparticles were utilized in LbL process, right after poly allylamine hydrochloride (PAH) and poly (sodium 4-styrenesulfonate) (SPS) were applied in desired number of layers on the silicon wafer substrates.

Dynamic light scattering (DLS) is employed to analyze size and surface charge distribution of bare and functionalized silica nanoparticles. The presence of functional groups was examined by Fourier-transform infrared spectroscopy (FT-IR) and nuclear magnetic resonance (NMR). The thickness, surface topography and roughness of thin films are measured by ellipsometry and atomic force microscopy (AFM). Scanning electron microscopy (SEM) was performed to analyze nanostructural morphology of silica nanoparticle and thin films.

The obtained results indicated that chemically crosslinked silica nanoparticle containing thin films exhibit better mechanical properties that make them useful for desired applications.

ÖZET

LBL KAPLAMA İÇİN YÜKSEK STABİLİTEYE SAHİP FONKSİYONEL SİLİKA NANOPARÇACIKLARIN SENTEZİ VE KARAKTERİZASYONU

Melike Barak

Yüksek Lisans Tezi, Temmuz 2018

Tez Danışmanı: Doç. Dr. Fevzi Çakmak Cebeci

Anahtar kelimeler: silika nanoparçacıklar, microemulsiyon, yüzey değişimi, fonksiyonel gruplar, çapraz bağlanma, LbL, elektrostatik etkileşim, dayanıklılık

Tabaka tabaka kaplama polielektrolit ve nano parçacık içeren su bazlı dağılımlarda ince film elde etmek için kullanılan üstün bir yöntemdir. Tabaka tabaka tekniği zıt yüklü malzemelerin elektrostatik etkileşimlerini kullanarak kontrollu yapı ve bileşime sahip uyumlu kaplamalar gibi ayrıcalıklı avantajlar sunar. Buna rağmen, bu etkileşimler ince filmlerde zayıf mekanik özelliklere neden olabilirler. Bu dezavantajı ortadan kaldırmak için, fonksiyonel groupların çapraz bağlanmasıyla zıt yüklü malzemelerin arasında kovalent bağ kurulabilir.

Silika nanoparçacıklar çoğunlukla yüzeylerde prüzlülük oluşturarak filmlerin tutunmalarını arttırmak için tabaka tabaka tekniğinde kullanılır. Bu parçacıklar aynı zaman da yüzey yükü düzenlenmesi, stabil dağılım ve iyi mekanik özellikler sağlayan yüzey değişimleri için de uygundur. Silan alkoksi grupları fonksiyonlandırma işlemleri için en iyi seçeneklerdendir. Bu bağlanma ajanları sabit fiziksel ve kimyasal kovalent bağlar oluşturarak yüzeyin mekanik sağlamlılığını yükseltir.

Bu çalışmada, silika nanoparçacıklar mikroemulsiyon yöntemi ile yüzey aktif madde/siklohegzan/amonyak ortamında tetraetil ortosilikatın (TEOS) hidroliz ve

yoğunlaşması ile sentezlendi. Tekdağılımlı ve yaklaşık 50 nm çapında silika nanoparçacıklar oluşumu ileriki safhalarda kullanılmak için elde edildi. Amino ve poli (etilen glikol)-arındırılmış alkoksi silanlar çapraz bağlanma ile silika nanoparçacıkların yüzyinde pozitif ve nagatif yüzey yüklerinin oluşumunu kesinleştirmek için kullanıldı. Fonksiyonlandırılmış silika nanoparçacıklar tabaka tabaka tekniğinde poli allilamin hidroklorür (PAH) ve poli (sodyum 4-stirensülfonat) (SPS) silicon plaka örneği üzerinde istenilen sayıda katmana uygulanmasından hemen sonrasında kullanıldı.

Dinamik ışık saçılması (DLS) fonksyonlandırılmış ve yalın haldeki silika nanoparçacıkların boyutunu ve yüzek yük dağılımını analiz etmek için kullanıldı. Fonksiyonel grupların varlığı Fourier-dönüşümü kızılötesi spektroskopisi (FT-IR) ve nükleer manyetik rezonans ile çalışıldı. İnce filmlerin kalınlığı, yüzy topoğrafisi ve prüzlülüğü elipsometri ve atomic kuvvet mikroskopu (AFM) ile ölçüldü. Taramalı electron mikroskopisi (TEM) ince filmler ve silika nanoparçacıkların nanoyapısal morfolojisini analiz etmek için kullanıldı.

Elde edilen sonuçlar kimyasal olarak çapraz bağlanmış silika nanoparçacıklar içeren ince filmlerin istenilen uygulama için faydalı hale getirdiği daha iyi mekanik özellikler sergilediğini gösterdi.

To my beloved family...

ACKNOWLEDGEMENT

First of all, I would like to say thank you to my supervisor, Fevzi Çakmak Cebeci for his great support under any circumstances. The most important thing is that he taught me how to fly just by my own self without further help. I appreciated to him for his offered opportunities in SUNUM and FENS facilities. Special thanks to Serkan Ünal for their encouraging comments and being my jury member. Also, my sincere gratitude to Burcu Dedeoğlu for attending as one of my thesis defense jury members by honouring me.

Special thanks to Emine Billur Seviniş Özbulut for her almighty help and suggestion. She always pushed me beyond any limits. and supported me to success everything. I will never forget what she did for me.

I am very grateful to meet every person who beautified my university life. Especially, my dear friends, Betül Altın and Nazife Tolay who are my family at Sabanci University. I always remember them with fun and enjoyable memories. I would also like to thank Hümeyra Nur Kaleli and Ebru Özer for their encouragement, Sezin Sayın for her cheerful attitudes, Yonca Belce for being my best teammate, Buse Bulut Köpüklü for her lovely contribution to happiness in our office, İsa Emami Tabrizi for his delicious cakes and Deniz Benli to make me relax.

Many thanks to Burçin Yıldız due to collaboration for NMR measurements and Süleyman Çelik for utilizing AFM. Special thanks to Ali Tufani for his major guidance in laboratory procedures. Although I want to express my sincere gratitude to Araz Sheibani Aghdam for his useful advices and helps.

The most special person I have earned at Sabanci University, Adnan Taşdemir. Time did not pass without drinking tea with his nice conversation. I want to thank him for always encouraging me to do my best. He is always with me for every moment during my thesis. I appreciate his unconditional help and support.

Finally, and most importantly, endless thank to my family for their unconditional love, trust, care and full support. I will never pay what they did for me.

This project was funded by Scientific and Technological Research Council of Turkey (TUBITAK) under the grant agreement number 115M407. Therefore, I would like to show my appreciation for all the support received from this organization, as well.

TABLE OF CONTENTS

LIST OF FIGURES

LIST OF TABLES

LIST OF ABBREVIATIONS

AFM	Atomic Force Microscopy
AHAPS	N-(6- aminohexyl) aminopropyltrimethoxysilane
APDMES	(3-Aminopropyl)dimethylethoxysilane
APS	3-(aminopropyl) trimethoxysilane
APTES	3-aminopropyltriethoxysilane
ATR	Attenuated Total Reflectance
bL	bi Layer
CMC	Critical Micelle Concentration
DETAS	N-[3-(trimethoxysilyl)propyldiethylenetriamine
DLS	Dynamic Light Scattering
DLVO	Derjaguin-Landau-Verwey-Overbeek
EDL	Electrical Double Layer
FT-IR	Fourier Transform Infrared Spectroscopy
HLB	Hydrophilic-Lipophilic Balance
LB	Langmuir-Blodgett
LbL	Layer by Layer
NMR	Nuclear Magnetic Resonance
NPC	N-trimethoxysilylpropyl-N, N, N-trimethylammonium chloride
O/W	Oil in water
PAH	Poly Allylamine Hydrochloride
PEG	Poly Ethylene Glycol
SEM	Scanning Electron Microscope
SPS	Poly (Sodium 4-Styrenesulfonate)
TEOS	Tetraethyl orthosilicate
W/O	Water in oil
ZP	Zeta Potential

1. INTRODUCTION

Thin film coatings have great importance for surface science and engineering. Layer by layer (LbL) assembly is one of the versatile deposition methods to form thin film coatings for many demanding surface applications such as, self-cleaning, antireflective, antifogging and ice-phobic surfaces. LbL assembly method presents exceptional advantages like conformal coatings with controlled structure and composition and having opposite charged materials can be coated sequentially by electrostatic interactions. To assemble nanostructures from water dispersions is quite challenging due to the colloidal instability of the solutions that results in agglomeration and precipitation problems. Addition of functional groups to the surfaces of the nanostructure materials is a quite common approach to improve stability of such solutions. Besides, LbL coated thin films still require further improvement to eliminate their relatively weak mechanical properties. To improve mechanical properties of the coatings, functionalized silica nanoparticles with proper functional groups can be used. These nanoparticles offer more crosslinking possibility with post processes to generate covalent bonds between oppositely charged materials. In this study, silica nanoparticles were functionalized with several functional groups, right after they were synthesized by water-in-oil microemulsion to get ready for LbL method.

1.1.Motivation

The scope of this study is to synthesize silica nanoparticles by controlling their size and to modify the surface of these nanoparticles with several functional groups that are capable of making covalent bonding within the thin film for LbL application having better mechanical properties surface.

Nanoparticles having large surface area tend to agglomerate due to Van der Waals forces to reduce surface or interfacial energy. For this reason, functional groups make the nanoparticle utilize to decrease agglomeration by crosslinking. Thereby, dispersion of

silica nanoparticles in aqueous solution and mechanical properties are expected to be better.

The fundamental mechanism of LbL assembly is to rely on electrostatic interactions between the deposition solutions. Silica nanoparticles can be used to provide adhesion on the substrate in order to increase sustainability of further steps in LbL method. Durability of thin film can be enhanced by functional groups showing favorable mechanical robustness by crosslinking.

1.2. Novelty of This Thesis

The assembly of functionalized silica nanoparticles for LbL procedure is the main approach of this thesis and the functional silica nanoparticles provide robust surface resulting from crosslinking. Besides, silica nanoparticles with functional groups have positive surface charge and they can be assembled with negatively charged polyelectrolytes or bare silica nanoparticles. Different kind of functional groups' behavior will be observed in point of thin film properties for LbL method.

1.3. Road Map of This Thesis

- Silica nanoparticles were synthesized with hydrolysis and condensation reaction taking tetraethyl orthosilicate (TEOS) as main source by microemulsion method.
- Silica nanoparticles were functionalized to change surface charge and property with several functional groups which contain silane alkoxy groups by covalent bond.
- Functionalized silica nanoparticles were deposited onto the substrate to analyze thickness, morphology and robustness of thin films.

2. LITERATURE SURVEY

2.1. Colloidal Science

A solution contains solute and solvent ion and the interaction of one to another is stimulated via an orientation of distinct particles composing of certain size, shape, and charge density in the molecular approach [1]. This interaction-namely intermolecular forces- are forces of attraction or repulsion of adjacent particles with opposite charge densities and they are rather weak forces compare to intramolecular forces holding a molecule together as covalent, ionic and metallic bonding.

The attraction and repulsion forces between particles play the main important role in adhesion, adsorption of surfactants at interfaces and stability of colloids and micellization of surfactants [2, 3]. These forces entitle different interaction as van der Waals forces, solvation and steric force and electrostatic double layer force. Since these forces are the main motive of this thesis, more explicit information should be given to elucidate all background clarification of this thesis. Starting by van der Waals force, it is an umbrella of three categories as London dispersion force, Keesom orientation force and Debye induction force which are interaction between two induced dipoles, interaction between two permanent dipoles and interaction between one permanent dipole and one induced dipole respectively [4, 5]. Attractive or repulsive interaction as dispersion force can bring molecules together or coordinate them ordinarily by using distribution or fluctuation and polarization of electrons in the molecules. Furthermore, this interaction is in control of bulk materials properties at long distance, and by the surface layer at short distance. Secondly, solvation or steric forces are emerged from repulsive forces and they are both arose from entropic origin. The solvation forces describe aligning of solvent molecules into individual layers between surfaces in very confined zone. The hydrated species on a particle surface can induce a repulsion when surfaces come close each other. In addition, polymeric steric forces describe the repulsion of two surface which polymeric macromolecules was attached to their front particles. When these two surfaces come close to each other, the polymer brushes lie over opposite surfaces and repulsive osmotic force is being formed by trapped chains in between surface particles. Governing system can contain protic solvent (methanol or ethanol) or aprotic solvent (acetone and benzene) with the interaction of surface group of polymeric brushes. When polymeric branches and charged particles attached to form a polymer layer with electric potential, electrostatic

repulsion and steric confinements hinders agglomeration. Stabilization is maintained thermodynamically so that particles are always re-dispersible in multiphase system [6]. Lastly, the electrostatic double layer force describes the interaction of fluid-fluid and liquid-solid interfaces [7]. These interfaces have charged molecules which may be originated from adsorption of charged ions at the interface or dissociation of an ionizable surface group. The adsorption of an ionic surfactant or a polyelectrolyte can exemplify the adsorption of a charged ion at the interface and the dissociation of -SiOH groups present on the surface of a solid can be an instance for dissociation of an ionizable surface group. Resulted surface after disengaged part attracts opposite charged ions by coulombic interaction. Conversely, osmotic pressure repels those ions not only from the surface but also from each other. This dispersion is favorable thermodynamically because of the increase in entropy. Double layer forms by increase in concentration of opposite charged ions as surrounding layer on a particle surface when electrostatic attraction and osmotic repulsion reach an equilibrium. Stabilization is maintained kinetically. The double layer force is highly essential to form stabilization of emulsions, foams, and colloids. On the other hand, the integrated effect of double layer and van der Waals forces between two surfaces is modeled by the Derjaguin-Landau-Verwey-Overbeek (DLVO) theory [8-10]. DLVO theory offers to maintain stabilization of a colloidal system which contains particles having Brownian motion and being exerted by van der Waals attractive and electrical double layer repulsive forces seen in Figure 2. 1. The colloidal system can maintain stability if only particles apply enough repulsion to each so that dispersion can defy flocculation, coagulation or agglomeration. DLVO theory has some criteria's to be applied a system. The dispersion must be dilute to prevent any interfere of other particles to charge density and distribution on each particle surface or any proximity change to each particle surfaces. Even though repulsive force creates an energy barrier to block particles to come closer, some particle can overcome that barrier by collisions then attractive force will be dominant to attached them irreversibly together. No other force is dominant than van der Waals force and electrostatic double layer force because gravitational force is negligibly small due to small sized particles. Particles generally have simple and similar geometry that surface properties of all particles are ideal in terms of surface charge density and distribution including the electric potential in the enclosing ambient. The double layer should be in diffusive form that electrostatic force, entropic dispersion and Brownian motion can play their roles freely to determine distributions of counter ions and charges [3, 11, 12]. Nano particle synthesis by colloid method are based

on DLVO theory; and this method is simply established by use of surfactants for stabilizing the colloidal suspension and controlling the particle size. Colloidal particles suspended in a solution form a charged layer that same number of oppositely charged ions surrounds the colloid particles which resulted in electroneutrality. Even though colloid method is applicable to DLVO criteria's in theory, it is very hard to maintain stability and control the particle size in practice. Zeta potential (ZP) is very efficient tool to observe stability in any suspension or any distribution in a solution. As aforementioned in criteria's for DLVO theory, liquid layer enclosing particle consists of two parts; an inner and an outer part. Inner part is called Stern where adsorbed ions firmly bounded each other, on the other hand, outer part is called diffuse layer which contains weakly interacted ions [13]. The ions within diffusive layer form a stable region having a notational boundary. By applying a force field such as electric field, particle displaces so the ions within the boundary (electrical double layer) will be displaced too. Those ions away from boundary stays with bulk dispersant however an interface between the mobile particles and dispersant is formed and called as slipping/shear plane of a colloid particle.

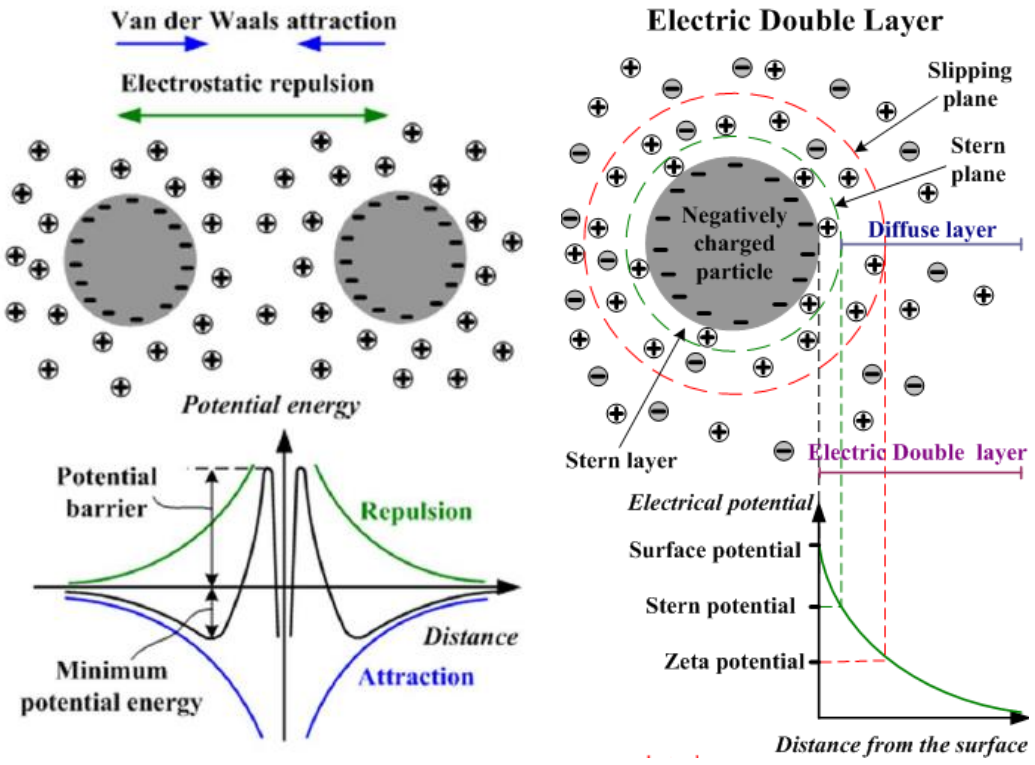

Figure 2. 1. Illustration of DLVO theory (left) and electrical double layer (right) [14].

ZP is electro-kinetic potential that plane of a colloid particle displacing under electric field [15]. If the magnitude of the zeta potential is -as general trend- more than +30 mV or less than -30 mV, particles will not tend to enclose each other or tend to expel each

other. Zeta potential values between +30 and -30 mV refers to instability or moderate stability of colloid otherwise colloid is highly stable if ZP > ±30 mV. However, there are some specific factors that affecting ZP and they are pH value, ionic strength, and concentration. pH effect on ZP is described as changing acidic (H^+) or basic (OH^-) components of particle to alter the range between pH value and the isoelectric point which is also called point of zero charge [16]. At zero charge point, particle does not move under the electric field to measure zeta potential. The isoelectric point is the where colloidal system is least stable according to pH value with respect to zeta potential, so that pH value should be far away from the isoelectric point to avoid agglomeration/flocculation. Ionic strength effect on ZP is described by the difference in valency of ions within EDL. Ions having higher valency forms a compressed EDL so that ZP lessen in magnitude. Concentration effect on ZP is described by change in surface adsorption by increase in concentration so that EDL thickness also changes. Zeta potential increases with the increase in concentration in dilute condition. However, zeta potential decreases at higher concentration so that it creates a low stability in colloidal system.

2.2. Silica Nanoparticles

The silica which is the main component of earth's crust consists of silicon and oxygen atoms, also called silicon dioxide (SiO_2). Silica has different phases divided into anhydrous crystalline silica (e.g. quartz, tridymite, and cristobalite) hydrated crystalline silica ($SiO_2.xH_2O$), anhydrous amorphous silica having anisotropic micro-porosity (e.g. fibers) anhydrous and hydrous amorphous silica having isotropic micro-porosity (e.g. sol, gel, and fine powders) and amorphous silica glass with massive dense. Silica in the crystalline consists of four or six oxygen atoms and each oxygen is bonded to two silicon atoms; however, amorphous silica has random packing of $[SiO_4]^{4-}$ units shown in Figure 2. 2 [17, 18].

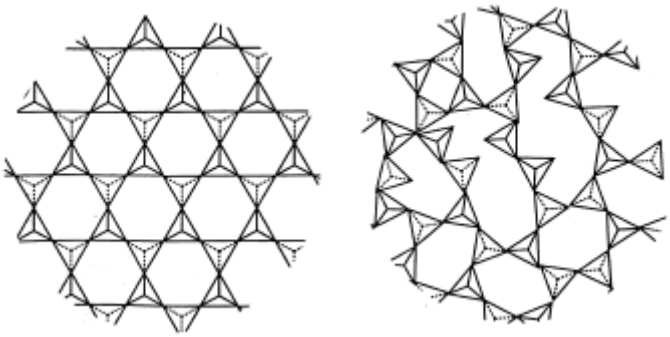

Figure 2. 2. Two dimensional representation of crystalline (left) and amorphous silica (right)[18].

The silica is a hydrophilic material because of the presence of silanol group (SiOH) on the surface of particles. The surface charge potential, density and stability alter by pH and ionic strength of solution. When silica nanoparticles disperse in aqueous solutions, silanol groups ionize to cause negative surface charge and pK_a of silanol is approximately 9.2 [17]. The stability-pH curve which metastable silica at zero surface charge indicates the poorest stability was indicated by Iler's work displayed in Figure 2. 3. The gel formation which occurs the collision of two silica particles with low enough charge on the surface forming siloxane bonds, filling volume of sol to get gel raises in the pH range between 3 and 5 until pH 6 and is proportional with hydroxyl ion concentration that behaves as catalyst to form siloxane linkage. The isoelectric point of silica achieves at around pH 2. The stability increases with catalytic at higher pH values that repulsion is dominant between the particles due to enough concentration of surface charge. In the pH range between 8 and 10 sols are generally stable that the particles suspend in the solution without aggregation [17-19]

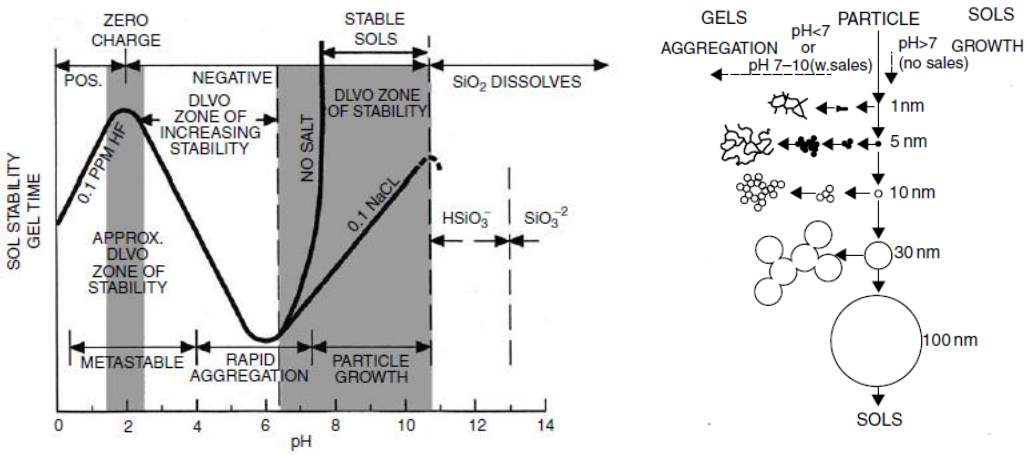

Figure 2. 3. pH versus stability graph of colloidal silica systems [17].

From the very beginning of civilization, silica has great importance for humanity. Nowadays, the usage of silica nanoparticles is very popular due to having simple preparation methods and modifying surface easily that enable to utilize them several applications such as biomedical, pharmacy, food, chromatography, ceramics, catalysts, metallurgy, thin film substrates, optics, elastomers, electronic and thermal insulators [18].

There are many different approaches for the synthesis of silica nanoparticles which basically includes sol-gel process (e.g. Stöber Method [20]) and microemulsion method [21].

2.3. Sol-Gel Process

The sol-gel processing of inorganic materials was mentioned for the first time by Ebelman [22]; however, it gained importance after Geffcken and Berger studies devised preparation of oxide films from sol-gel precursors [23]

A colloid is the dispersion of very small particles (range 1-1000 nm) in a suspension and van der Waals interaction due to particles surface charges becomes dominant because gravitational force exerting on particles are negligible and particles depict Brownian motion [24]. The sol-gel which require transition of colloidal suspension (sol) into continuous liquid phase (gel) is the process for preparation of silica nanoparticles. The sol defined as a dispersion of colloid in a continuous liquid phase in the size range between 1 and 100 nm and gel is three-dimensional interconnected solid network in liquid with sub-micron size pores [25, 26]. There are four steps in the sol gel process which are;

- A sol is formed with the desired colloidal particles to disperse in a liquid.
- The sol solution is generated on the substrates by dipping, spinning and spraying.
- While stabilizing agents are removed, the particles are polymerized in the sols and develop a gel as a continuous network.
- The residual organic or inorganic components are formed an amorphous or crystalline coating by final heat treatment, respectively [24].

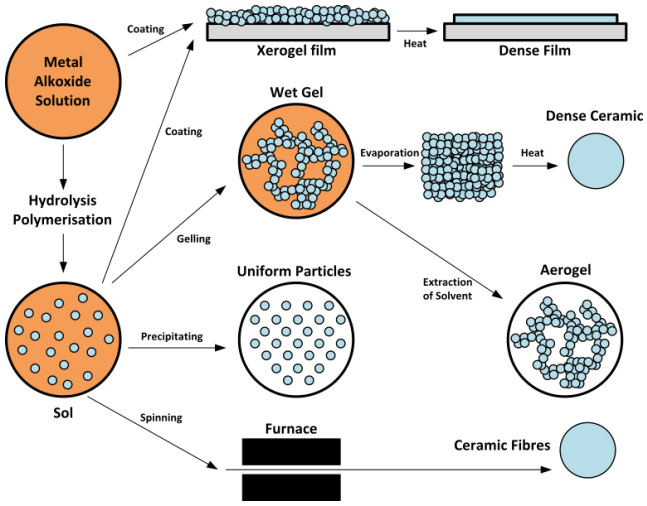

Figure 2. 4. Schematic representation of synthesis of nanomaterials by the sol-gel procedure

The sol-gel process shown in **Error! Reference source not found.** [24] enables to synthesize and produce materials for diverse application areas which are controllable, ultra-fine, spherical shape nanoparticles, thin film coatings, ceramic fibers, membranes, ceramics, glasses and porous aerogel materials. The sol-gel process also presents several advantages, such as obtaining homogenous multi-component system easily, minimizing defects during processing powders, observing defects of gel after drying, formation of fibers, films or composites in the cause of rheological properties of sols or gels.

2.3.1. Hydrolysis and Condensation Reactions

Traditionally, inorganic or metal organic precursors are used for sol-gel processing which occurs by hydrolysis and condensation reactions. The most commonly used reactant is tetraethyl orthosilicate (TEOS) in silica nanoparticle synthesis [27]. Hydrolysis and condensation reactions can be catalyzed by acid, base or humidity shown in Figure 2. 5 and Figure 2. 6 [23]. Indeed, the hydrolysis reaction can start in the absence of catalysts because of humid environment, but the presence of catalysts enhances its reaction rate. The type of catalyst can change the product features, for example, an acidic media enables to form a gel, on the other hand stable sol occurs in a basic media [19, 23].

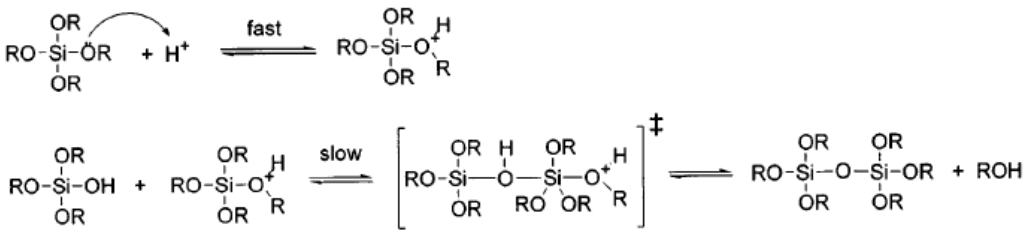

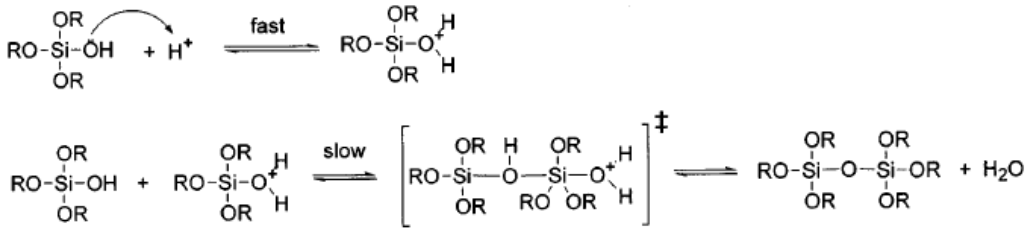

Figure 2. 5. Hydrolysis and condensation under acidic environment.

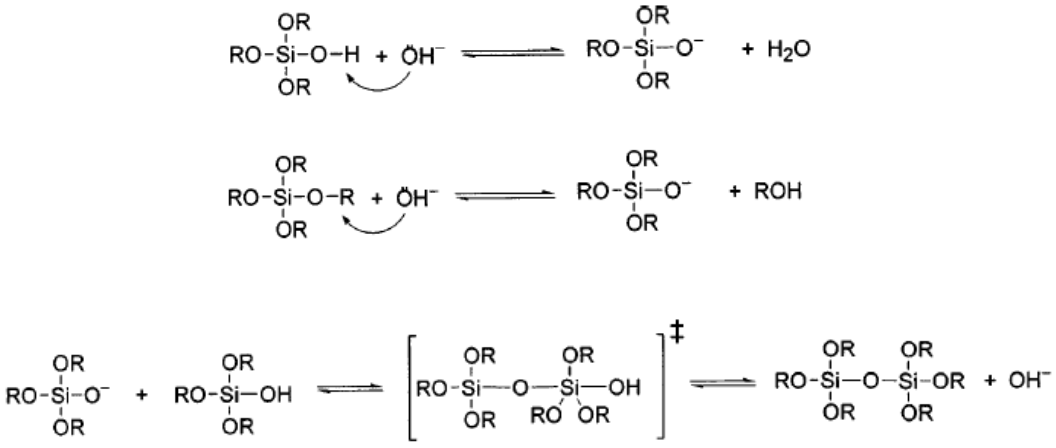

Figure 2. 6. Hydrolysis and condensation under basic environment.

Hydrolysis reaction can initiate in the presence of catalyst or humidity and at the same time alkoxy groups eliminate from the main structure in order to form silanol groups. Immediately after the condensation reactions start and the reaction rate accelerates with heat.

The parameters of the silica nanoparticle synthesis including temperature, pH of catalyst (acid or base), nature of the solvent, and the type of alkoxide precursor [25, 28] are critical on particle size, morphology and strength indicated in Figure 2. 7 [23].

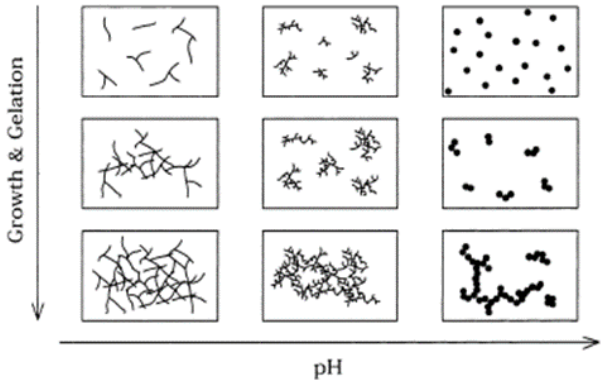

Figure 2. 7. pH versus growth & gelation behavior of the colloidal silica nanoparticles

2.3.2. Stöber Method

In 1968, Stöber et. al. developed a pioneering method to synthesize monodispersed spherical silica nanoparticles with the diameter range from less than 50nm to 2μm [29]. The Stöber method is a one-pot reaction and it is carried out by hydrolysis and condensation reactions of tetraethyl orthosilicate (TEOS) in alcohol-based medium with an ammonia solution as a catalyst under a vigorously stirring [20, 28-34].

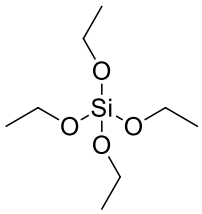

Figure 2. 8. Schematic representation of TEOS

In the hydrolysis reaction, ammonia solution provides hydroxyl ions to medium and these hydroxyl ions attack to silane in TEOS. The ethoxy groups of TEOS are eliminated from the main structure to form silanol groups. After starting the hydrolysis reaction, the alcohol and water condensations take place to generate siloxane bonds following the silica structure are produced. Hydrolysis and condensation reactions are shown below, representatively in Figure 2. 9.

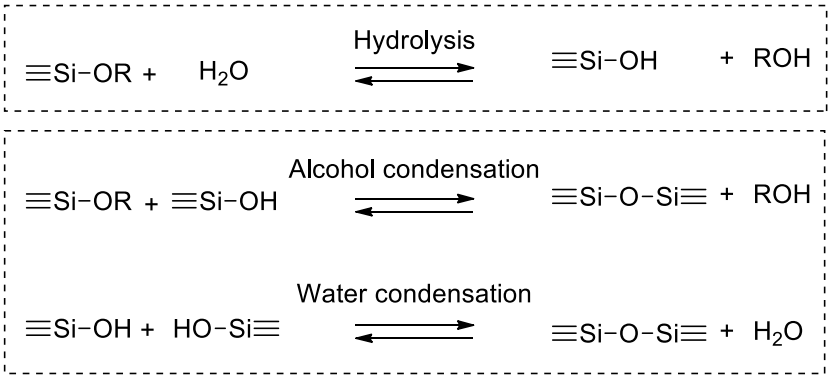

Figure 2. 9. Hydrolysis and condensation demonstrations of TEOS

Ammonia solution is used as a catalyst and the amount of ammonia solution directly affects the silica nanoparticle size, shape and morphology. The particle surface has a negative charge at high pH value, hence, its sol can be obtained without aggregation [19].

The final size and shape are governed by the concentration of water and ammonia solutions, the chain length of alcohol-based solvents (methyl, ethyl, propyl, butyl alcohol) and the reaction temperature. The reaction rates can change with respect to the chain

length of solvent, for instance, the fastest reaction takes place in methyl alcohol, but the slowest one is in *N*-butyl alcohol. There is an inversely proportional relationship between the reaction rate and the particle size [29].

Two models basically explain the chemical and physical growth mechanisms of silica nanoparticles which are monomer addition [19] and controlled aggregation [28] and both of methods can be attributed to nucleation and growth mechanism.

The superiority of this method is that the final product does not contain any surfactant-based impurities. On the other hand, controlling the synthesis of silica particle with a size less than 100 nm is a major encountered problem in Stöber method, as a consequence, the particles are obtained in high poly-dispersed condition.

2.4. Microemulsion

Microemulsions are macroscopically homogenous, but microscopically heterogenous mixtures [35]. The microemulsion method enable to synthesize uniform, monodispersed and spherical shaped silica nanoparticles less than 100 nm and many nanomaterials having different shape and morphology as an alternative to Stöber Method [21, 36-38].

In 1943, Hoar and Schulman [39] were prepared homogenous solution with combination of water, oil, surfactant and cosurfactant in their studies for the first time (Figure 2. 10) yet the microemulsion term was proposed by Schulman et. al in 1959 [40]. Microemulsion consists of minimum three components existing water, oil and surfactant that is optically isotropic, macroscopically homogenous and thermodynamically stable liquid solution. In microemulsion the surfactant has two part as the polar and non-polar phase to form interfacial film and the surfactant molecules surrounded at the interface of oil and water [41].

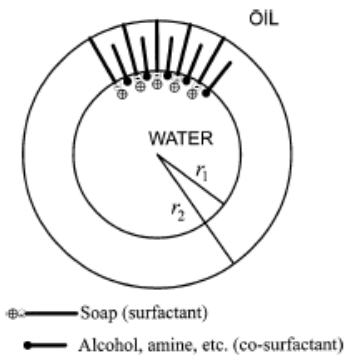

Figure 2. 10. The first representation of water in oil microemulsion by Schulman.

Microemulsions have wide application areas from traditional one (e.g. detergency) to advance one (e.g. nanoparticle synthesis, catalyst, solar energy conversion, cosmetic, drug delivery, pulp and paper industry, concentrate and asphalt, petroleum industry, food and beverages [42].

2.4.1. Surfactant

Nanoparticle synthesis in liquid phase includes numerous components to modify resulting shape, morphology and size, the most important key component to change final properties is surfactant that is the primary difference, as compared to sol-gel method. The aim of surfactant usage is to control the dispersion preventing agglomeration during chemical synthesis [35].

The surfactant molecules are amphiphile because they consist of at least two parts which one of them is soluble in polar solvents called as hydrophilic and the other one is insoluble in water defined as hydrophobic. The hydrophilic and hydrophilic parts are indicated in the head and tail groups, respectively (Figure 2. 11) [43]. These two parts in the surfactant molecules having opposite solubility provide unique features which is able to adsorb at the surfaces and interfaces. The result of these, microemulsion reveals by decreasing the surface tension and forming aggregations in the solution [42]. That is why surfactant word is derived from surface active agent due to the fact that it reduces the interfacial tension between hydrophilic and hydrophobic phases [44].

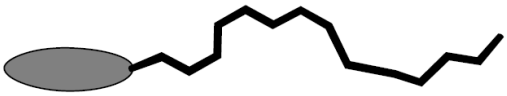

Figure 2. 11. Schematic representation of surfactant molecules with hydrophilic head group and hydrophobic tail.

Hydrophobic group in the surfactant avoid contacting in water in aqueous solutions, but it can dissolve in the aqueous solution at the low concentrations. When the concentration of surfactant exceeds a value referred CMC (critical micelle concentration), the surfactant molecules adjust spontaneously in micelles [44, 45].

Micelles formation is entropy driven process. The water can be supposed to have 3-D structure of hydrogen bonds with cavities. During the destruction and formation of hydrogen bonds, free water molecules move through the cavities. When hydrocarbon exists in the system, the cavities is filled by hydrocarbon molecules and movement of water is restricted. As a result, hydrophobic solute is surrounded by water molecules

which become more ordered. Hydophobic tail of surfactant transfers from ordered water phase to oil phase during micellization that causes disorderness in water molecules surrounding the hydrophobic molecules, consequently the entropy increases in the system and the microemulsion stabilies [44].

Surfactants are divided into two groups that are ionic (e.g. cationic, anionic and zwitterionic) and non-ionic according to their hydrophilic head groups. Non-ionic surfactants whose hydrophilic head is generally formed a short polyethylene oxide chain or seldom a polyhydroxy chain do not have any charge. Non-ionic surfactants are not sensitive to water different from ionic surfactants and compatible to use together with other surfactants, hence their usage increases day by day.

The properties of the surfactants are designated to hydrophilic-lipophilic balance (HLB) defined in 1949 by William Griffin [46]. HLB values (Figure 2. 12) for non-ionic surfactants changes from 1 to 20. 1 HBL number is assigned to most lipophilic molecule nonetheless 20 HBL number is assigned to the most hydrophilic molecule [44-46].

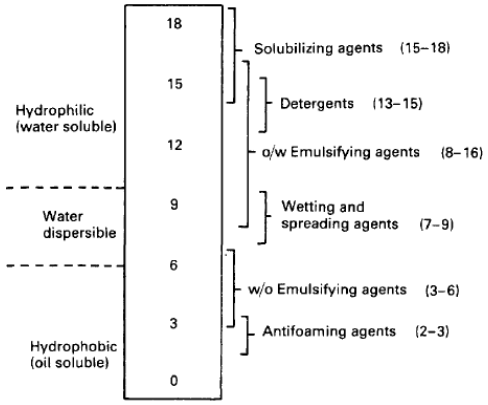

Figure 2. 12. The range of HLB of surfactants [47].

The amount of surfactant determines the coverage of surface consequently, the extent which is the size and number of droplets. When the major component is the oil, the water phase forms the droplets or reverse micelles which the hydrophilic head group of surfactant points inside toward the water phase as hydrophobic points outside toward the oil phase. Water in oil microemulsion (reverse microemulsion) will be explained detailly in Chapter 2.4.3. The radius of droplet is influenced with some parameters such as, amount of water and surfactant

2.4.2. Type of Microemulsion

According to one consider, microemulsions are droplet type of dispersion dividing into oil in water (O/W) and water in oil (W/O) with drop diameter changing between 10 and 100 nm as a kind of emulsions. However, microemulsions and emulsions have important differences that emulsions are thermodynamically unstable, static system and having relatively large droplets but microemulsions are thermodynamically unstable, dynamic system and having small aggregates that have a reverse situation in this way high energy is not necessary to form them [43, 48].

One of the most well-known classifications of microemulsion systems is specified by Winsor [49] to explain phase forming separating four displayed in Figure 2.10. :

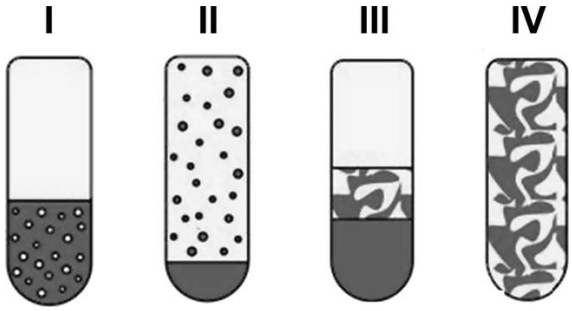

Figure 2. 13. Schematic illustration of Winsor model [50].

Winsor I: Oil in water (O/W) microemulsion phase placed in below is equilibrium with the upper excess oil. The surfactant is favorable soluble in water.

Winsor II: Water in oil (W/O) microemulsions phase placed in above is equilibrium with lower excess water. The surfactant is preferentially soluble in oil.

Winsor III: There are three phases which are excess oil, O/W and W/O as bicontinuous and excess water from top to down.

Winsor IV: A isotropic micellar solution which forms by adding sufficient amount of surfactant and alcohol.

2.4.3. Water in Oil (W/O) Microemulsion

Water in oil microemulsion is well known method since 1960s [51], but used as nanoreactors for producing nanoparticle in 1982 [52]. W/O microemulsion forms homogenous solution when nanometer sized water droplets are dispersed in a hydrocarbon based continuous phase with the help of surfactants. The hydrophilic head group of surfactants are oriented to the water phase, but the hydrophobic tail group of

surfactants points toward the oil phase. Thus, the surfactant composes aggregates defined as reverse or inverted micelles which minimize the energy thermodynamically by forming spherical shape [53]. The polar and ionic components are portioned in the center part of surfactant in reverse micelles as a result of which inorganic and organic materials in oil is dispersed well [41].

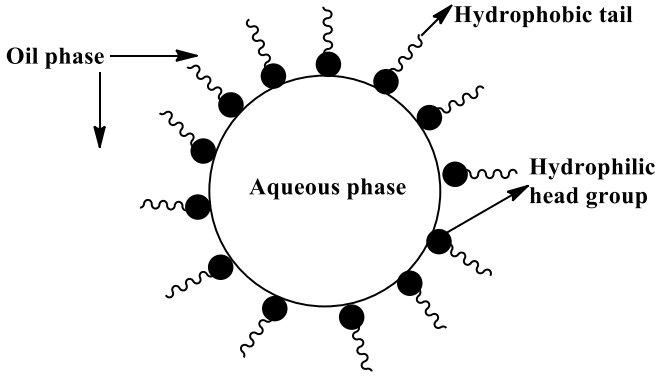

Figure 2. 14. Typical structure of water in oil microemulsion.

The water droplets in the W/O microemulsion behave as nanoreactors for controlled nucleation and growth to synthesize silica nanoparticles (Figure 2. 14). The particle size and shape which is spherical can be controlled by the help of water pool throughout the synthesis [54]. The particle formation is affected by the reactant distribution in the nanodroplets and the dynamics of inter-droplet exchange. The surfactant stabilized nanodroplets show a cage effect that inhibits nucleation and growth of particles [55]. The surfactant performs as stabilizing ligand with weak interaction between particles and hydrophilic head group and also, the steric stabilization provided by the surfactant prevents the aggregation of particles at the final step of particle growth [56]. Besides, the surfactant provides to form particle arrangement with a remarkable ordered on the solvent volatilization [57].

There were many articles about the silica nanoparticle synthesis by microemulsion method. One of the main articles published by Osseo-Asare and Arriagada that silica nanoparticles were synthesized by hydrolysis and condensation of TEOS in surfactant/organic solvent/ammonia media in the size range between 30 and 70 nm [21, 57, 58]. In their study, the particle size and morphology of silica nanoparticles were affected by concentration of ammonia, surfactant and TEOS. The same authors were developed in the study and they reported that size of silica nanoparticles was influenced by water to surfactant molar ratio (R) seen in Figure 2. 15. The particle size decreased

when R value increased until R value reaching 1.8 which referred the minimum particle size. After 1.8 value, particle size raised with R. Hydrolysis and nucleation of silica nanoparticles were not allowed to rise at low R value, but they promoted when ammonia concentration was increased by raising hydroxyl ion concentration. Thus, increase in number of nuclei caused to generate small particle size. Moreover, irregular particle shape was obtained with reducing ammonia concentration, that effect observed better at high R value. Another situation explained particle size change at large R value that nucleation was advisable. Both high R and ammonia concentration led up to intermicellar nucleation by this way aggregation occurred [21]. Another study showed the same results that particles grew by adding hydrolyzed monomer to nuclei thereby, the high amount of nuclei caused the small particle size [59]

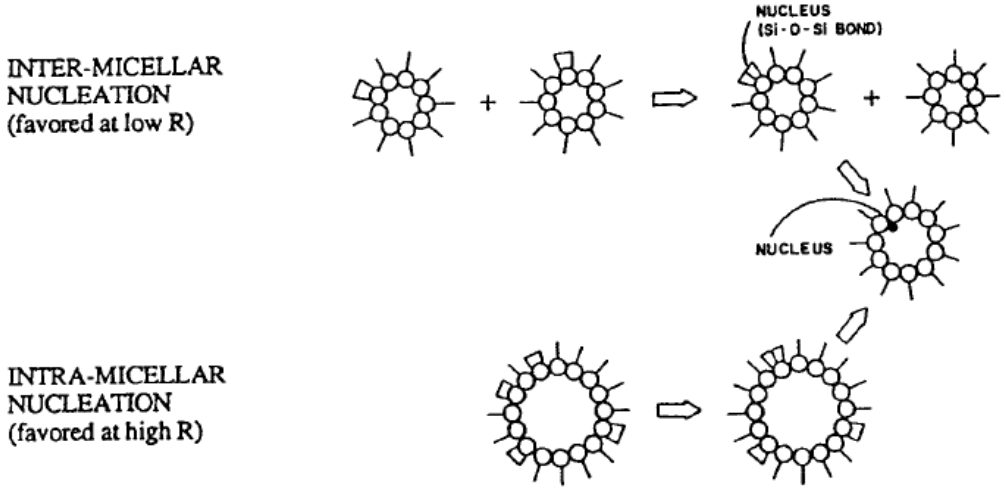

Figure 2. 15. Comparison between nucleation between low and high R value

Silica nanoparticles are bio-compatible materials and they are preferred to perform bioanalysis and biotechnological applications. Bagwe et al. developed dye doped silica nanoparticles as biomarkers by reverse microemulsion method. Similar with Arriagada and Osseo-Asera studies, particle size can be reduced with increasing ammonia concentration due to raising of nucleation rate according to type of bio-application [60].

Pileni achieved pioneering study about several parameters affecting particle size and shape. Regular crystal growth, shape control and nanorod and nanowire formation was explained broadly [61, 62].

Detailed research on the particle growth kinetic in reverse microemulsion system and microemulsion dynamics were presented by Lopez et al. [38, 56] and Osseo-Asare and Arriagada [58].

Briefly, W/O microemulsion is significantly promising method to prepare monodispersed silica nanoparticles. The synthesis is fulfilled quickly in a spatially and geometrically closed area, so the particle size and morphology control are enabled with high homogeneity in nano-scale. The interfacial tension is decreased by surfactant wall in the microemulsion method thereby, the system exhibits excellent morphology control. The water in oil microemulsion offers favorable conditions to produce monodispersed silica nanoparticles. The formation of nanoreactors provide to obtain less than 100 nm silica nanoparticles. That is why we chose the microemulsion method to synthesize monodispersed and 50 nm silica nanoparticles.

2.5. Functionalization of Silica Nanoparticles

Surface functionalization adjusts the physical and chemical features of materials in the wide range of applications [63]. It is one of the superior procedure to modify on the nanoparticles or surfaces which can be used in many applications such as water repellents, antireflective coatings, antifogging, adhesives, paints and inks [64]. The surface modification of the nanoparticles enables to control surface chemistry for chemical loading, provide crosslinking, dispersion of nanoparticles, colloidal stability against aggregation, enhance compatibility between inorganic and organic materials, different surface charge by different kind of functional groups, better adhesion and improvement of mechanical properties [65-69]. There are two ways to achieve surface modification which is via physical interactions and covalent couplings using silane coupling agents [70]. Schematic illustration of silane coupling agent is displayed in Figure 2. 16.

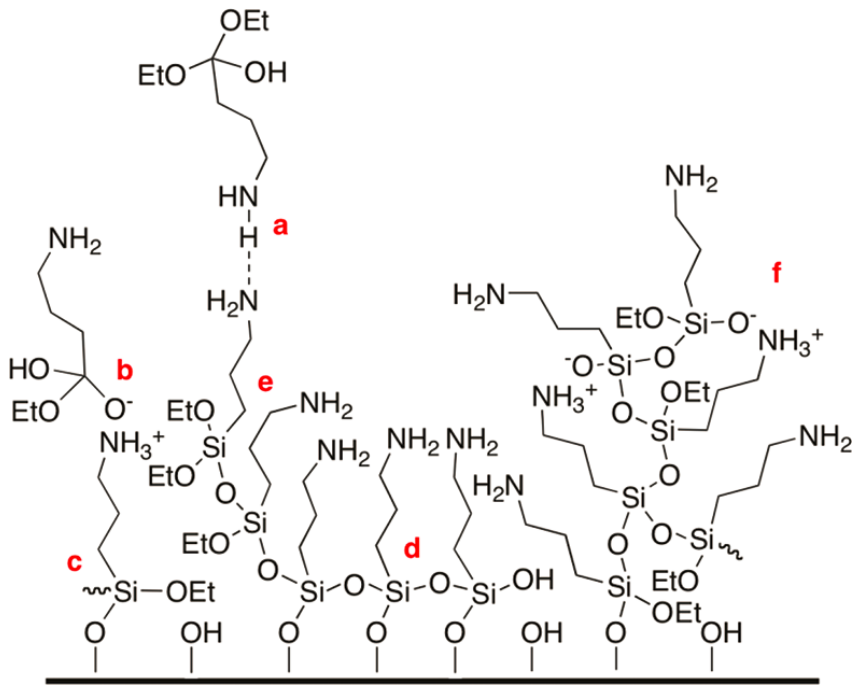

Figure 2. 16. Schematic illustration of silane coupling agents' interactions (a) hydrogen bonding, (b) electrostatic attraction, (c) covalent bonding, (d) horizontal polymerization, (e) vertical polymerization, (f) polymeric silane

2.5.1. Silane Coupling Agents

The silane coupling agent as listed in Table 2. 1 [69] can be expressed as $R_nSiX_{(4-n)}$ which R represents a nonhydrolyzable organic moiety such as, alkyl, aromatic or organofunctional groups and X is alkoxy moieties (generally methyl or ethyl) [64].

The characteristics of functionalized particle or surfaces alter in terms of wetting or adhesion.

The silane coupling agents can be used as surface modifier, a primer or an adhesive. A reactive silanol is formed after the hydrolysis and then, condensation reactions are taken place with other silanol groups to form the siloxane bond. In these reactions, the coupling agents have different type of functional groups which help the surface to react with silanol groups by covalent bonds [71-73].

One of the most widely used coupling agents is amino silanes because of their bifunctional nature. In early days, amino functionalized silica was utilized in filler industry for rubber and plastic to better strength, resistance and rheology [74]. Nowadays, amino terminated silica nanoparticles are very promising from biomedical applications [65, 66, 75-78] to thin film technology [67, 79-81]

Amino silanes are bonded to the surface by covalent bond resulting Si-O-Si structure. In aqueous media, $-NH_3^+$ groups arising from amino silanes increase to develop the relevance of surface chemistry due to their positive surface charges which enable the attachment of negative charged groups such as nanoparticles and DNA for the applications. Furthermore, amino silanes have an extraordinary surface reaction in order to contain a built-in catalyst different from other silane agents [82, 83].

Table 2. 1. Typical silane coupling agents to modify silica particles

Name	**Abbreviation**	**Structure**
3-aminopropyltrimethoxysilane	APS	$H_2N(CH_2)_3Si(OCH_3)_3$
3-aminopropyltriethoxysilane	APTES	$H_2N(CH_2)_3Si(OC_2H_5)_3$
aminopropyl methyldiethoxysilane	APMDES	$H_2N(CH_2)_3(CH_3)Si(OC_2H_5)_2$
(3-acryloxypropyl) methyldimethoxysilane	APMDMOS	$CH_2=CHCOO(CH_2)_3(CH_3)Si(OCH_3)_2$
(3-acryloxypropyl) trimethoxysilane	APTMS	$CH_2=CHCOO(CH_2)_3Si(OCH_3)_3$
aminophenyltrimethoxysilane	APTMS	$H2NPhSi(OCH_3)_3$
bis(triethoxysilylpropyl)tetrasulfane	TESPT	$(C_2H_5O)_3Si(CH_2)_3S_4(CH_2)_3Si(OC_2H_5)_3$
dimethyldichlorosilane	DDS	$(CH_3)_2SiCl_2$
3-glycidoxypropyltrimethoxysilane,	GPS	$CH_2(O)CHCH_2O(CH_2)_3Si(OCH_3)_3$
3-isocyanatopropyltriethoxysilane	ICPTES	$OCN(CH_2)_3Si(OC_2H_5)_3$
methacryloxymethyltriethoxysilane	MMS	$CH2=C(CH_3)COOCH_2Si(OC_2H_5)_3$
3-methacryloxypropyltrimethoxysilane	MPS	$CH=C(CH_3)COO(CH_2)_3Si(OCH_3)_3$
methacryloxypropyltriethoxysilane	MPTES	$CH=C(CH_3)COO(CH_2)_3Si(OC_2H_5)_3$
mercaptopropyl triethoxysilane	MPTS	$SH(CH_2)_3Si(OC_2H_5)_3$
methyltriethoxysilane	MTES	$CH_3Si(OC_2H_5)_3$
phenyltrimethoxysilane	PTMS	$PhSi(OCH_3)_3$
vinyltriethoxysilane	VTES	$CH=CHSi(OC_2H_5)_3$
vinyltrimethoxysilane	VTS	$CH=CHSi(OCH_3)_3$

2.5.2. Covalent Couplings

Crosslinking which provides the chemical reaction with two or more molecules by covalent bond is occurred throughout the silica functionalization process. Binding affinity or covalent bond are generally favored to functionalize the silica nanoparticles due to reduction of desorption from the surface resulted in robust rather than adsorption and electrostatic interaction. [70, 72, 75, 84, 85].

Waddell et al. reported that aminopropyl silane film was formed by hydrolysis of alkoxy group following covalent attachment of hydroxy silane groups in silicon oxide surface and APTES reaction [86]. In addition to this study, Pasternack et al. indicated that to obtain dense amino propyl film and having ordered Si-O-Si bonds without unreacted byproduct as fully as possible can be produced by pre-annealing and reveal better stability in aqueous solution [87].

The very basic report for the colloid science and interfaces was the functionalization of silica particles with organo-trialkoxysilanes mentioned by Van Blaaderen et. al in 1993. The functionalization reaction was performed with a based catalyzed system in a mixture of ammonia solution and ethanol. That was the new procedure to obtain hybrid materials which made the particles suitable in colloidal systems. The different from bare silica, the organo-silica particles had higher surface charge and low density [20]. However, the organo-silica particles loss their functionality in aqueous media in time. This fundamental problem was investigated by Smith et al. The degradation was catalyzed with either to form five-membered cyclic intermediate or intermolecularly interactions. They denoted the importance of the alkyl linker length in amino silanes to minimize the detachment of functional groups from silica nanoparticles. The results indicated that aminopropyl silane was not a good candidate in the aqueous environment according to either having shorter and longer amine-based alkyl linker because of their ability of intramolecular interaction [88]. The similar report was supported the results of Smith et al. study that throughout hydrolysis primer amine in the APS and APTES catalyzing the formation of siloxane bond and hydrolysis made the silane layer unstable. Indeed, the intramolecular interactions also attained denser structure to organo-silica particles, so mechanically robust functional silica particle was obtained in this approach.

N-(2-aminoethyl)-3-aminopropyltriethoxysilane and N-(2-aminoethyl)-3-aminopropyl trimethoxysilane were determined as the best candidate because detachment of bond was prevented by steric effect. N-(6-aminohexyl) amino methyl triethoxy silane was not catalyzed intramolecularly, so it was not stable enough [82].

Graf et al. investigated the colloidal stability of the functionalized silica nanoparticle in the different media comprehensively. Amino acid, amino, and poly (ethylene glycol)-terminated alkoxy silanes covalently is bound to the silica nanoparticles in order to form positive and negative surface charges in physiological medias. The most promising results were achieved for N-(6-aminohexyl)-3-aminopropyltrimethoxy-silane (AHAPS), and 2-[methoxy(polyethleneoxy)propyl]- trimethoxy-silane (PEG) functionalized silica nanoparticles in all media [63].

There are many bio-applications about the dye doped functional silica nanoparticles because the silica nanoparticles can be functionalized with several functional groups additionally, dye can be covalently bonded on the silica surface. The dye helped the

particle detect for bioassays and bioanalysis. Thus, those nanoparticles could be utilized for optical bioimaging in vivo and vitro [89-91].

The effect of different functional groups was investigated with regard of agglomeration by Bagwe et al in 2006. The silica nanoparticles were functionalized with the methyl phosphonate as inert group and amino silane. The amine groups provided to obtain high agglomeration and low surface charge. However, the particles acted as well disperse due to have high negative surface charge when methyl phosphonate was added that size also decreased because of electrostatic repulsion. Thereby, many bio-based application was resulted by using the surface modification [92].

An et al. analyzed that covalent bond formation of amino and carboxyl functional groups on the surface of silica nanoparticles. In that study, the silicon substrate was terminated with amine groups and following functionalized with carboxylic acid by amide bond formation. The carboxyl surface was determined as more active to further reactions [85].

Howarter et al. demonstrated that adhesion between silica substrate and organic or metallic compounds is enhanced by using APTES thin films which enable to use in various areas to illustrate from advanced materials to bio-based applications. The different film morphologies such as, smooth thick and rough surfaces were observed in that study. Hydrolysis of APTES in the solution based and at the hydrated surface was illustrated in Figure 2. 17[93].

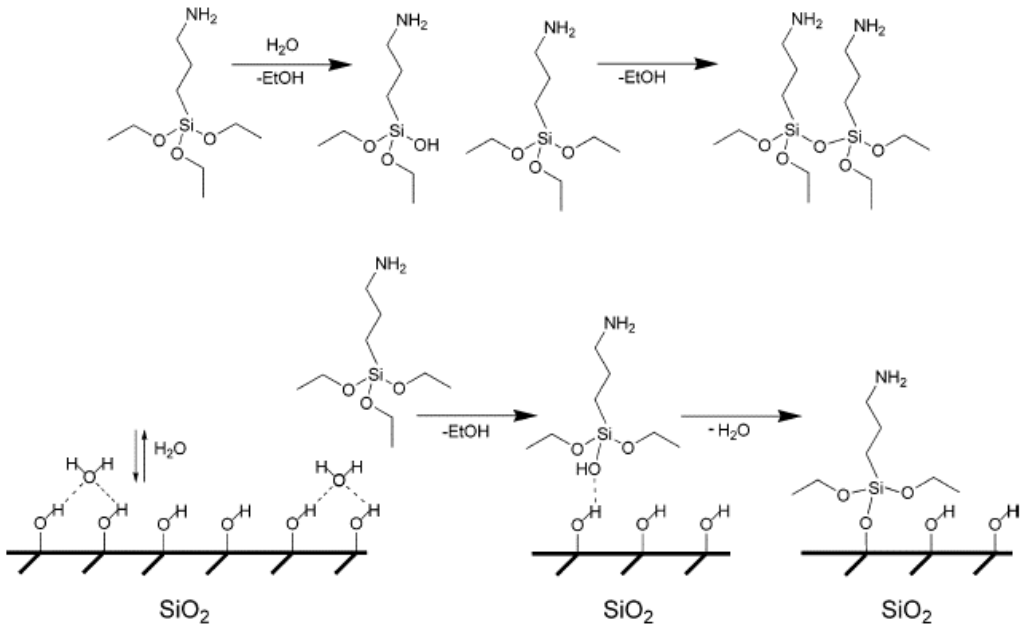

Figure 2. 17. Demonstration of hydrolysis of APTES in the solution (Top) and at the hydrated surface (Bottom)

There are many studies about the APTES functionalization of the silica nanoparticles or silicon substrates in non-aqueous media which was investigated the effect of experimental parameters by using several characterization tools [93-98]. The aim of hydrolysis of APTES in non-aqueous media is to utilize a monolayer grafting throughout the modification, but solvent removal process is not easy resulting impurity in the product and also, the process proceeds long with low efficiency [99].

2.5.3. Physical Interactions

Non-covalent modification of silica nanoparticles is based upon the adsorption or electrostatic interactions with large molecules such as polymers, lipids, proteins or antibodies [65, 70]. The fundamental advantages of the physical interactions method are being simple and cheap without further purification process. On the other hand, bound molecule can be disassociated from the nanoparticle surface by the weak interaction [100].

Surface charges of nanoparticles in a solution provide the dispersion of nanoparticles by electrostatic repulsion preventing interaction/aggregation. Nevertheless, adding ions and ionic surfactants on the nanoparticle surface can modify their surface charge, so that electrical double layer can be formed around each nanoparticle. Formed structure has inner and outer layers which is called stern layer and diffusion layer alternatively. The zeta potential is evaluated by the movement of these two layers under an electric field. All in all, zeta potentials determine the degree dispersion of the solution consisting of physical repulsion and interaction. Moreover, zeta potential data is used to explore bound functional groups onto nanoparticle surface which helps to modify overall surface charge [101, 102].

Polyethylene glycol (PEG) is one of the polymers which forms a protective layer around the silica nanoparticles to prevent agglomeration. Branda et al. functionalized amine based PEGylated silica nanoparticles. PEG concentration was adjusted to get long term stability concurring both steric and electrostatic effect [103]. Xie et al. studied that mesoporous silica nanoparticles were functionalized with carboxyl groups then conjugated with folate via PEG in order to accomplish nanocarrier for diagnosis simultaneously [104]. Another study was fulfilled by Beyer et al. which the surface modification was taken placed by reactive polymer interlayers. Thus, polymer supported bilayer introduced compatible properties to tune the surface with other molecules [105].

Xu et al. reported that physical or chemical interaction of PEG to silica nanoparticle indicated the biocompatibility for biomedical applications. The LbL will be explained in detail in the next chapter. To sum up, having two opposite charged polyelectrolytes are developed on the silica nanoparticles surface to mediate with the charged compounds such as biomolecules [106-109] in LbL process.

2.6. Layer by Layer (LbL) Assembly

Layer by layer (LbL) assembly is one of the easiest techniques to generate thin film coatings on various substrates with polymers, colloids and bio-compounds. It presents outstanding control and versatility according to other thin film deposition methods [110]

Actually, one technique was developed to fabricate thin films in the past known as the Langmuir-Blodgett (LB) technique which is defined as transferring one or more monolayers on the water surface onto solid support [111, 112]. That technique was applied on synthetic nanosized heterostructures of organic compounds by Kuhn et al. [113]. However, the LB technique has some limitation in terms of controlled thickness and stable films.

The fabrication of opposite charged particles which are polyanion and polycation onto a substrate was demonstrated by Decher et al. at first [114-117]. There are many advantages such as being easy, simple and cheap with respect to LB and self-assembly techniques [118]. It is green technique because of aqueous based solution.

Concisely, negative charged glass substrate is coated with having opposite charged materials which can be nanoparticles, polymers, proteins or viruses to change the substrate charge and these steps can be repeated in a cycle until the desired film thickness and film properties are achieved. Schematic illustration of dip and spray coating can be observed in Figure 2. 18**Error! Reference source not found.** [119].

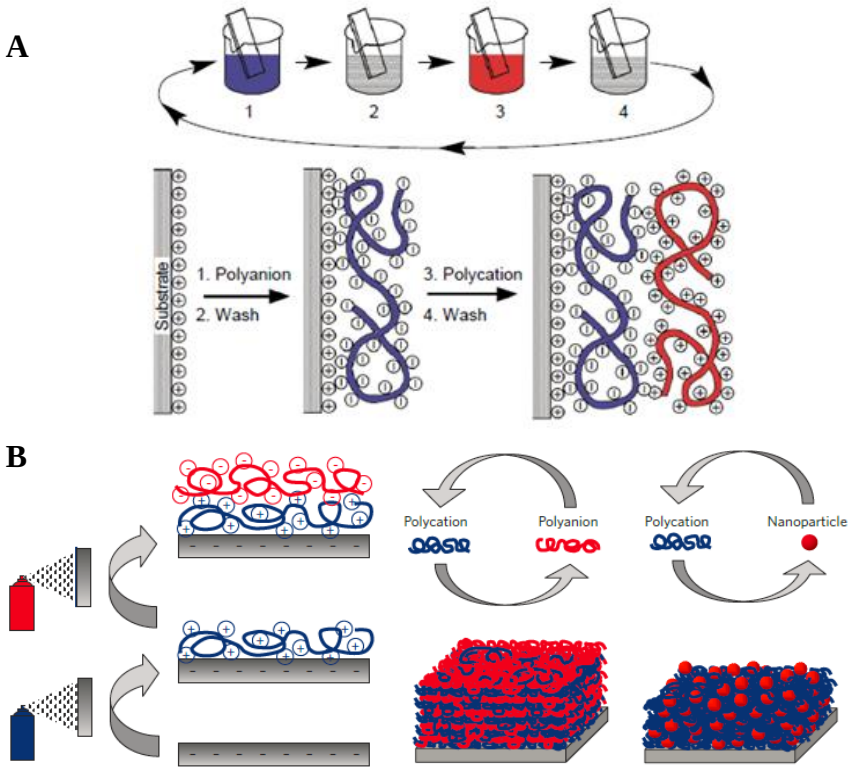

Figure 2. 18. Dip coating of polyanion and polycation and spray coating of polyanion/nanoparticle and polycation

Multilayer thin films can be used on corrosion resistant [120], anti-reflective [121-123], antifogging [121-127], superhydrophilic and superhydrophobic [121-123, 127, 128], antibacterial coatings [126], antifouling [128] by conducting some steps.

3. EXPERIMENTAL WORK

3.1. Materials

Cyclohexane (Sigma-Aldrich, 99.5%), Igepal CO-520 (Sigma-Aldrich, 99%), ammonia solution (Sigma-Aldrich, 25 wt. %), were used as received without further purification, but tetraethyl orthosilicate (TEOS, Sigma-Aldrich, 98%) was used freshly distilled before using for silica synthesis. 3-(aminopropyl) trimethoxysilane (APS, Sigma-Aldrich, 97%), N-trimethoxysilylpropyl-N,N,N-trimethylammonium chloride (NPC, ABCR, 50% in methanol), N-(6- aminohexyl)aminopropyltrimethoxysilane (AHAPS, ABCR, 95%), 3-Aminopropyl(dimethyl)ethoxysilane (APDMES, ABCR, 97%), N-[3-(trimethoxysilyl)propyldiethylenetriamine (DETAS, ABCR, 95%) and 2-[methoxy(polyethyleneoxy) propyl]trimethoxysilane with 6-9 polyethylene oxide units (PEG-silane, ABCR, 90%) were used as silane coupling agents for functionalization process as visualized in the Figure 3. 1. Ethanol (Sigma-Aldrich, 99.8%) was used to purify all of the nanoparticles by recentrifugation and redispersion process. Poly allylamine hydrochloride (PAH, M_w: 15000) and poly (sodium 4-styrenesulfonate) (SPS, M_w: 70000) were purchased from Sigma -Aldrich as positive and negative polyelectrolyte, respectively. Deionized water (>18MΩcm, Millipore Milli-Q) was utilized in all water-based solutions and rinsing procedures throughout the LbL assembly.

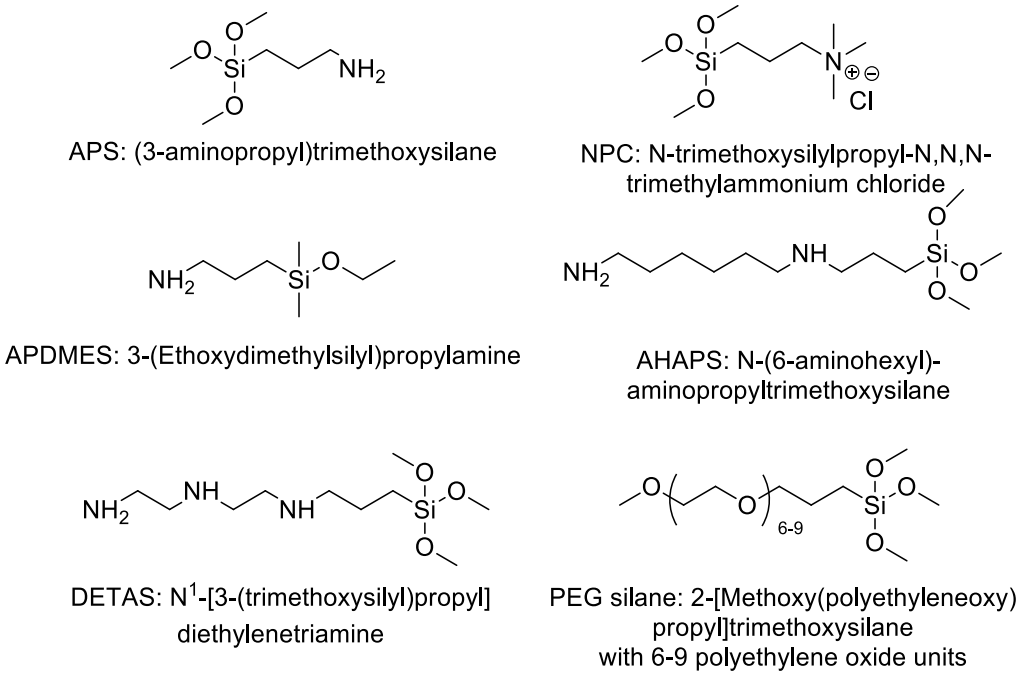

Figure 3. 1. Chemical structure of silane coupling agents

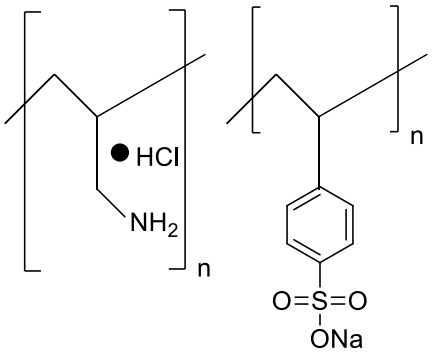

Figure 3. 2. Schematic illustration of poly allylamine hydrochloride (PAH) (left) and poly (sodium 4-styrenesulfonate) (SPS) (right)

3.2.Synthesis of Silica Nanoparticle by Water in Oil Microemulsion Method

In this study, silica nanoparticles were prepared by hydrolysis and condensation of TEOS used as silica source in a nonionic surfactant/cyclohexane/ammonium hydroxide solution. Igepal CO-520, cyclohexane, and 25% wt. concentrated ammonium hydroxide were used as non-ionic surfactant, solvent, and catalyst respectively.

During the experiment, remodified microemulsion system was executed for synthesis of silica nanoparticles [21, 63]. 100 mL (0.9 mol) cyclohexane and 5.11 g (0,06 mol) Igepal CO-520 was put into glass bottle, then, 0.606 mL (6.5 mmol) ammonia hydroxide (25% wt.) was mixed under the magnetic stirring at 600 rpm until microemulsion solution became transparently clear. Afterwards, 0,626 mL (7 mmol) TEOS was added to the microemulsion under magnetic stirring for 5 min. The microemulsion was kept in the storage for 3 days without disturbance. After 3 days of storage, the microemulsion was precipitated by supplement of 10 mL acetone and washed by isopropyl alcohol, 3 times with ethanol and 3 times with deionized water, alternately by repeated centrifugation process which was at 11000 rpm at least 15 min long in each step.

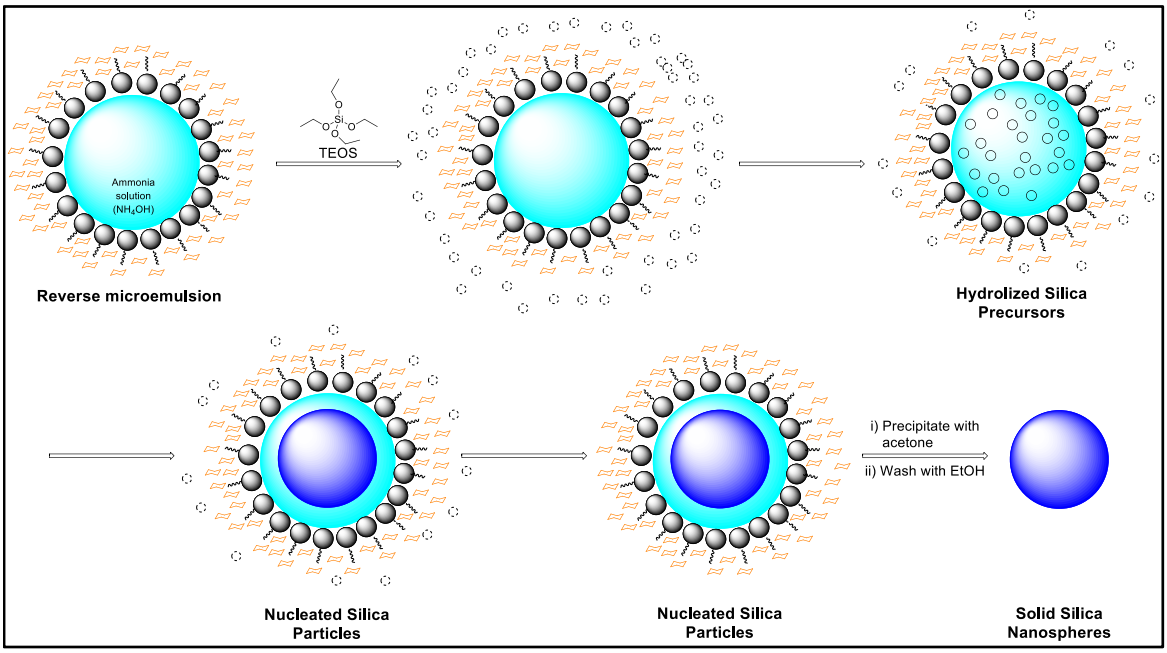

Figure 3. 3. Schematic representation of synthesis of silica nanoparticles by water in oil microemulsion method

3.3.Functionalization of Silica Nanoparticles

3.3.1. Functionalization of Silica Nanoparticles with APS, NPC, APDMES and AHAPS

Functionalization of silica nanoparticles were prepared using the functionalization procedure described by Graf et.al [63]. Three-necked flask was used with a magnetic bar during the experiment after nitrogen flashing by injection. 5 mL ethanol and 2 mL ammonia solution (25% wt.) were dispersed in a beaker for 1 minute. In another place, 0.1 g silica nanoparticles were dispersed in 5 mL ethanol until acquiring homogenous dispersion. First of all, ethanol and ammonia mixture were added to the flask under magnetic stirring at 600 rpm in the dry nitrogen ambient, and subsequently 10 mg/mL silica dispersion was placed in flask to reach final silica nanoparticles concentration. 9 mmol functional group (APS, NPC, APDMES and AHAPS) solution was added in the mixture and stirred overnight at room temperature. Following that, mixture was refluxed at 80 °C for 3 h after removing nitrogen inlet. Lastly, the mixture was centrifuged three times at 4000 rpm for 15 min in ethanol to collect the pure functionalized silica nanoparticle as far as possible.

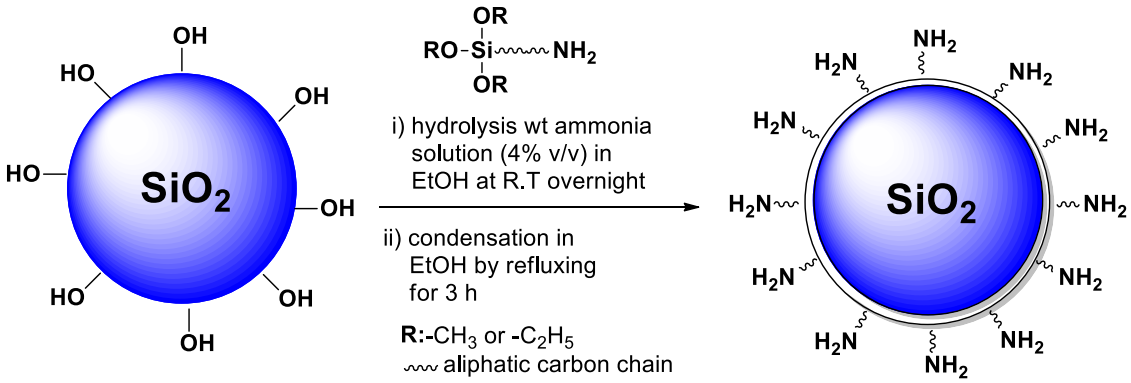

Figure 3. 4. Schematic illustration of functionalization of silica nanoparticles with amine based functional group by hydrolysis and condensation reactions

NMR chemical shifts of APS, NPC, APDMES and AHAPS functionalized silica are given in below;

Si-APS: ^{1}H NMR (500 MHz, D_2O) δ 2.93-2.90 (m, 2H), 1.74-1.68 (m, 2H), 0.61-0.57 (m, 2H).

Si-NPC: ^{1}H NMR (500 MHz, D_2O) δ 3.33-3.30 (m, 2H), 3.10 (s, 9H), 1.91-1.85 (m, 2H), 0.64-0.61 (m, 2H).

Si-APDMES: ^{1}H NMR (500 MHz, D_2O) δ 2.94 (m, 2H), 1.68 (m, 2H), 0.65 (m, 2H), 0.15-0.14 (m, 6H).

Si-AHAPS: ^{1}H NMR (500 MHz, D_2O) δ 2.99-2.90 (m, 6H), 1.77-1.73 (m, 2H), 1.65-1.62 (m, 4H), 1.41-1.38 (m, 4H), 0.62-0.59 (m, 2H).

3.3.2. Functionalization of Silica Nanoparticles with PEG Silane

10 mg/mL silica nanoparticles dispersion in ethanol was added to the flask, and 0.1 mL PEG and 2 mL ammonia was mixed under magnetic stirring. The mixture was heated to 80 °C on the magnetic stirrer with 600 rpm under dry nitrogen atmosphere overnight. The final product was purified by recentrifugation and redispersion three times to remove excess PEG at 4000 rpm for 15 min with ethanol.

NMR chemical shifts of PEG functionalized silica are given in below;

Si-PEG: ^{1}H NMR (500 MHz, D_2O) δ 3.70 (s, 36 H), 3.53 (m, 2H), 3.38 (s, 3H), 1.71 (m, 2H), 1.27 (m, 2H).

3.3.3. Functionalization of Silica Nanoparticles with DETAS

10 mg/mL silica nanoparticle dispersion in toluene was added to a three necked round bottom flask connected to condenser within argon ambient while solution was stirred by a magnetic stirrer during 30 minutes at 100 rpm speed. In the next step, 1 mL ammonia solution was introduced to reaction mixture and resulted mixture was stirred vigorously during 2 hours at room temperature. Then, temperature of yielded solution was set to 85 °C, then 8 µL DETAS was added to reaction mixture under vigorous stirring and reflux was started under argon flow. Then, the same amount of DETAS was added three times

within each 1.5 h periods. Then, particles inside the final solution was precipitated by using a centrifuge and precipitated particles was washed several times with toluene and ethanol. The final product was dried at 80 °C for 24 hours.

NMR chemical shifts of DETAS functionalized silica are given in below;

Si-DETAS: ^{1}H NMR (500 MHz, D_2O) δ 3.56-3.37 (m, 4H), 2.97-2.55 (m, 6H), 1.70 (m, 2H), 0.64 (m, 2H).

3.4. Layer by Layer Assembly

Dip spin LbL was carried out during LbL assembly process. Dipping time was determined as 10 min for polyelectrolytes and nanoparticles. Subsequently, rinsing procedure was applied in the sample immersed into distilled water for rinsing procedure as 2 min and two times 1 min to remove residual charge. The substrates which were glass slides or silicon wafer were cleaned in the glass cleaning solution (4% in water) and then, in deionized water by ultrasonic bath for 15 min each step before coating. Plasma treatment was performed on the cleaned substrate for the purpose of surface charging for 2 min. PAH (+) and SPS (-) were prepared as 10 mM and their pH values were adjusted to 4.0 pH value by using 0.05, 0.1, 0.5, 1 M hydrochloric acid (HCl) and sodium hydroxide (NaOH) solutions. Functionalized silica nanoparticles were dispersed in deionized water as concentration of 0.15/1L and its pH value was also reduced to 4 by having same concentration HCl and NaOH solutions. The charge of silica nanoparticles was changed according to their functional group. First, adhesion layer was transferred onto substrate surface with PAH (4.0) /SPS (4.0) as 5 bilayer (bL). Afterwards, the same process was repeated for functionalized SiO_2 (4.0) /SPS (4.0) as coating with desired number of layer (5, 10, 15, 20). Lastly, the coated substrate was dried by the help of dry nitrogen to get ready for characterization.

3.5.Characterization

3.5.1. Dynamic Light Scattering (DLS)

Hydrodynamic size of silica nanoparticles and zeta potential of functional silica nanoparticles were investigated by performing Dynamic Light Scattering (DLS) analyzer which is Zetasizer Nano ZS, Malvern Instruments Ltd. 0.15 g/L of silica solution was prepared in deionized water for size and zeta potential measurement. The ultrasonic bath and probe sonication method were used to prevent agglomeration of silica nanoparticles

for all DLS measurements. pH of all silica solution was tuned by HCl and NaOH for zeta potential measurement. All resulted samples were surveyed at 25 ˚C in disposable low volume cuvette and disposable folded capillary zeta cell for size and zeta potential measurement, respectively. Nanoparticle sizes determined for 10 cycles with 3 measurements to obtain mean particle size and number of percentages were considered. Zeta potential was explored to examine the particle surface charge implying bounded functional groups on silica nanoparticles.

3.5.2. Scanning Electron Microscopy (SEM)

Morphology, size and distribution of the samples were visualized with a Zeiss Leo Supra 35 Field Emission Scanning Electron Microscope. Silica nanoparticles were dispersed in a 15 mg/L dilute solution of nanoparticles and distilled water. 100 μL of resulted solution were dropped on silicon wafers and then they were dried for an hour in an oven. The functional silica nanoparticles were deposited onto silicon wafer by LbL assembly and those wafers were cut by diamond cutter in order to fit on SEM stubs. Samples loaded silicon wafers were placed into Desk V HP, Denton Vacuum sputtering machine then samples were coated with gold/palladium for 2 minutes. Following these, silicon wafers were placed on SEM stubs by two-sided carbon tape which helps gold/palladium coated part to be in contact with stubs in order to maintain electrical conductivity. SEM stubs then placed in SEM sample stage as last step of sample preparation procedure of SEM analysis. Silica nanoparticles were monitored by using secondary electron detector powered 3 keV within 7-10 mm working distance.

Morphological and microstructural analysis of silica nanoparticles were observed and silica nanoparticles with different functional groups were studied according to their particles size, homogeneity in distribution and sample geometries, agglomeration states by SEM analysis.

3.5.3. Fourier Transformation Infrared Spectroscopy (FTIR)

Fourier transform infrared spectroscopy (FT-IR) were operated via Bruker Equinox 55 FTIR spectrometer with Attenuated Total Reflectance (ATR) attachment. FTIR data were collected from 4000 to 650 cm^{-1} range to examine structural properties of sample by inquiry of existing vibrational bonds of samples. Samples were used in their powder form and measurements was conducted without further preparation. FTIR spectroscopy was carried out in standard ATR mode and the machine was waited 15 minutes in nitrogen

ambient before measurements were started. Background scan was obtained before sample were analyzed and background noise was subtracted from samples data. All measurements were evaluated 64 repetitive scan and final data were obtained as average automatically.

3.5.4. Nuclear Magnetic Resonance Spectroscopy (NMR)

NMR spectra was performed on a spectrometer Varian Unity Inova 500MHz spectrometer. The spectra were recorded at room temperature with a 500Mhz 1H-19F(15N-31P) 5mm PFG Switchable Probe. Samples were dissolved in D_2O (99.96 %). 10-20 mg of sample is dissolved in 600 µL of deuterated solvent. The proton NMR spectra were acquired using S2PUL sequence (32K data points, acquisition time 1.892 s, pulse width 7.2µs, repetition delay 10s). Chemical shifts were referenced with respect to water signal at 4.8 ppm if D_2O used.

3.5.5. Ellipsometry Analysis

Ellipsometry uses two different polarized light (s-polarized and p- polarized) having 90-degree phase shift but same frequency and polarized lights reflects from the sample by elliptical changes resulting in information of angle and amplitude change. In other word, ellipsometry is a great tool to obtain extinction coefficient, refractive index and thickness of thin film. Ellipsometry generally has a light source, a polarizer which polarizes the light on the specimen, and a detector which measures the amount of light polarization after reflection from the specimen. In this study, M2000 spectroscopic ellipsometry (J. A.Wollam Co., Inc) was used to measure the thickness of functionalized silica nanoparticles coated silicon wafer by LBL method. Ellipsometry data is collected either as a function of wavelength or the incidence angle, or both. Functionalized silica nanoparticles coated silica on wafers were placed in device and thickness measurements were received at 65, 70, and 75 incidence angles while using light wavelength between 315 to 718 nm range. The Cauchy model or b-spline were executed to fit data for all thickness measurements. The thickness value was recorded according to transparent value of the coatings on wafer and change in thickness value was collected as a function of time.

3.5.6. Atomic Force Microscopy (AFM)

Atomic force microscopy was performed in dynamic mode (ezAFM, Nanomagnetics Instruments) To perform the experiment coated silicon wafer was cut in suitable size by

diamond cutter. The surface was cleaned with drynitrogen to remove residual. 5µmx5µm area was scanned by using tip in tapping mode.

4. RESULTS&DISCUSSION

4.1. Preparation of Silica Nanoparticles

Silica nanoparticles were synthesized by water in oil (W/O) microemulsion in the surfactant/ammonia/cyclohexane media. TEOS was employed for hydrolysis and condensation reactions under ammonia catalyst to produce monodisperse spherical silica nanoparticles. In the hydrolysis reaction, silanol groups were formed by removing ethanol and silicon-oxygen-silicon bonds were appeared by either water or ethanol extraction. The wall creating by the surfactant molecules enclosed nano-droplets and those walls behaved as cages to prevent growth of particles. Additionally, surfactant molecules involved in stabilization of nuclei and prevention of particles against their aggregation by a repulsive force. Consequently, satisfactory results anticipated in the microemulsion method by comparison to other synthesis methods with regard of final size and geometrical shape.

The water to surfactant ratio (***R***), ammonia (***A***) and TEOS concentration (***T***) are critical parameters of the silica nanoparticle synthesis on the particle size, shape, morphology, monodispersity and particle distribution. The appropriate silica nanoparticle to utilize in further steps was determined as reference (***S***) can be seen in Table 4.1.

4.2. Characterization of Silica Nanoparticles

4.2.1. Particle Size Distribution of Silica Nanoparticles

The particle size of silica nanoparticles was analyzed by using dynamic light scattering (DLS) and scanning electron microscopy (SEM) instruments which revealed to hydrodynamic diameter of the silica nanoparticles, so the results did not represent the real diameter of particles given idea about the size. The silica nanoparticles' diameters were found from 40 to 80 in the nanometer range as listed in the Table 4. 1. The effective particle size was determined as 50 nm because of monodisperse nature of the sample and suitable particle size for LbL applications.

In the beginning of experiment, the cyclohexane was recovered by rotary evaporation system to synthesize silica nanoparticles. However, we observed residual surfactant on the surface and inside of the silica nanoparticles after a while. Thus, the new procedure

was revised as precipitating silica nanoparticles in acetone instead of precipitating them with centrifuge after removal of cyclohexane by rotary distillation process.

The Figure 4. 1 was demonstrated the difference of producing silica by rotary evaporation or acetone precipitation. The surfactant was not able to remove from the system as observed in Figure 4. 1 (a), so silica nanoparticles seem agglomerated and stick each other. Also, ordered structure was observed due to the surfactant effect. Figure 4. 1(b) indicated the well-dispersed silica nanoparticles and the particles did not lap over in the solution.

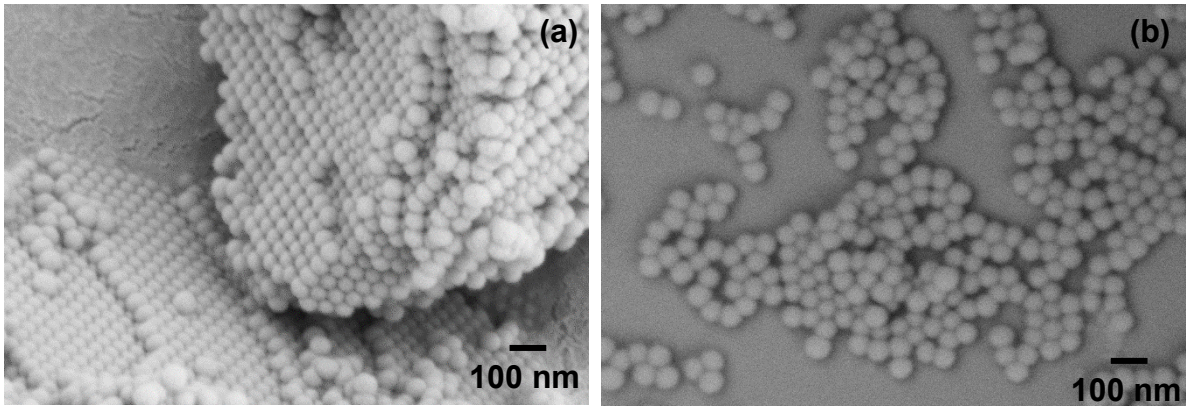

Figure 4. 1. Comparison between cyclohexane recovery types which are by rotary evaporation (a) and acetone precipitation (b)

Table 4. 1. Particle size difference regarding to water/surfactant ratio, ammonia and TEOS concentration

Sample	Water/Surfactant (*R*) Ratio	Ammonia (*A*) (mM)	TEOS (*T*) (mM)	D_{DLS} (nm)	D_{SEM} (nm)
R	1.01	0.026	0.15	58.73	61.51
***R*/2**	0.51	0.025	0.14	78.87	69.83
2*R*	2.02	0.027	0.15	62.27	67.16
2*A*	2.02	0.052	0.15	49.01	44.47
***A*/2**	0.51	0.013	0.14	62.07	63.73
2*T*	1.01	0.026	0.29	59.20	62.28
***T*/2**	1.01	0.026	0.07	52.60	53.94

4.2.1.1. Effect of water/surfactant molar ratio

While all other variables were taken constant, the water to surfactant ratio (***R***) was changed according to ***S*** sample which had 1.01 ***R*** value.

At low ***R*** value water was bound to the surfactant and so, hydroxyl ions mobility was decreased because of that the hydrolysis and nucleation reaction were not applicable for having low ***R*** microemulsion. Moreover, the number of TEOS monomers was low in each aggregate, so that intra-micellar nucleation was not favorable. On the contrary when ***R*** was increased from 0.51 to 1.01, the aggregates reduced in reverse micelle as well and the amount of unbounded water had tendency to rise in the aggregates. Thus, nuclei formation facilitated by hydrolysis of TEOS, which that state caused in smaller particle size at high ***R*** value displayed in Figure 4. 3(a). When ***R*** value become approximately 1.8, the particle size rises with increasing ***R*** which is supported by Arriagada and Ossea-Asare's work too. Therefore, the sample ***2R*** tended to have particle growth by aggregation given in Figure 4. 3(c) [21].

Uniform particle distribution was obtained in ***R/2*** (Figure 4. 3(b)) because of the high concentration of surfactant. The minimum particle size was observed in ***R***, meanwhile, the maximum particle size was found in ***R/2***.

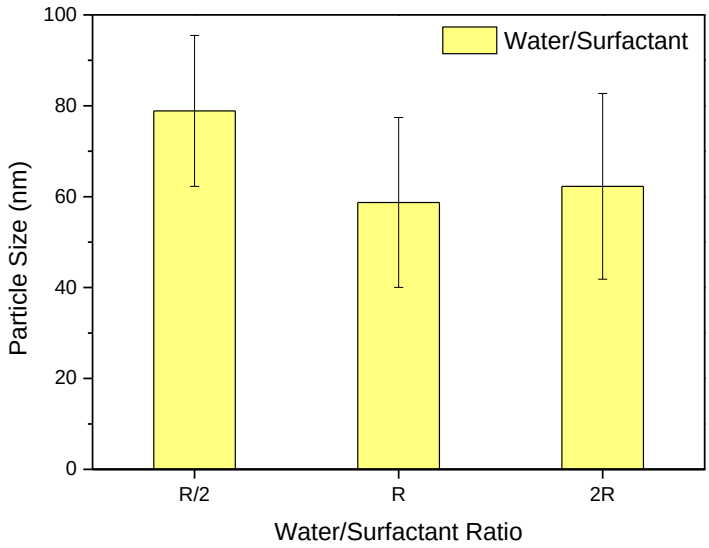

Figure 4. 2. Particle size change versus water surfactant molar ratio

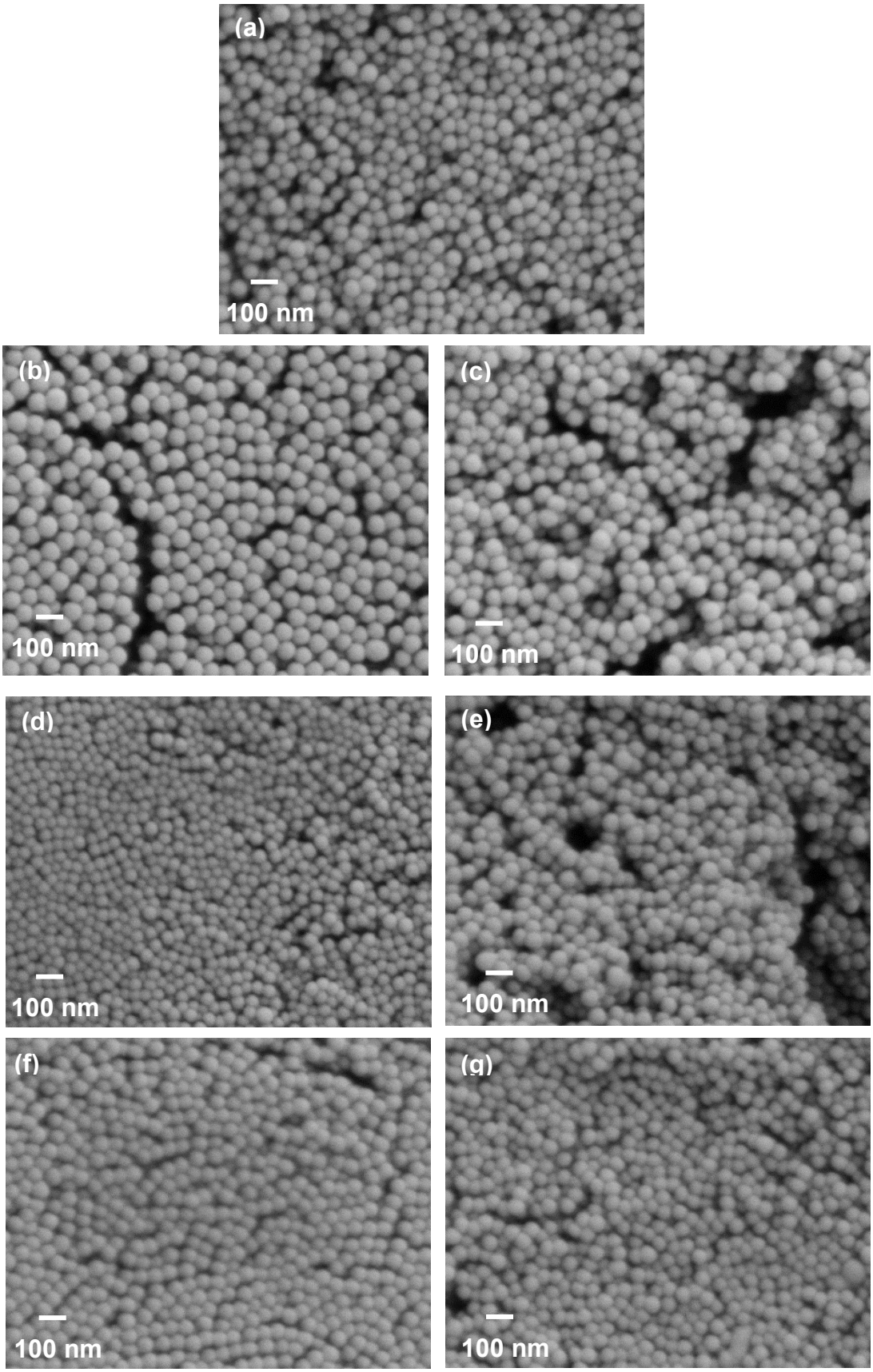

Figure 4. 3. Effect of W/S, ammonia and TEOS concentration on the particle size and morphology of silica nanoparticles (a) ***S***, (b) ***R/2***, (c) ***2R***, (d) ***2A***, (e) ***A/2***, (f) ***2T***, (g) ***T/2***.

4.2.1.2. Effect of ammonia concentration

When the water to surfactant ratio was smaller than 1.8, the particle size was decreased by increase in ammonia concentration as seen in Figure 4. 4 [21]. Hydroxyl ion concentration raised by increasing ammonia concentration thereby, hydrolysis and nucleation took place abundantly. Thus, smaller particle size could be obtained by raising nuclei rather than low ammonia concentration.

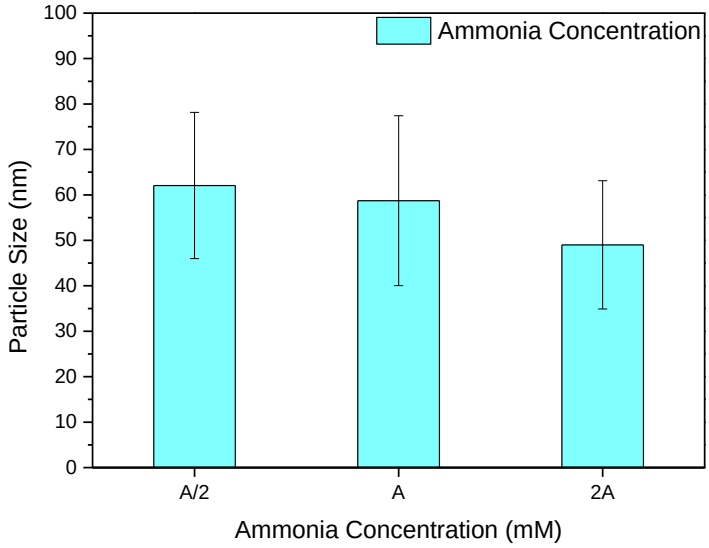

Figure 4. 4. Particle size change versus ammonia concentration

Low ammonia concentration led to nonuniform particle size and shape (Figure 4. 3(e)) when compared to high ammonia concentration (Figure 4. 3(d)). Low concentrated ammonia ingredient caused to form lesser nuclei thus, large particles were obtained in the growth process.

4.2.1.3. Effect of TEOS concentration

The particle size increased as TEOS concentration raised at the low ***R*** value according to Arriagada, F. and K. Osseo-Asare's research [21]. Differently from Stöber method, noticeable change in the particle size was not observed with respect to TEOS concentration (Figure 3.4.). Bagwe et al. [60] reported that TEOS concentration from 0.025 to 0.1 mM did not influence the particle size other variables taken constant. The studies of Arriagada and Osseo-Asare [21] was analogous to support the results as illustrated by Figure 3.4.

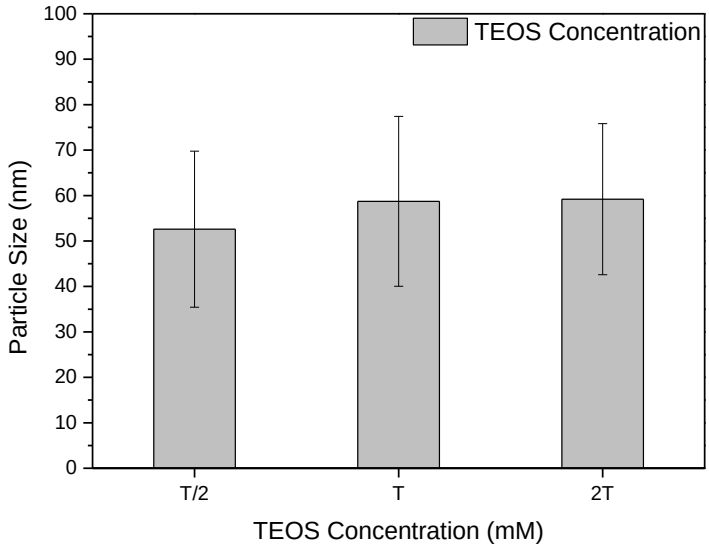

Figure 4. 5. Particle size change versus TEOS concentration

4.2.2. Zeta Potential Results of Bare Silica Nanoparticles

According to DLVO theory, the colloidal solution establishes a stable dispersion in the exact zeta potential values which must be higher than +30 mV for the positive charged nanoparticles and lower than -30 mV for the negative charged nanoparticle. If the zeta potential values are out of this range, the nanoparticles tend to precipitate because of colloidal instability.

Zeta potential graph of bare silica nanoparticles can be observed in Figure 4. 6. In this plot, the favorable nanoparticles dispersion was validated between 5.0 and 9.5 pH values. The results Figure 4. 6 were consistent with previous works by Zu, Ma and Metin et al. who investigated the stability of bare silica nanoparticles [129-131].

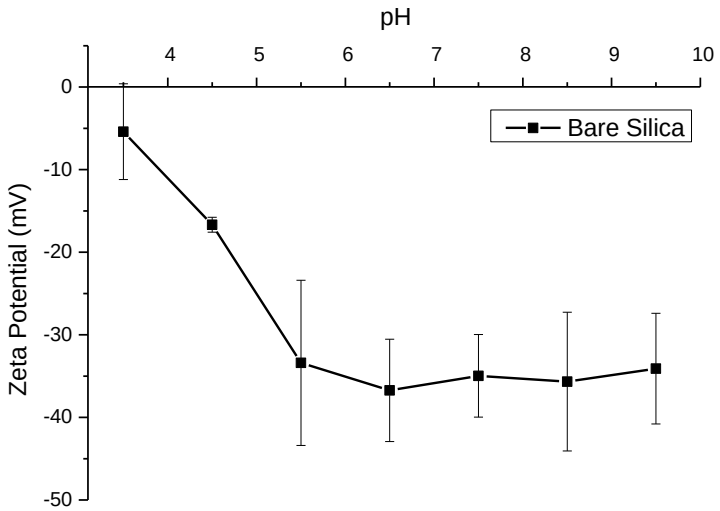

Figure 4. 6. Zeta potential versus pH graph of bare silica nanoparticles

4.2.3. FTIR Results of Bare Silica Nanoparticles

FTIR spectrum of bare silica nanoparticles is given in Figure 4. 7. Both broad peak between 3600 and 3300 cm^{-1} , and 1632 cm^{-1} were stretching peaks of Si-OH since silica adsorbed OH groups arising from water and humidity due to the hydrophilic nature of silica after drying [132]. The asymmetric and symmetric stretching of Si-O-Si band was seen at 1080 and 800 cm^{-1}, respectively and they were proof of existence of silica molecules coming from TEOS during the synthesis process. Also, the band at 955 cm^{-1} belonged to additional stretching of Si-OH [133].

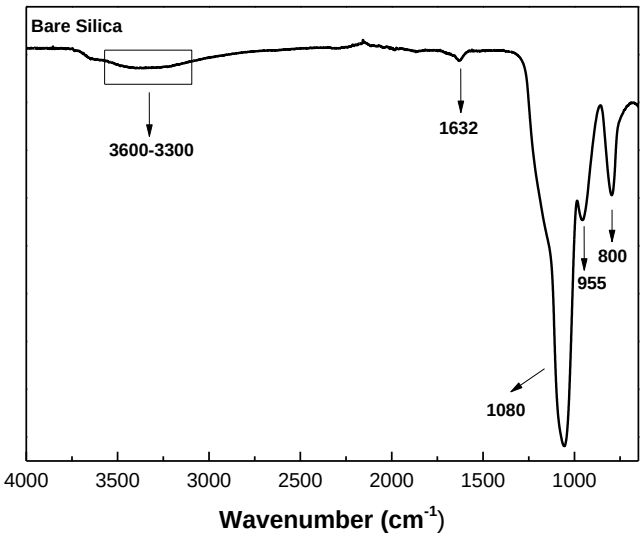

Figure 4. 7. FTIR spectrum of bare silica nanoparticles synthesized by microemulsion method

4.2.4. NMR Results of Bare Silica Nanoparticles

The silica nanoparticles were synthesized by using TEOS as the main source. The ethoxy groups were not observed in the NMR spectrum seen in Figure 4. 8 indicated the formation of silica nanoparticles. Only solutions which were D_2O, ethanol and acetone were found in the results.

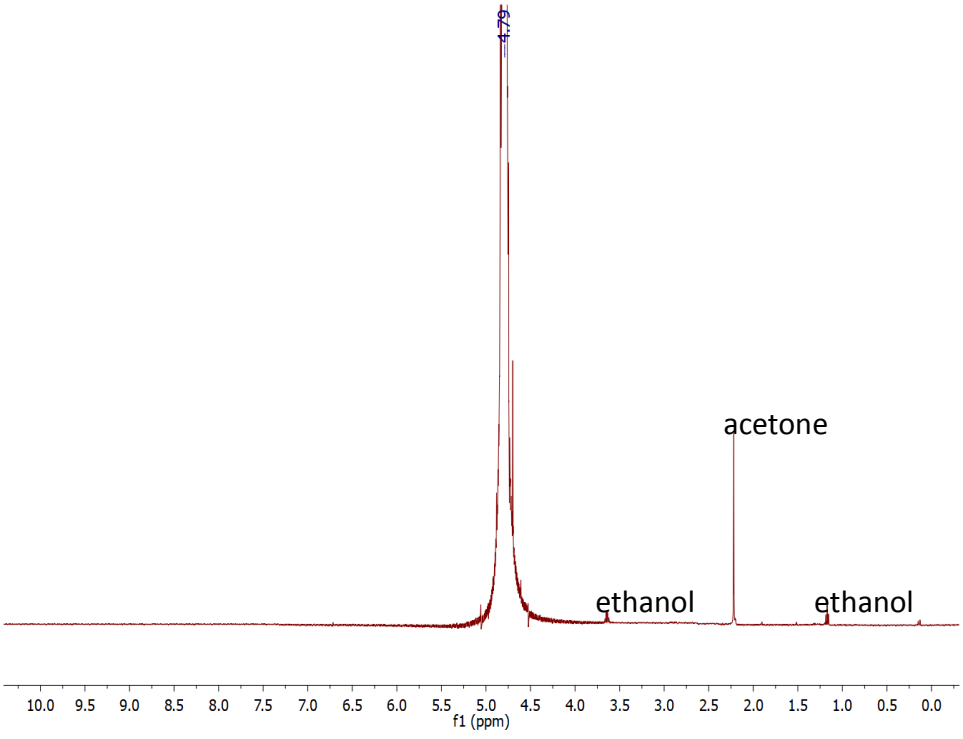

Figure 4. 8. ^{1}H-NMR spectra of bare silica nanoparticles in D_2O

4.3. DLS, FT-IR, NMR, and TGA Analysis of Functionalization of Silica Nanoparticles

The incorporation of a functional group on silica nanoparticle can alter the surface charge. It can be controlled via the type and amount of functional group, for instance, the amine functionality naturally has a positive surface charge and also the amount of amine group on the surface effects in direct proportion to the particle charge. In this study, all functional groups have silane alkoxy groups which react with the silanol groups on the silica nanoparticle. Functionalization of silica nanoparticles includes two sequent steps: hydrolysis and condensation. This is one pot reaction in ethanol media, and the ammonia solution used as a base catalyst to accelerate the rate of hydrolysis. After the overnight mixing at room temperature, the reaction solution was refluxed for 3 hours to terminate the condensation. APS, NPC, AHAPS, APDMES, PEG-Silane, and DETAS were utilized for the functionalization of silica nanoparticles. These functional silica particles were characterized with DLS, FT-IR, NMR, and TGA. The results are given in detail following titles.

4.3.1. Characterization of APS (3-aminopropyltrimethoxysilane) Functionalized Silica Nanoparticles

The zeta potential was measured in order to detect surface charge which is important to identify charge change at certain interval. FTIR and NMR were performed to evaluate the NH_2 and CH_2 bonds on the silica nanoparticle surface as shown in Figure 4. 9.

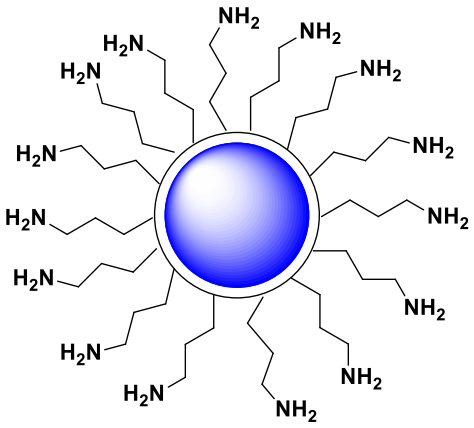

Figure 4. 9. Schematic demonstration of 3-aminopropyltrimethoxysilane (APS) functionalized silica nanoparticles

4.3.1.1. Zeta Potential Results of APS Functionalized Silica Nanoparticles

The zeta potential versus pH graph explained the colloidal stability of APS functionalized silica nanoparticles seen in Figure 4. 10. According to the graph, APS functionalized silica nanoparticles were stable between 3.5 and 8.5 that were indicated having huge pH range when compared with others. The isoelectric point was determined as 9.2 pH value. Amine groups at the end of APS molecules provide to modify surface charge of silica nanoparticles from negative to positive. APS functionalized silica nanoparticles indicated the great stability and the superior zeta potential value right after pH treatment. On the other hand, primer amine in the APS catalyzes to form siloxane bond and hydrolysis resulting to break Si−O bond and the amine groups are detached from the surface can be observed in Figure 3. 4. All of the consequences concluded in colloidal instability after a while.

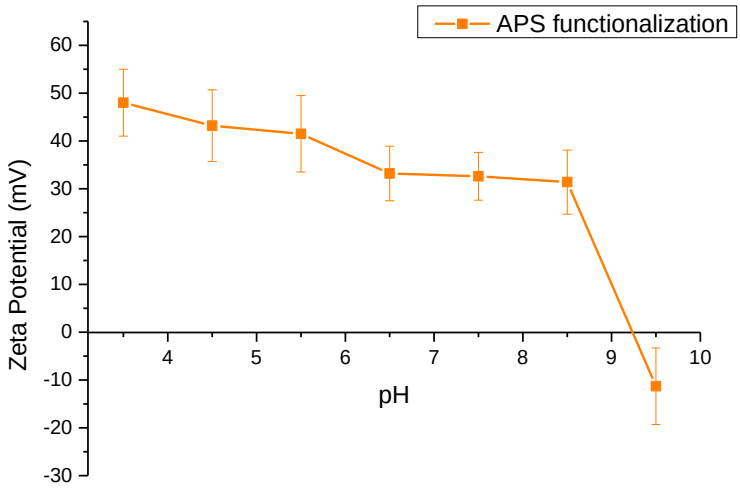

Figure 4. 10. Zeta potential versus pH graph of NPC functionalized silica nanoparticles

4.3.1.2. FTIR Results of APS Functionalized Silica Nanoparticles

FTIR spectrum of the APS functionalized silica nanoparticles is given in the Figure 4. 11. Peaks between 3400 and 3000 cm^{-1}, and 1628 cm^{-1} corresponded to N-H bending vibrations, but they were also superposed with vibrational stretching of Si-OH groups that is the reason we could not clearly identify the exact type of vibrational peaks for both groups [134]. The asymmetric stretching vibrations of $-CH_2$ was clearly verified by 2935 cm^{-1} peak arising from propyl groups. 1558 cm^{-1} absorption was assigned to the $-NH_2$

groups [135, 136]. The weak neck at 1487 cm^{-1} was attributed to existence of symmetric $-NH_3^+$ deformation mode [87].

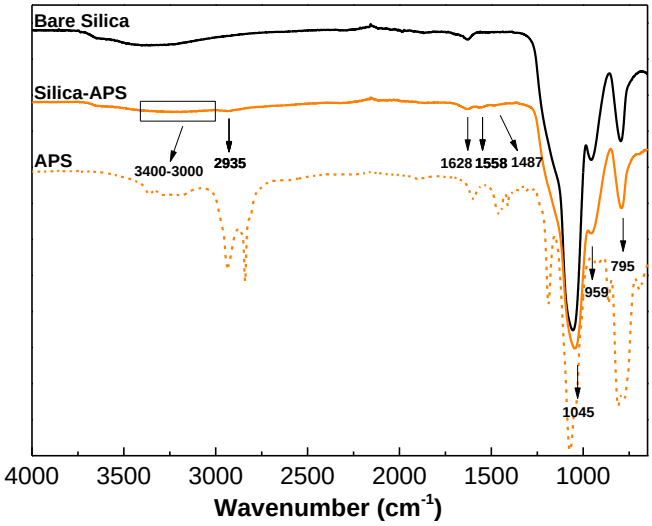

Figure 4. 11. FTIR spectrum of bare silica, bare APS and APS functionalized silica

4.3.1.3. NMR Results of APS Functionalized Silica Nanoparticles

Every NMR spectrum results showed proofs of functionalization of silica nanoparticles by not containing any regarding spectrum of alkoxy and silanol groups on the data.

The ^1H NMR spectrum displayed multiplet resonance at 2.93-2.90 ppm (H_2N-C**H**$_2$-CH_2), 1.74-1.68 ppm (CH_2-C**H**$_2$-CH_2) and 0.61-0.57 ppm (CH_2-C**H**$_2$-Si) which confirmed the attachment of APS molecules to the silica nanoparticles can be seen in Figure 4. 12.

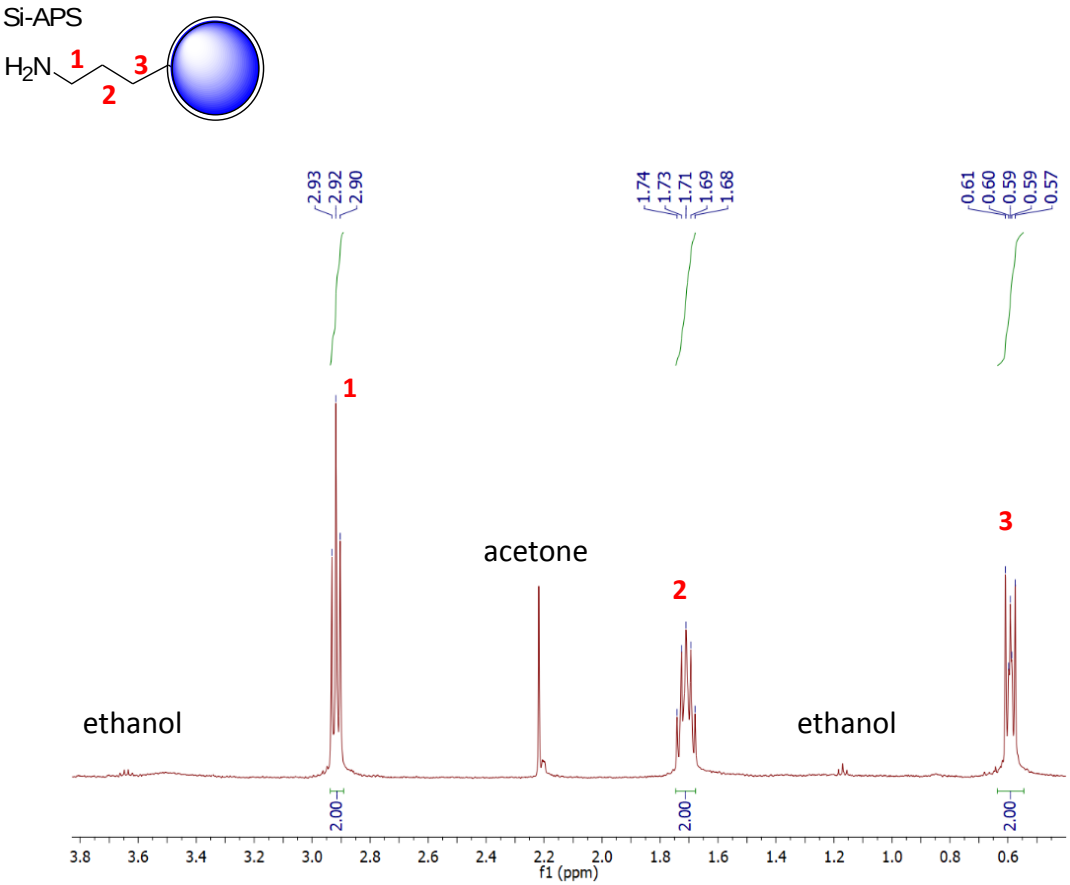

Figure 4. 12. ^{1}H-NMR spectra of APS functionalized silica nanoparticles in D_2O

4.3.2. Characterization of NPC (N-trimethoxysilylpropyl-N, N, N-trimethylammonium chloride) Functionalized Silica Nanoparticles

The zeta potential was measured in order to detect surface charge which is important to identify charge change at certain interval. FTIR and NMR were performed to evaluate the $NH4^{+}$ CH_2 and CH_3 molecules on the silica nanoparticle surface displayed in Figure 4. 13.

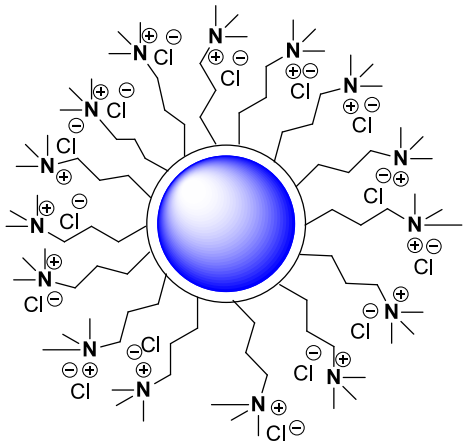

Figure 4. 13. Schematic demonstration of N-trimethoxysilylpropyl-N, N, N-trimethylammonium chloride (NPC) functionalized silica nanoparticles

4.3.2.1. Zeta Potential Results of NPC Functionalized Silica Nanoparticles

Zeta potential value of NPC functionalized silica nanoparticles with respect to pH value adjusted by using 0.05 and 0.1 M HCl, and 0.05 and 0.1 M NaOH for each zeta potential measurement given in the Figure 4. 14 ranging between 3.5 and 9.5 pH values. NPC functionalized silica nanoparticles have positive surface charge arising from NH_3^+ groups as seen in Figure 4. 13. The electrostatic repulsion was created in the acidic medium between positive surface charged particles and positive charged environment, so NPC functionalized silica nanoparticles was stable between 3.5 and 5.0 pH values. However, it also showed high colloidal stability at 9.5 pH which is in DLVO range for ideal dispersion. The isoelectric point of the sample which exhibits unstable was placed at around 6.5 pH and the colloidal solution precipitated in that pH value.

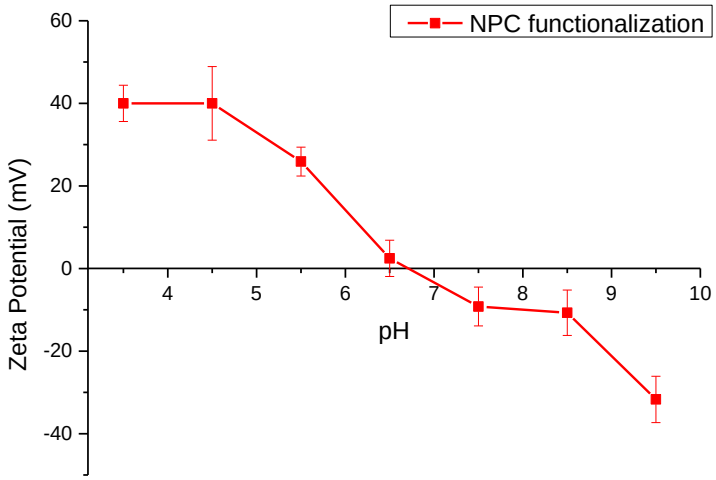

Figure 4. 14. Zeta potential versus pH graph of NPC functionalized silica nanoparticles

4.3.2.2. FTIR Results of NPC Functionalized Silica Nanoparticles

The Figure 4. 15 reveals the FTIR spectrum of NPC functionalized silica nanoparticles. The broad peak ranging from 3400 to 3000 cm^{-1} and 1632 cm^{-1} peak belonged to stretching and bending vibrations respectively that are whether N-H or Si-OH groups [134]. Similar with APS functionalized silica, these peaks could not be distinguished exactly. The absorption peak at 2982 cm^{-1} referred to asymmetric stretching of CH_3 sourced from trimethylammonium chloride sites. In a similar way, ammonium chloride groups with three methyl showed evidence of the formation of NH_3^+ groups at 1489 cm^{-1} [94].

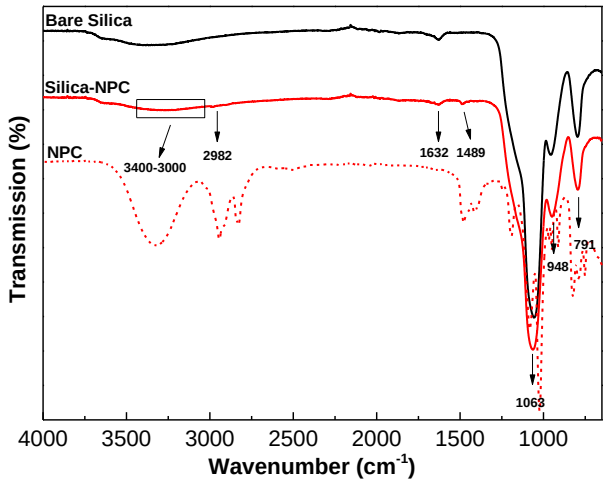

Figure 4. 15. FTIR spectrum of bare silica, bare NPC and NPC functionalized silica

4.3.2.3. NMR Results of NPC Functionalized Silica Nanoparticles

The ^{1}H NMR spectrum displayed multiplet resonance at 3.33-3.30 ppm (N^{+}-C**H**$_2$) 3.10 ppm (C**H**$_3$-N^{+}) 1.91-1.85 ppm (CH_2-C**H**$_2$-CH_2) 0.64 ppm (C**H**$_2$-Si) which confirmed the attachment of NPC molecules to the silica nanoparticles can be seen in Figure 4. 16.

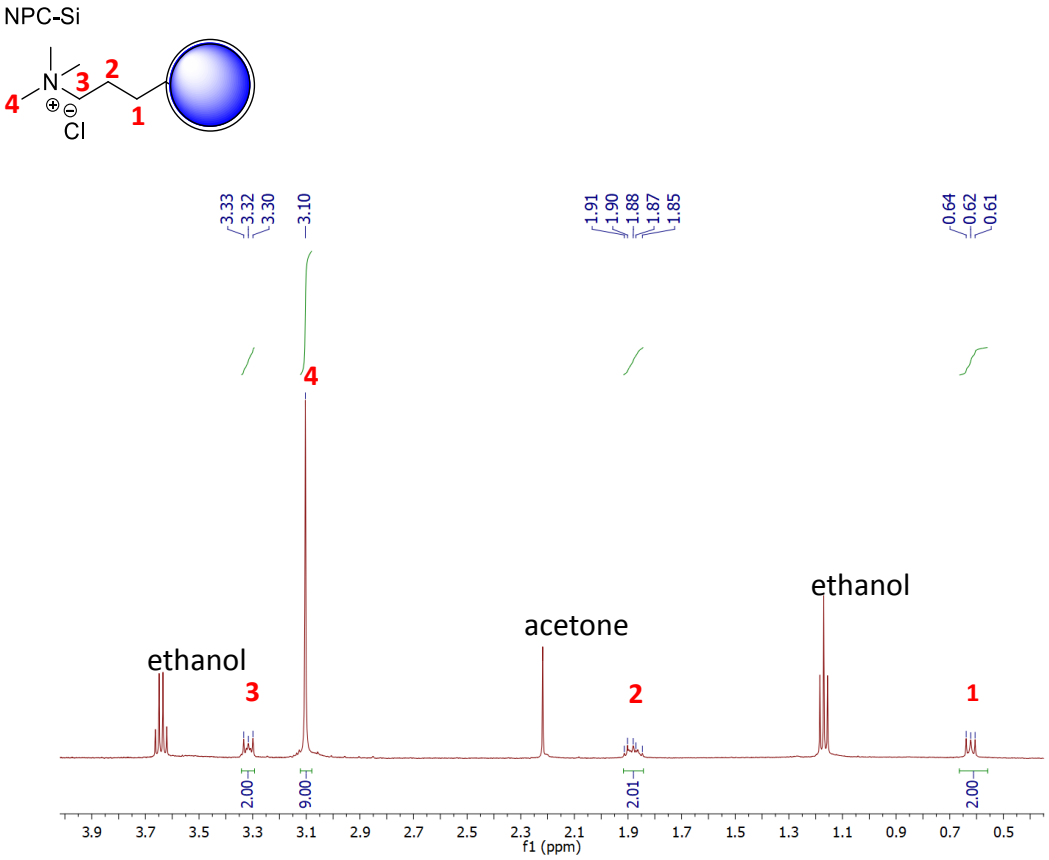

Figure 4. 16. ^{1}H-NMR spectra of NPC functionalized silica nanoparticles in D_2O

4.3.3. Characterization of APDMES (3-Aminopropyl(dimethyl)ethoxysilane) Functionalized Silica Nanoparticles

The zeta potential was measured in order to detect surface charge which is important to identify charge change at certain interval. FTIR and NMR were performed to evaluate the NH_2 and CH_2 bonds on the silica nanoparticle surface as illustrated in Figure 4. 17.

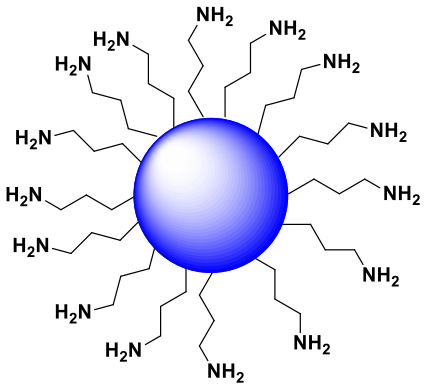

Figure 4. 17. Schematic demonstration of 3-Aminopropyl(dimethyl)ethoxysilane) (APDMES) functionalized silica nanoparticles

4.3.3.1. Zeta Potential Results of APDMES Functionalized Silica Nanoparticles

Figure 4. 18 represents the zeta potential graph of APDMES functionalized silica nanoparticles in the solution with a pH range from 3.5 to 9.5. NH_2 groups were caused to create positive surface charge as similar to the AHAPS functionalized silica nanoparticles as indicated in Figure 4. 17. Electrostatic repulsion that provides to obtain colloidally stable nanoparticles dispersion in the solution was confirmed arising from acidic media. The sample presented good stability from 3.5 to 4.5 pH and also from 8.5 to 9.5 which elicited an alteration of surface charge from positive to negative by adding the base to the system. Apart from all these functional groups, APDMES supported to generate vertically growth on silica nanosphere since dimethyl silyl groups were not allowed binding, so the silica was able to bound to only ethoxy sites by removal of ethanol. As a result of that, silica cannot be functionalized all of its entire surface and positive surface charge could be lost after pH treatment even at the low pH values.

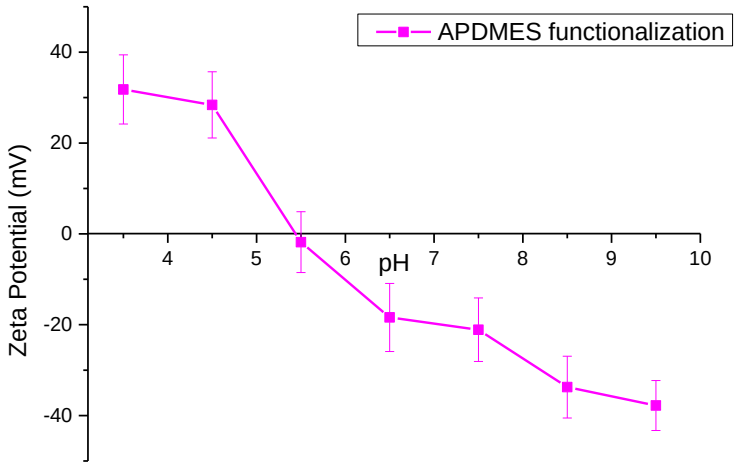

Figure 4. 18. Zeta potential versus pH graph of APDMES functionalized silica nanoparticles

4.3.3.2. FTIR Results of APDMES Functionalized Silica Nanoparticles

The FTIR spectrum of APDMES functionalized silica is illustrated in Figure 4. 19. The wide peak 3400 to 3000 cm^{-1}; and 1627 cm^{-1} peak were originated from stretching N-H or Si-OH and bending N-H or Si-OH vibrational bands respectively. Nearly identical with NPC, 2983 cm^{-1} absorption peak depicted the asymmetric stretching of CH_3 stemming from dimethyl groups. The bending of C-H groups displayed at 1450 cm^{-1} as described in AHAPS functionalized silica nanoparticles FTIR profile.

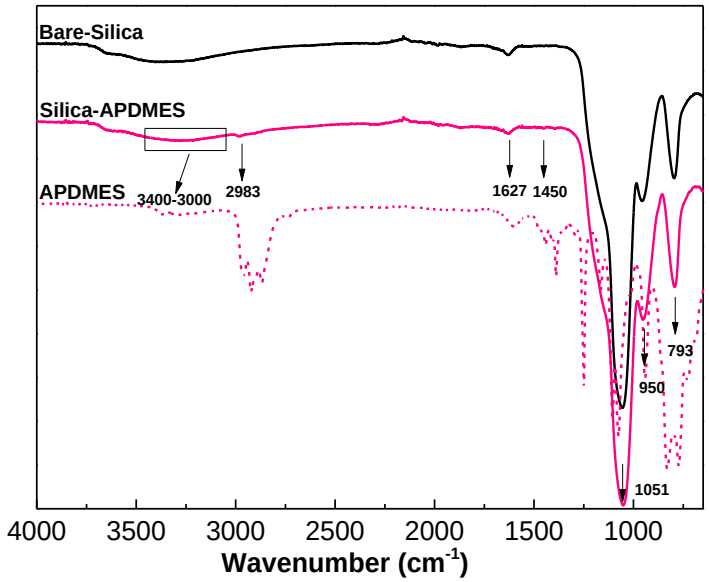

Figure 4. 19. FTIR spectrum of bare silica, bare APDMES and APSMES functionalized silica

4.3.3.3. NMR Results of APDMES Functionalized Silica Nanoparticles

The ^{1}H NMR spectrum displayed multiplet resonance at 2.94 ppm (H_2N-C**H**$_2$-CH_2) 1.68 ppm (CH_2-C**H**$_2$-CH_2), 0.65 ppm (C**H**$_2$-Si) and 0.15-1.14 ppm (Si-C**H**$_3$) which confirmed the attachment of APDMES molecules to the silica nanoparticles can be seen in Figure 4. 20.

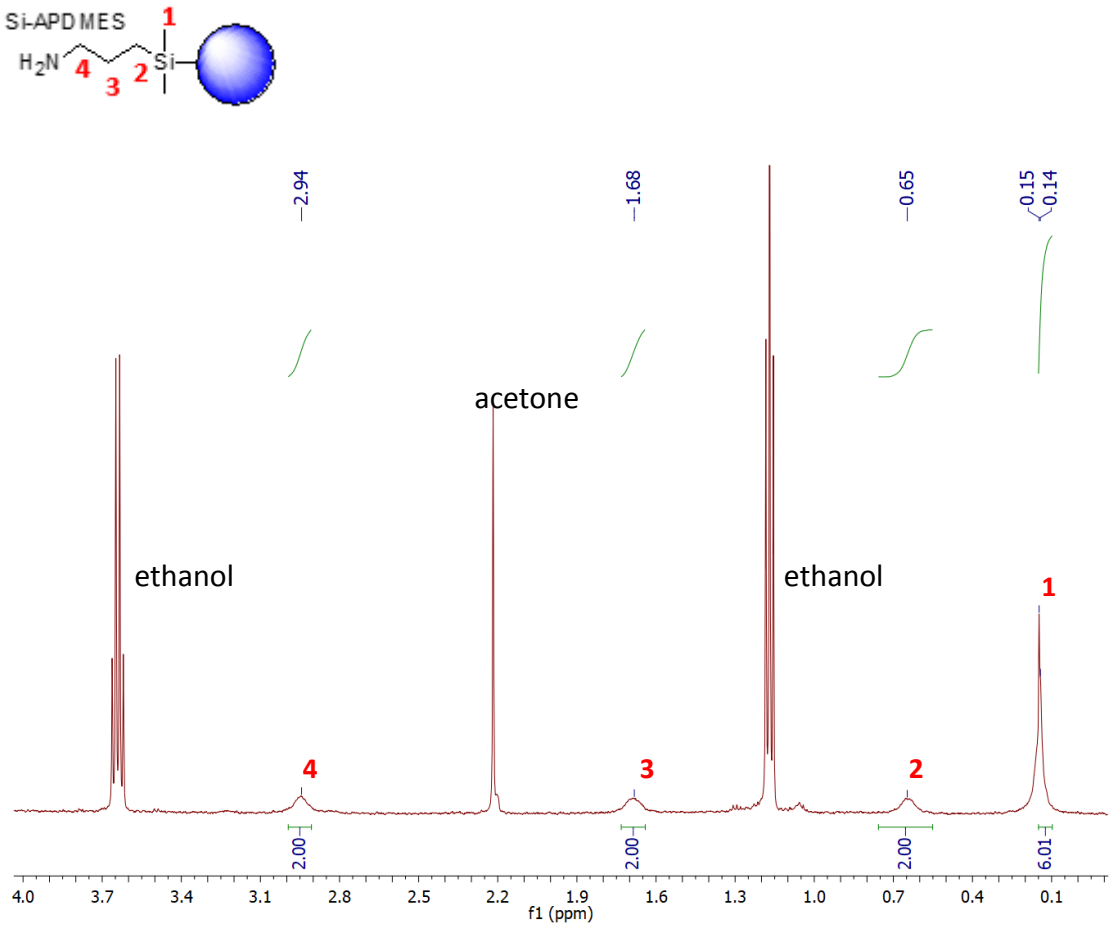

Figure 4. 20. ^{1}H-NMR spectra of APDMES functionalized silica nanoparticles in D_2O

4.3.4. Characterization of AHAPS (N-(6-aminohexyl) aminopropyltrimethoxysilane) Functionalized Silica Nanoparticles

The zeta potential was measured in order to detect surface charge which is important to identify charge change at certain interval. FTIR and NMR were performed to evaluate the NH, NH_2 and CH_2 molecules on the silica nanoparticle surface as indicated in Figure 4. 21.

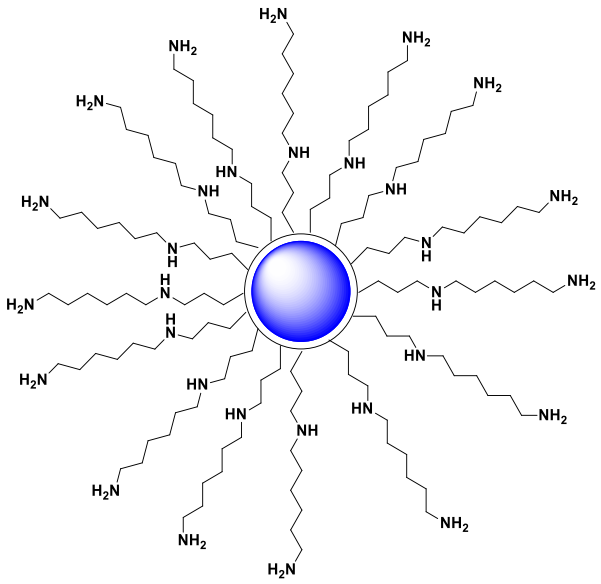

Figure 4. 21. Schematic demonstration of N-(6- aminohexyl) aminopropyltrimethoxysilane (AHAPS) functionalized silica nanoparticles

4.3.4.1. Zeta Potential Results of AHAPS Functionalized Silica Nanoparticles

Zeta potential graph of AHAPS functionalized silica nanoparticles is illustrated in Figure 4. 22 according to pH values. AHAPS functional groups were gained to the silica nanoparticles positive surface charge by amine groups given in Figure 4. 21. AHAPS functionalized silica nanoparticles displayed excellent stability from 3.5 to 6.0 pH values by being secondary amine groups. Differently from other functional groups, they were stable because of steric hinderance during hydrolysis catalyzed intramolecularly analogous to Zhu et al. study [82]. The colloidal stability of nanoparticles was the lowest value at the isoelectric point which was pH 9.0 value.

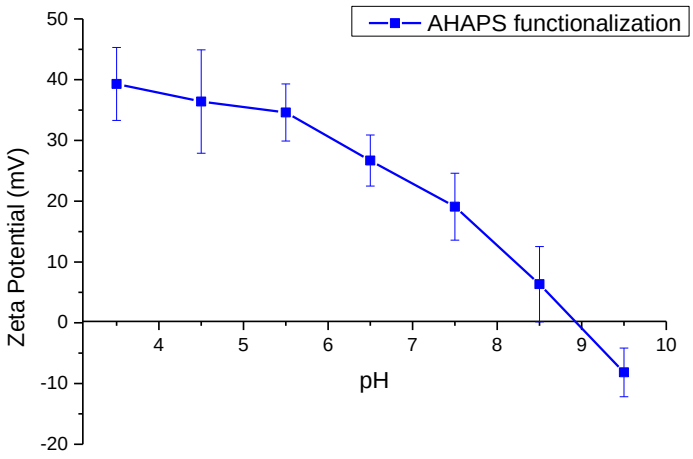

Figure 4. 22. Zeta potential versus pH graph of AHAPS functionalized silica nanoparticles

4.3.4.2. FTIR Results of AHAPS Functionalized Silica Nanoparticles

The FTIR spectrum of AHAPS functional silica nanoparticles can be found in Figure 4. 23. In a similar way, peaks which are 3400 and 3000 cm^{-1}; and 1622 cm^{-1} were correlated to N-H stretching or Si-OH stretching; or N-H bending or Si-OH bending vibrational bonds. The absorption peak of 2931 cm^{-1} confirmed the existence of asymmetric stretching of -CH_2 coming from alkyl chains same as APS functionalized silica nanoparticles. The bending of C-H groups displayed at 1454 cm^{-1} which can validate the bonded functional groups [137].

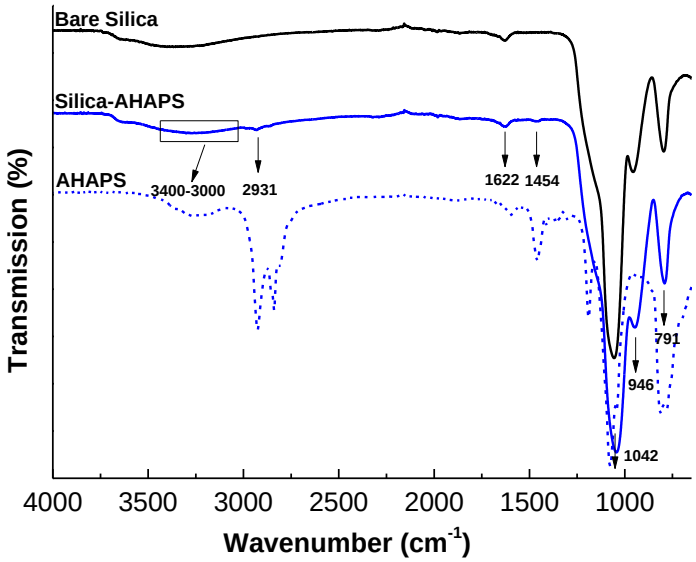

Figure 4. 23. FTIR spectrum of bare silica, bare AHAPS and AHAPS functionalized silica

4.3.4.3. NMR Results of AHAPS Functionalized Silica Nanoparticles

The ^1H NMR spectrum displayed multiplet resonance at 2.99-2.90 ppm (H_2N-C**H_2**), 1.77-1.73 ppm (CH_2-N**H**-CH_2), 1.65-1.62 ppm (NH_2-CH_2-C**H_2** and C**H_2**-CH_2-Si), 1.41-1.38 ppm (CH_2-C**H_2**-CH_2), 0.62-0.59 ppm (C**H_2**-Si) which confirmed the attachment of AHAPS molecules to the silica nanoparticles can be seen Figure 4. 21

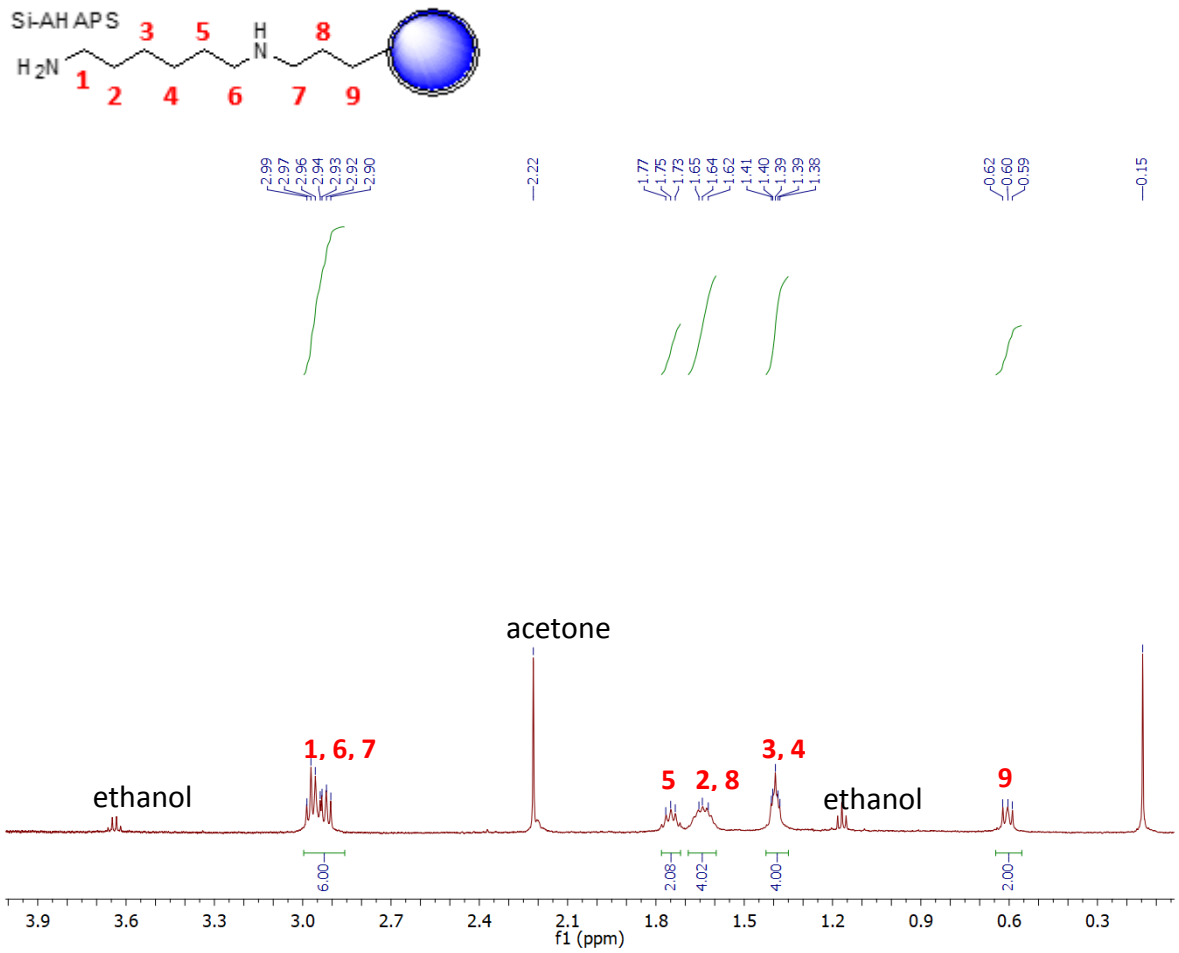

Figure 4. 24. ^{1}H-NMR spectra of AHAPS functionalized silica nanoparticles in D_2O

4.3.5. Characterization of PEG-Silane (2- [methoxy(polyethyleneoxy) propyl] trimethoxysilane with 6-9 polyethylene oxide units) Functionalized Silica Nanoparticles

The zeta potential was measured in order to detect surface charge which is important to identify charge change at certain interval. FTIR and NMR were performed to evaluate the bonding of PEG-Silane molecules on the silica nanoparticle surface can be observed in Figure 4. 25.

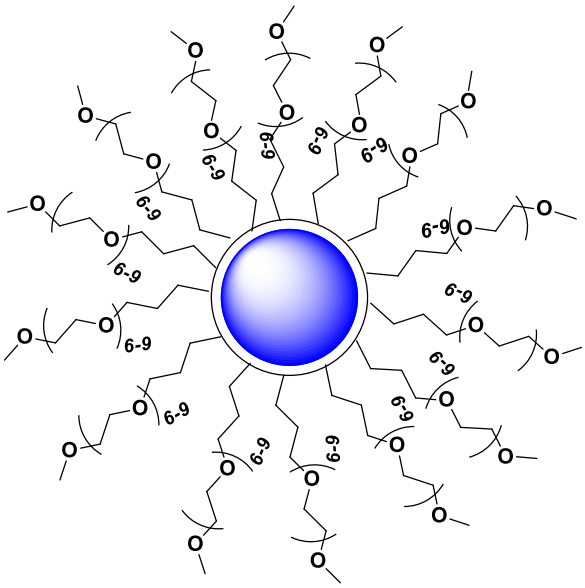

Figure 4. 25. Schematic demonstration of (2- [methoxy(polyethyleneoxy) propyl] trimethoxysilane with 6-9 polyethylene oxide units) (PEG-Silane) functionalized silica nanoparticles

4.3.5.1. Zeta Potential Results of PEG-Silane Functionalized Silica Nanoparticles

Data in Figure 4. 26 indicate the zeta potential versus pH graph of PEG-Silane functionalized silica nanoparticles. Comparable to other functional silica nanoparticles, they possessed negative surface charge by reason of having non-charged functional group that produced steric hinderance. Thus, better dispersity was expected in the stable colloidal solution according to bare silica nanoparticles. The most stable was 9.5 pH value.

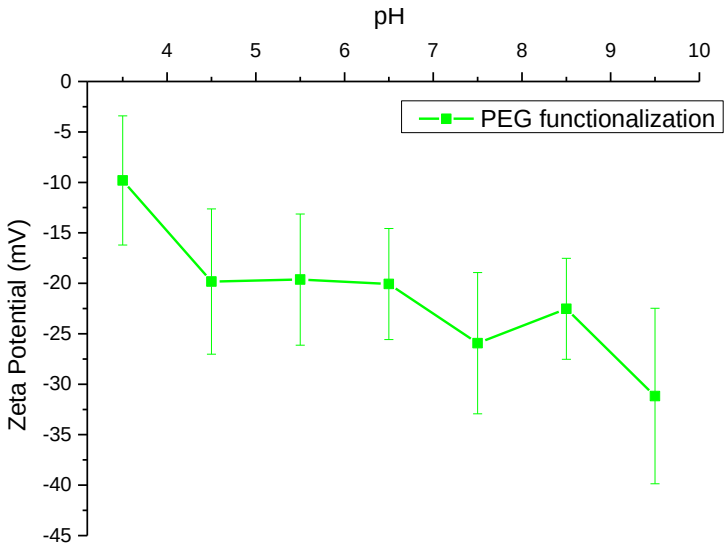

Figure 4. 26. Zeta potential versus pH graph of PEG-Silane functionalized silica nanoparticles

4.3.5.2. FTIR Results of PEG-Silane Functionalized Silica Nanoparticles

The FTIR spectrum of PEG-Silane functionalized silica is illustrated in Figure 4. 27. Apart from others, the wide peak 3400 to 3000 cm^{-1} and 1630 were resulted from the stretching and bending of Si-OH vibrational bands respectively due to the absence of amine groups. The shoulders at 2917 and 2860 cm^{-1} ascribed asymmetric and symmetric stretching of -CH_2 respectively. The bending of C-H groups illustrated at 1461 cm^{-1} like AHAPS and APDMES functionalized silica nanoparticles

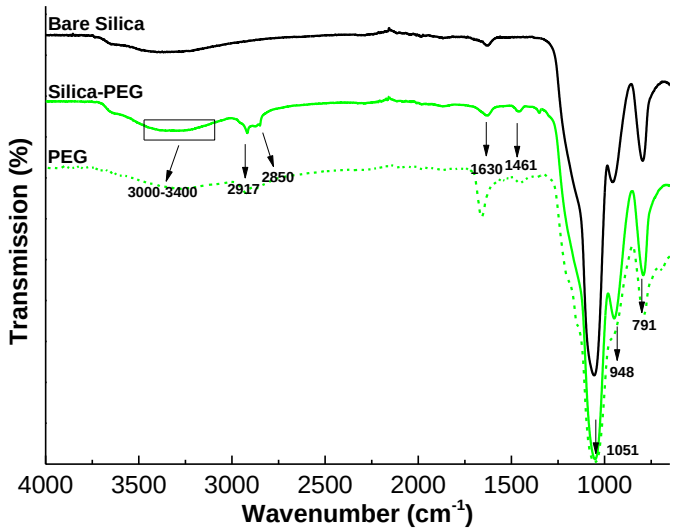

Figure 4. 27. FTIR spectrum of bare silica, bare PEG-Silane and PEG-Silane functionalized silica

4.3.5.3. NMR Results of PEG-Silane Functionalized Silica Nanoparticles

The ^1H NMR spectrum displayed multiplet resonance at 3.7 ppm (O-C**H**$_2$-CH_2), 3.53 ppm (O-C**H**$_2$-CH_2-CH_2-CH_2-Si), 3.38 ppm (C**H**$_3$-O), 1.7 ppm (CH_2-C**H**$_2$-CH_2), 1.27 ppm (C**H**$_2$-Si) which confirmed the attachment of PEG-Silane molecules to the silica nanoparticles can be seen Figure 4. 28.

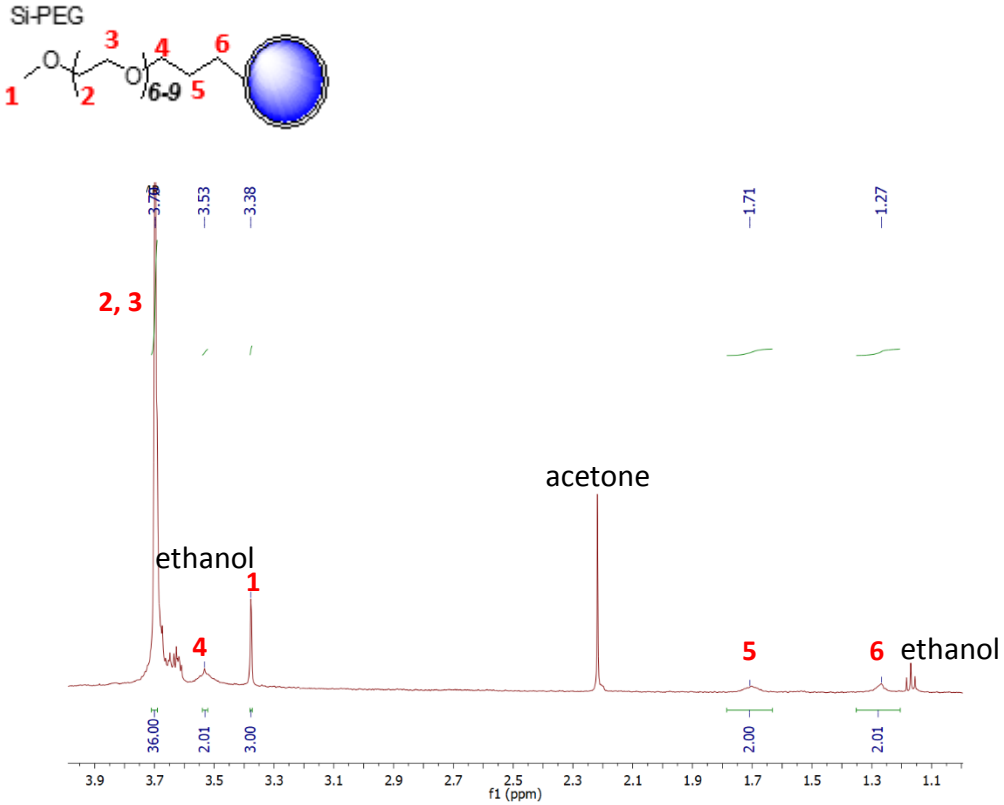

Figure 4. 28. ^{1}H-NMR spectra of PEG-Silane functionalized silica nanoparticles in D_2O

4.3.6. Characterization of DETAS (N-[3-(trimethoxysilyl)propyldiethylenetriamine) Functionalized Silica Nanoparticles

The zeta potential was measured in order to detect surface charge which is important to identify charge change at certain interval. FTIR and NMR were performed to evaluate the NH_2 and CH_2 molecules on the silica nanoparticle surface can be observed in Figure 4. 29.

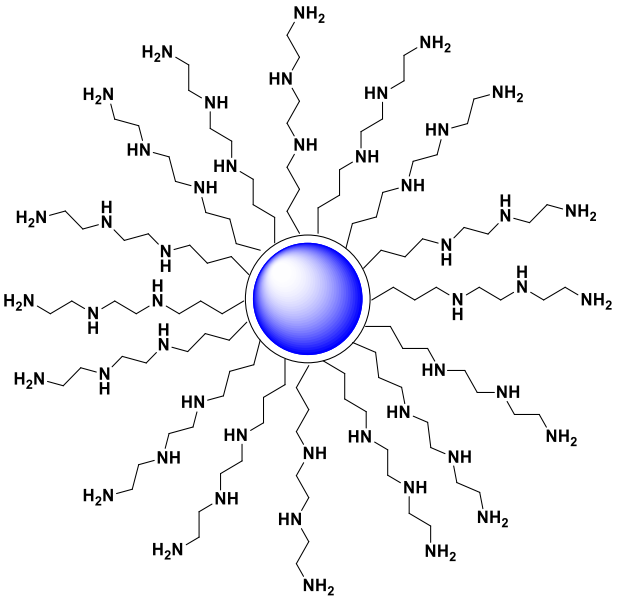

Figure 4. 29. Schematic demonstration of N-[3-(trimethoxysilyl)propyldiethylenetriamine) (DETAS) functionalized silica nanoparticles

4.3.6.1. Zeta Potential Results of DETAS Functionalized Silica Nanoparticles

Zeta potential graph of DETAS functionalized silica nanoparticles is displayed in Figure 4. 30 according to pH values. DETAS molecules were provided positive surface charge by amine groups given in Figure 4. 29. The positive surface charge was observed ranging from 3.5 to 9.0 pH values arising from secondary amine groups. The colloidal stability of nanoparticles was the lowest value at the isoelectric point which was pH 9.0 value.

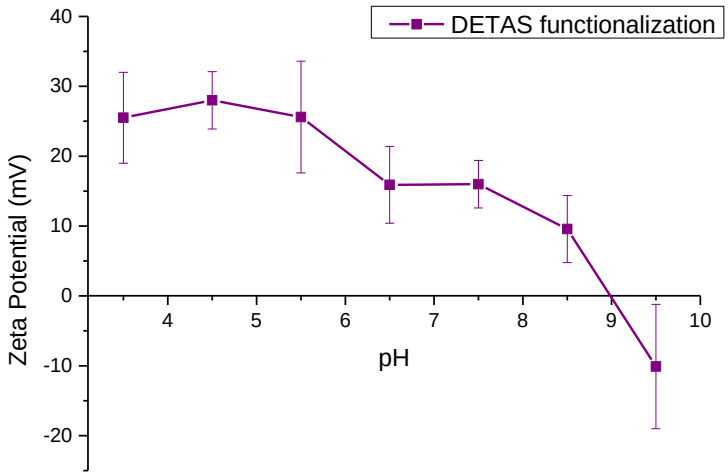

Figure 4. 30. Zeta potential versus pH graph of DETAS functionalized silica nanoparticles

4.3.6.2. FTIR Results of DETAS Functionalized Silica Nanoparticles

Figure 4. 31 demonstrates the FTIR spectrum of DETAS functionalized silica nanoparticles. The stretching N-H or Si-OH and bending N-H or Si-OH vibrational bands were determined by the peak of 3400 to 3000 cm^{-1}; and 1660 cm^{-1} respectively. The asymmetric and symmetric stretching of -CH_2 were identified by the shoulders at 2931 and 2866 cm^{-1} respectively [87]. The bending of C-H groups was repeated at 1455 cm^{-1} likewise all other functional groups.

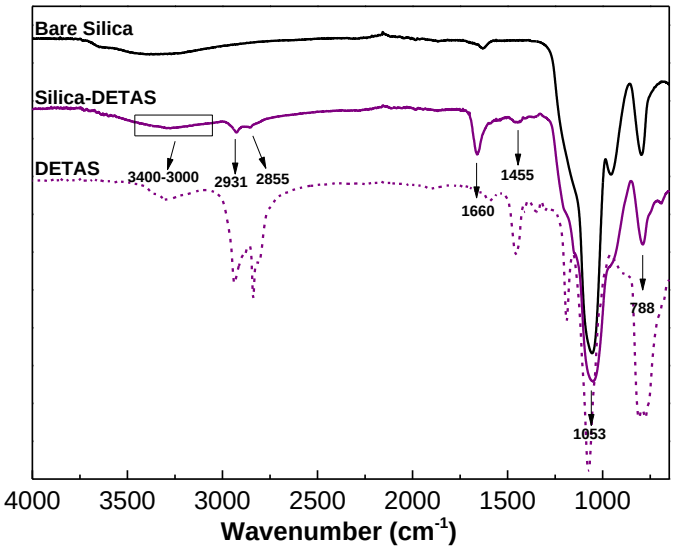

Figure 4. 31. FTIR spectrum of bare silica, bare DETAS and DETAS functionalized silica

4.3.6.3. NMR Results of DETAS Functionalized Silica Nanoparticles

The ^1H NMR spectrum displayed multiplet resonance at 3.56-3.37 ppm (H_2N-CH_2-CH_2) (H_2N-CH_2-CH_2-NH), 2.97-2.55 ppm (NH-CH_2-CH_2), 1.7 ppm (CH_2-CH_2-CH_2) and 0.64 ppm CH_2-Si which confirmed the attachment of DETAS molecules to the silica nanoparticles can be seen Figure 4. 32.

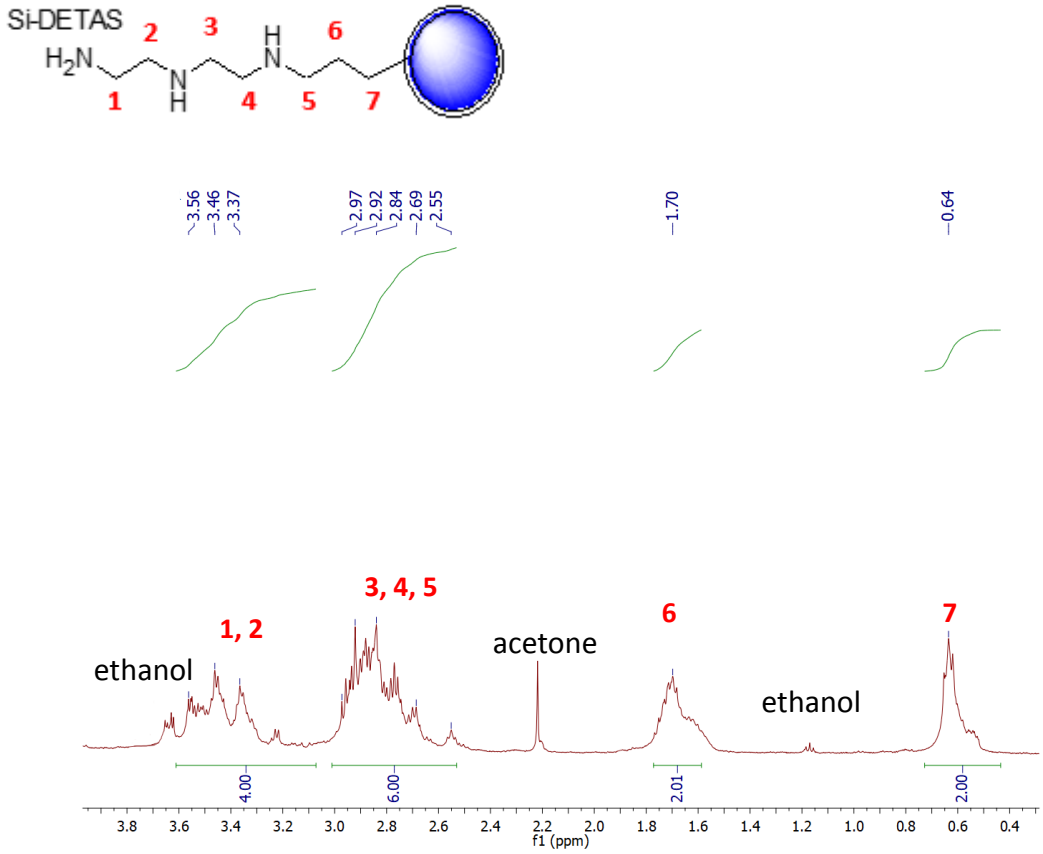

Figure 4. 32. ^{1}H-NMR spectra of DETAS functionalized silica nanoparticles in D_2O

4.3.7. Overview of All Functionalized Silica Nanoparticles and Bare Silica in terms of FTIR Analysis

Different from others, APDMES and NPC functionalized silica nanoparticles had CH_3 groups. Si-OH or N-H peaks were shifted according to bare silica spectrum in Figure 4. 33 and that proved the binding of functional groups.

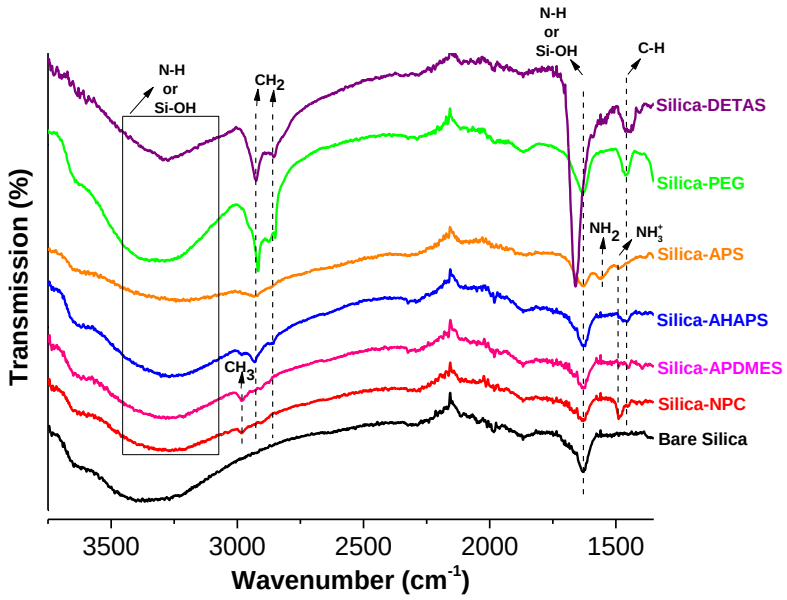

Figure 4. 33. Schematic illustration of FTIR spectrum of functional groups ranging from 3750 to 1350 cm^{-1}

The same effect was watched in Figure 4. 34 that Si-O-Si, Si-OH and Si-O-Si peaks were shifted. Silicon dioxide has oxygen and silicon atoms containing lattice which silicon atoms have oxygen atoms around with stochiometric ratio 1:2. Naturally, it has specific vibrational resonance frequency. However, by adding functional groups to oxygen or silicon site bring a new vibrational frequency. Thus, the FTIR spectrum shift according to new doping functional group atoms and their corresponding frequency. All in all, silicon dioxide natural frequency was distorted aforementioned new frequency that is caused of spectrum shift.

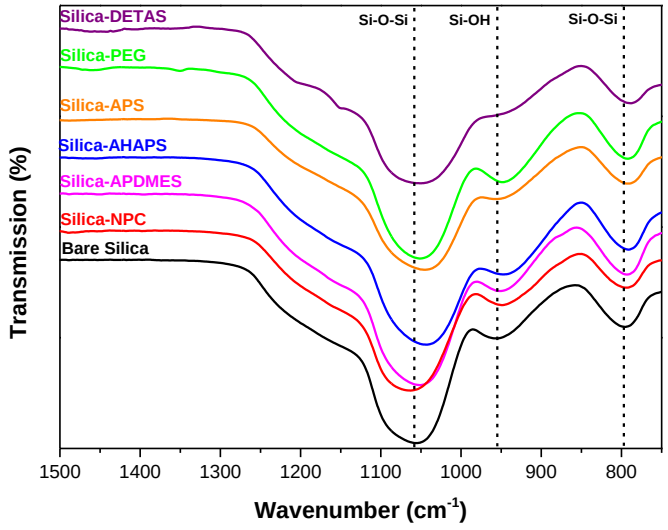

Figure 4. 34. Schematic illustration of FTIR spectrum of functional groups ranging from 1500 to 750 cm^{-1}

4.4. Layer by Layer Assembly of Functionalized Silica Nanoparticles

4.4.1. Characterization of LbL Thin Films Coated with Functionalized Silica Nanoparticles by SEM

The functionalized silica nanoparticles were deposited onto the silicon wafer substrates via LbL self-assembly approach. Firstly, adhesion layers were applied as 5 bL on the substrate in order to increase cohesion. pH of using cationic and anionic polyelectrolytes which were PAH (+) and SPS (-), respectively was set the pH value of 4.00. Later, functionalized silica nanoparticles were coated on the surface with the desired number of bilayers. Since plasma treated silicon wafer exhibit negative surface charge, substrates firstly were immersed into positively charged polyelectrolyte solution.

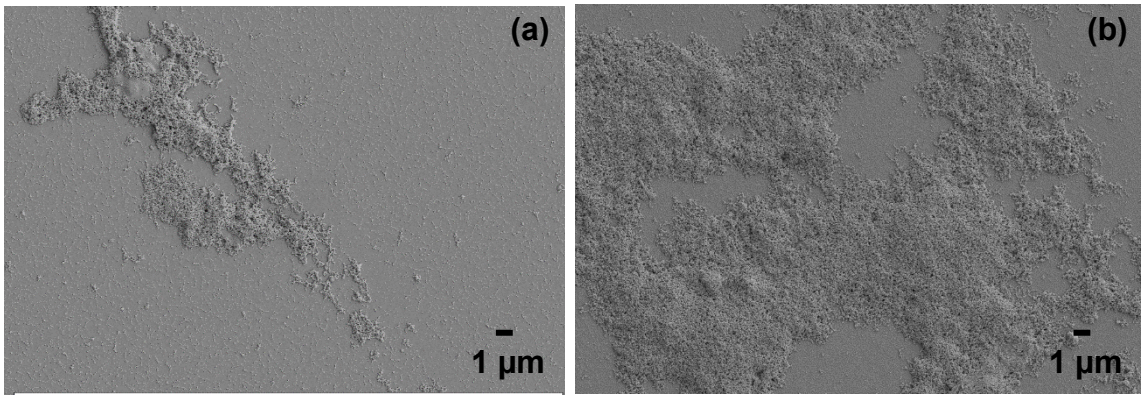

Figure 4. 35. SEM micrographs of APS factionalized silica nanoparticles thin films coated by LbL in 5 bL (a) and 10 bL (b) on silicon wafer.

Figure 4. 35 illustrates SEM images of APS functionalized silica nanoparticles thin films coated by LbL on silicon wafer. It is clearly seen from the images that APS functionalization is triggered agglomeration of silica nanoparticles and prevented to form a uniform thin film layer. Thin films were grown on silicon wafer which was dipped in a solution of pH 4. Regarding SEM results of APS functionalized silica nanoparticles LbL films, it can be inferred that colloidal suspension of that nanoparticles was not stable during the coating process and silica nanoparticles interacted and attracted each other more than silicon wafer surface so that island like thin film growth was yielded. Besides, when the number of bilayers was doubled from 5 bL to the 10 bL, there was no drastic change in the surface coverage of thin films as shown in the Figure 4. 35(b). Even it seems an increase in surface coverage, silica particles were still grown on themselves. APS effect can be explained by charge attraction of silica particles due to APS

functionalization rather than attraction by wafer surface as supported by Graf et al. and Asenath-Smith et al. reports [63, 88].

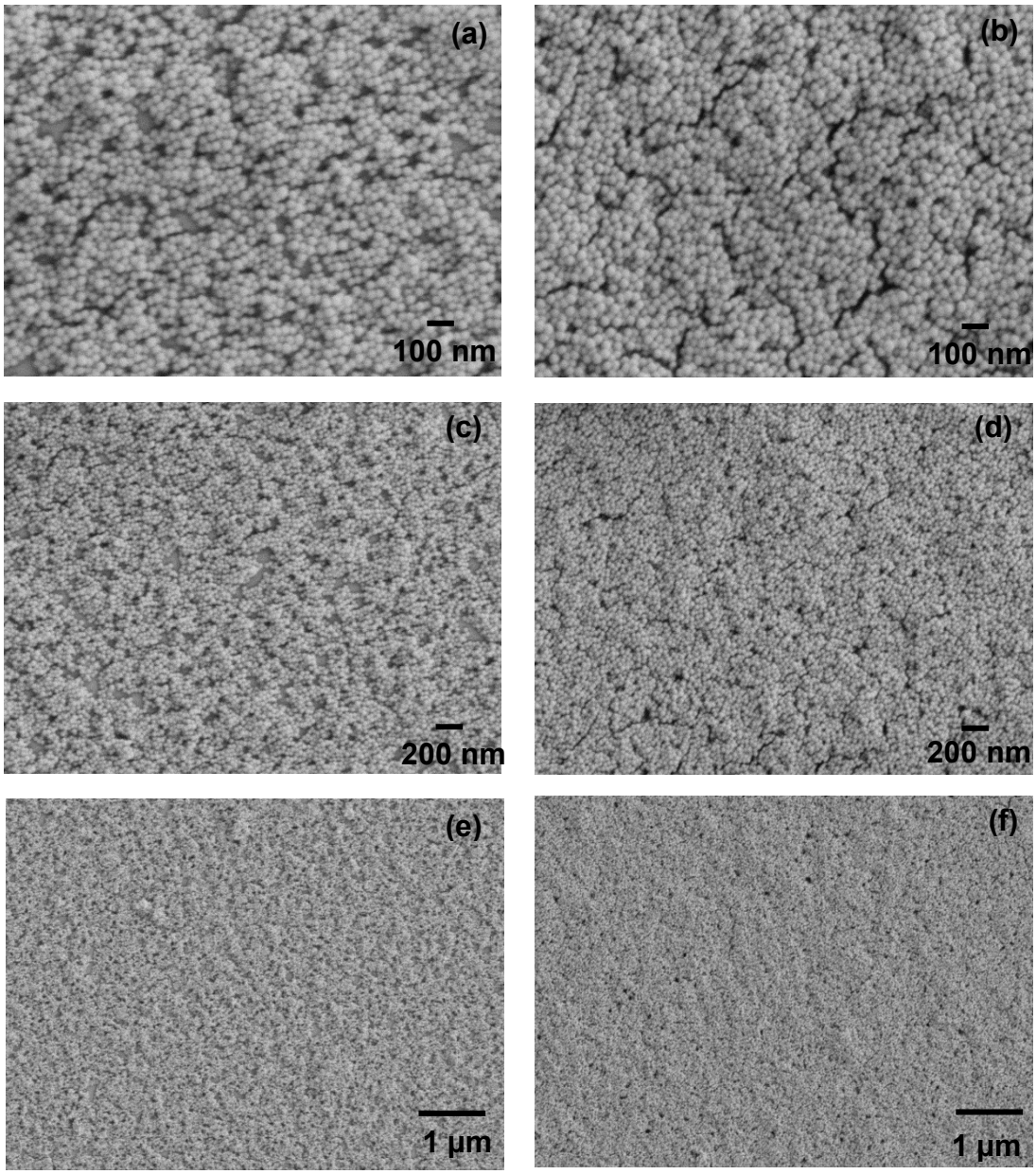

Figure 4. 36. SEM micrographs of NPC factionalized silica nanoparticles thin films coated by LbL in 5 bL (a, c, e) and 10 bL (b, d, f) on silicon wafer at 100 nm, 200 nm and 1 um magnification scale.

SEM analysis of NPC functionalized silica nanoparticles thin films coated by LbL with different bL numbers is demonstrated in Figure 4. 36 with several magnifications. SEM analysis revealed that coatings were grown homogeneously and well dispersed with same morphology on every magnification. Compared to 5 bL, coating with 10 bL number observed as thicker layer than coatings with 5 bL number and it is formed on silicon wafer stiffer as anticipated. In addition, coating with 10 bL number seems to have porous formation by spacing between silica nanoparticles adding up on each other's.

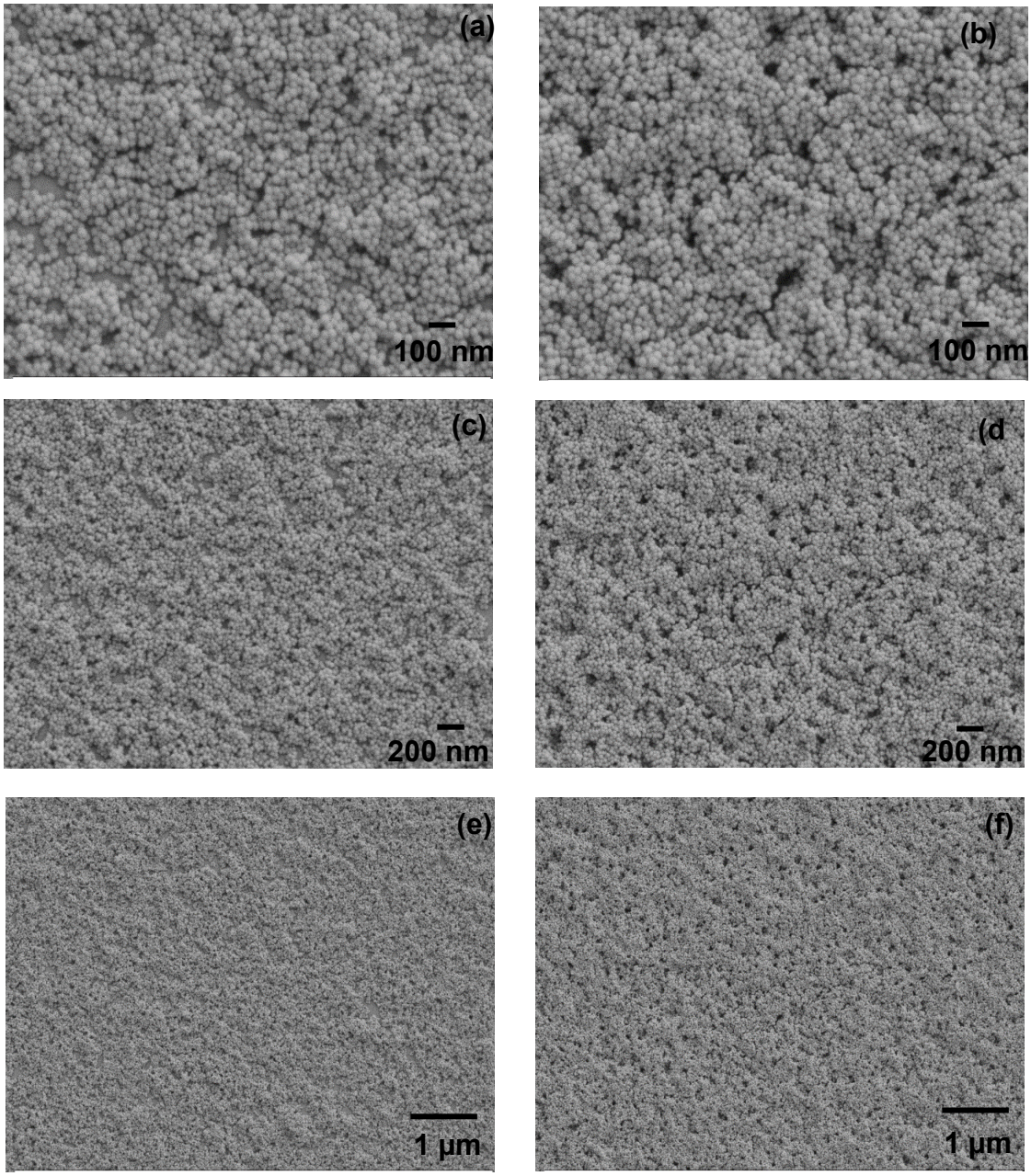

Figure 4. 37. SEM micrographs of APDMES factionalized silica nanoparticles thin films coated by LbL in 5 bL (a, c, e) and 10 bL (b, d, f) on silicon wafer at 100nm, 200nm and 1 um magnification scale.

Morphological analysis of APDMES factionalized silica nanoparticles thin films coated by LbL with 5 and 10 bL number is illustrated in Figure 4. 37 with 100nm, 200nm and 1 um magnification scale. As shown in Figure 4. 37 homogenous morphology is dominated every part of coatings with both 5 and 10 bL numbers. Figure 4. 37 displays that APDMES functionalized silica nanoparticles well dispersed on all over the silicon wafer and all nanoparticles have same shape and geometry. Coating with 10 bL has thicker thin film formation with more porous form than coatings with 5 bL numbers and it has more crackly separations.

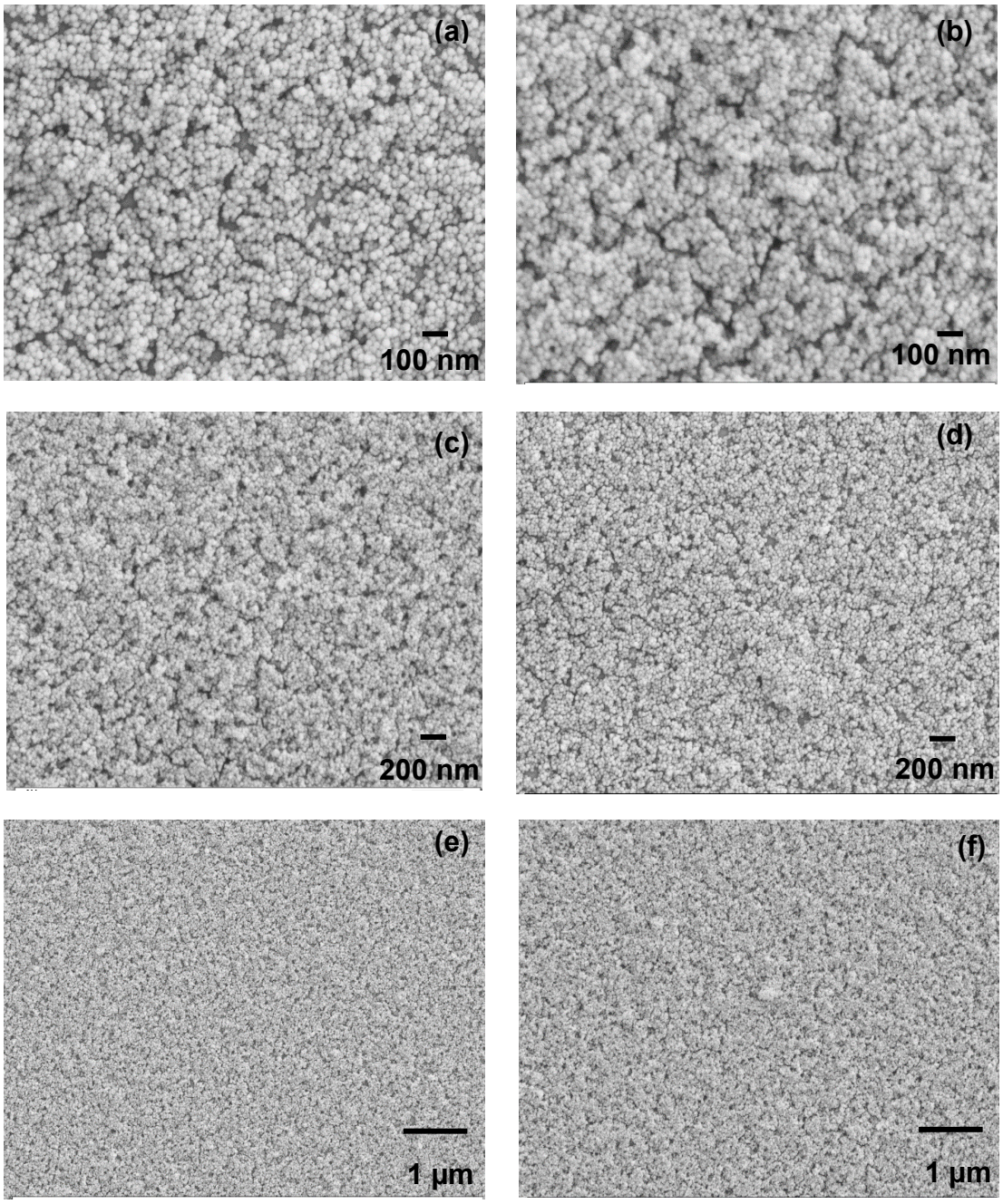

Figure 4. 38. SEM micrographs of AHAPS factionalized silica nanoparticles thin films coated by LbL in 5 bL (a, c, e) and 10 bL (b, d, f) on silicon wafer at 100nm, 200nm and 1 um magnification scale.

Figure 4. 38 displays the morphological analysis of AHAPS functionalized silica nanoparticles thin films coated by LbL with 5 and 10 bL numbers with few magnification scales. SEM analysis confirms that coatings have homogenously grown on silicon wafer and well dispersed which indicates stable dispersion of colloidal solution used for LbL. It appears that increase in bL numbers is yielded a thicker thin film growth and stiffer coating as compared coating with 10 bL numbers to 5 bL numbers. Similar to other

functionalization's, AHAPS functionalization on silica nanoparticles thin films resulted porous formation as well.

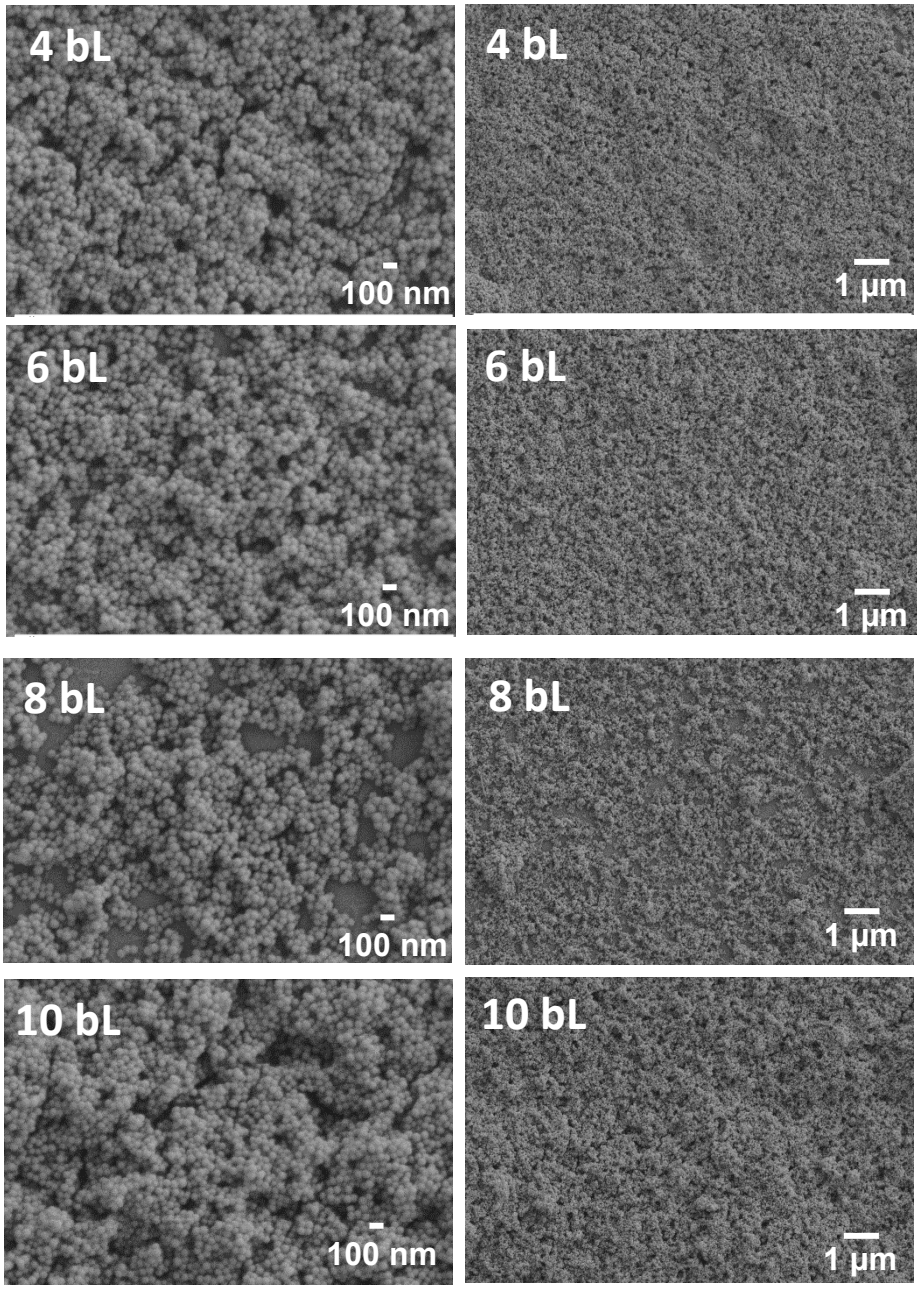

Figure 4. 39. SEM micrographs of AHAPS/PEG-Silane factionalized silica nanoparticles thin films coated by LbL in 4 bL, 6 bL, 8 bL and 10 bL on silicon wafer at 100nm and 1 um magnification scale.

Apart from all other coatings having just positive or negative surface charged functionalized silica nanoparticles, Figure 4. 39 shows both positive charged functionalized (AHAPS) and negative charged functionalized (PEG) silica nanoparticles ordered layer coatings by LbL on each other's. It observed that coating have more thickness this time when compared to all previous coatings. First layer was grown by positive surface charged AHAPS included solution with pH 4 because silicon wafer has

negative surface charge and then negative surface charged PEG included solution with pH 7 was used for second layer growth in LbL process and order established as this sequence. It is indicated that thickness is increased by the increase of bL number and this coating has greater thickness than the previous coating with single group functionalized silica thin films by LbL. It showed that two different and opposite surface charged functional groups decorated silica layer on each other did not form a homogenous coating and thin film was grown as in more island formation when compared to previous single type functionalized silica nanoparticle coatings.

4.4.2. Thickness Measurement of LbL Thin Film Coatings

Ellipsometry determined the change in height of the bilayers in each functional group can be seen histogram graphs at below. The thickness of coating increased from 100 nm in 5 bL to 200 nm in 10 bL for NPC and APDMES functionalized silica nanoparticles. The linear trend was attained in the results which are visible in Figure 4. 40 and Figure 4. 41.

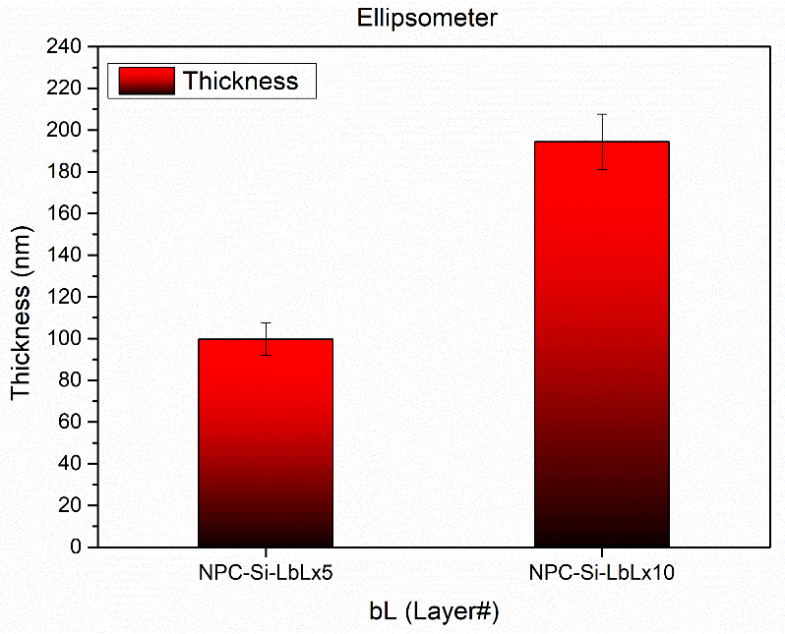

Figure 4. 40. Thickness measurements of NPC functionalized silica nanoparticles with respect to bL numbers by ellipsometry

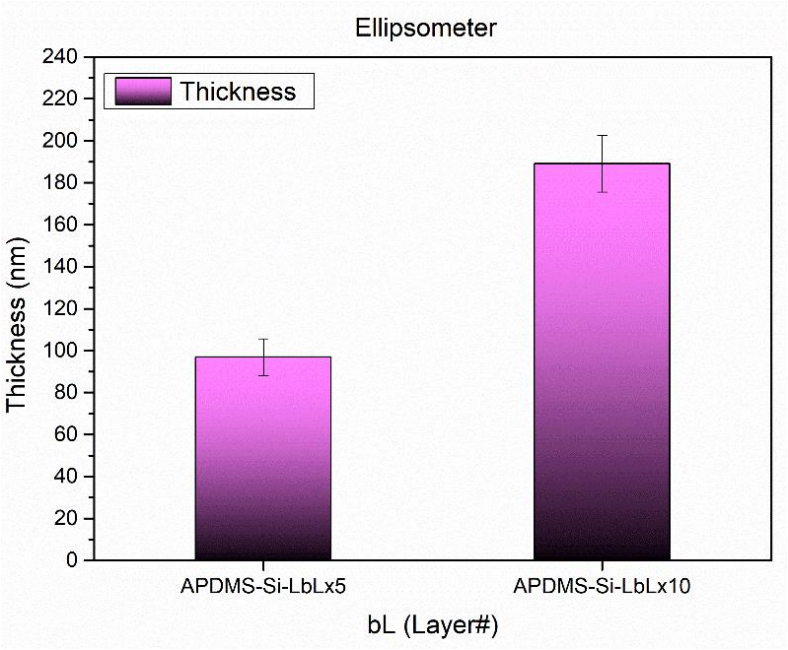

Figure 4. 41. Thickness measurements of APDMES functionalized silica nanoparticles with respect to bL numbers by ellipsometry

The thickness of AHAPS functionalized silica nanoparticles was measured approximately 100 nm in 5 bL. 50 nm increase was achieved in 10 bL particularly identified in Figure 4. 42. The reason of that can be explained that the charge of the 5 bL allowed the coating of 50 nm thickness due to charge transfer from negative to positive charged solution bath.

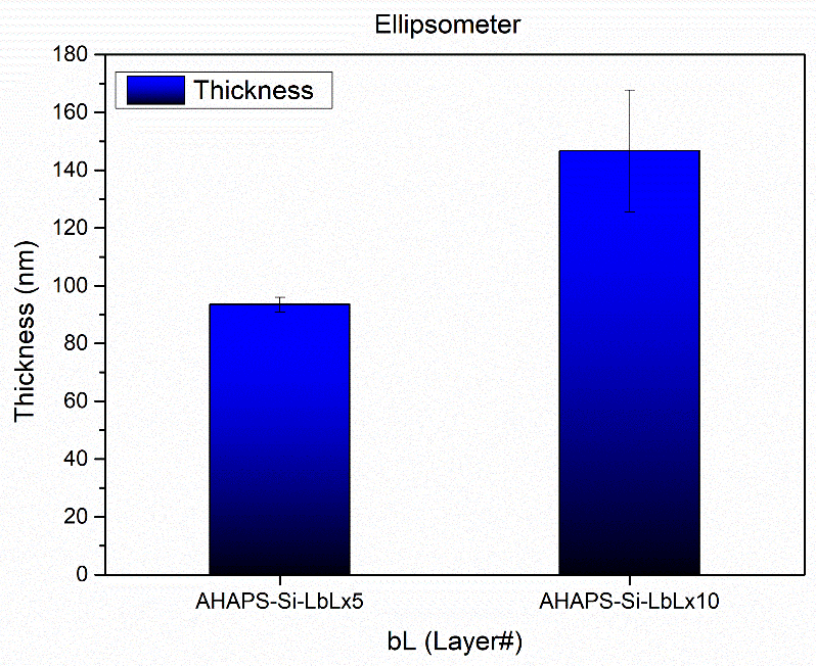

Figure 4. 42. Thickness measurements of AHAPS functionalized silica nanoparticles with respect to bL numbers by ellipsometry

The highest thickness was derived in AHAPS/PEG blend functionalized silica nanoparticles. In that case, positive and negative silica nanoparticles were coated onto silicon wafer one after another. The coating thickness of 4 bL, 6 bL, 8 bL and 10 bL were measured as 100, 150, 250 and 300 nm, respectively.

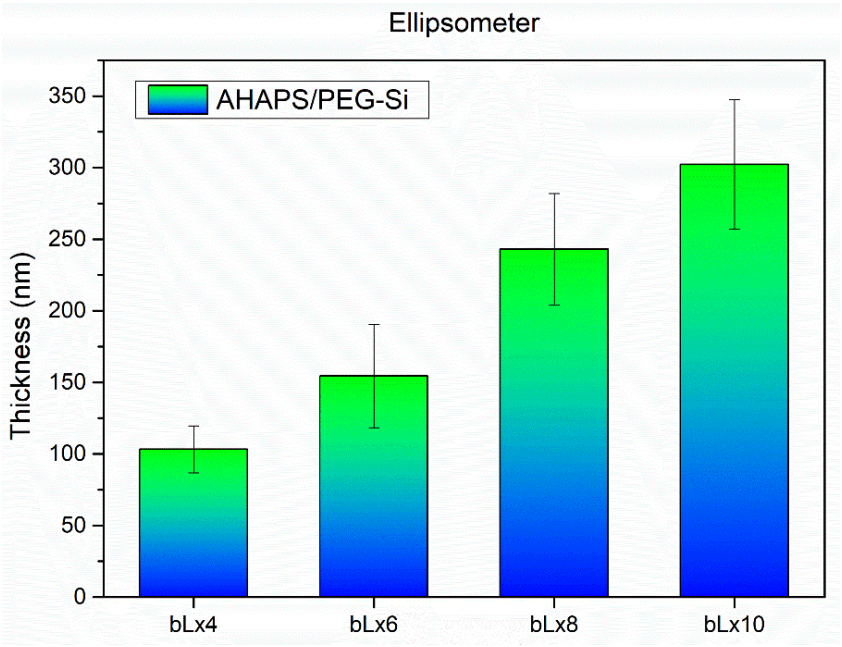

Figure 4. 43. Thickness measurements of AHAPS/PEG Blend functionalized silica nanoparticles with respect to bL numbers by ellipsometry

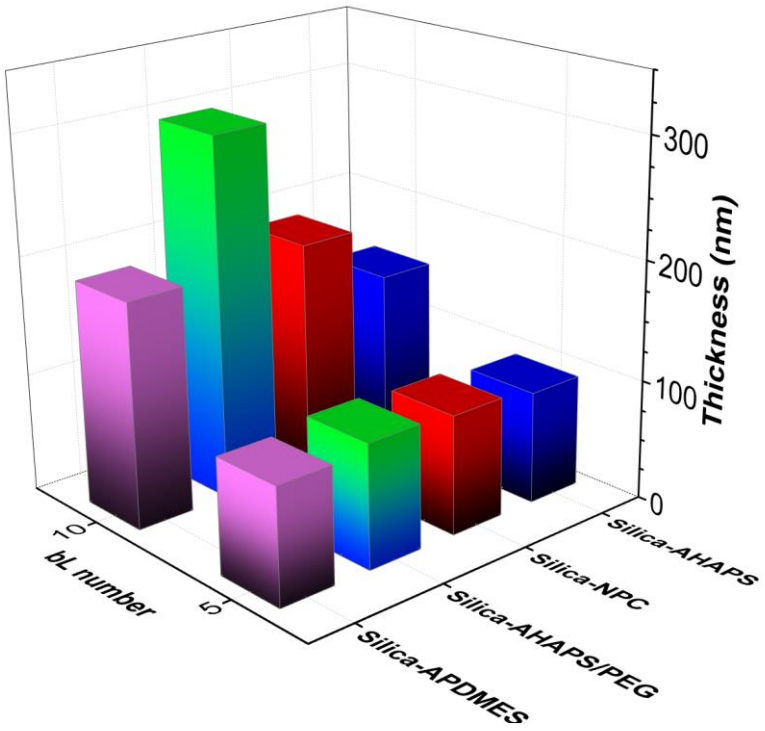

Figure 4. 44. 3-D representation of thickness comparisons between various functional groups

4.4.3. AFM Measurement of LbL Thin Film Coatings

The AFM measurement were performed to NPC, AHAPS, APDMES and AHAPS/PEG blend functionalized silica nanoparticles with 10 bL. The AFM topographies data indicated that 186 nm was the highest point of NPC functionalized silica nanoparticles coating having 19 nm roughness.

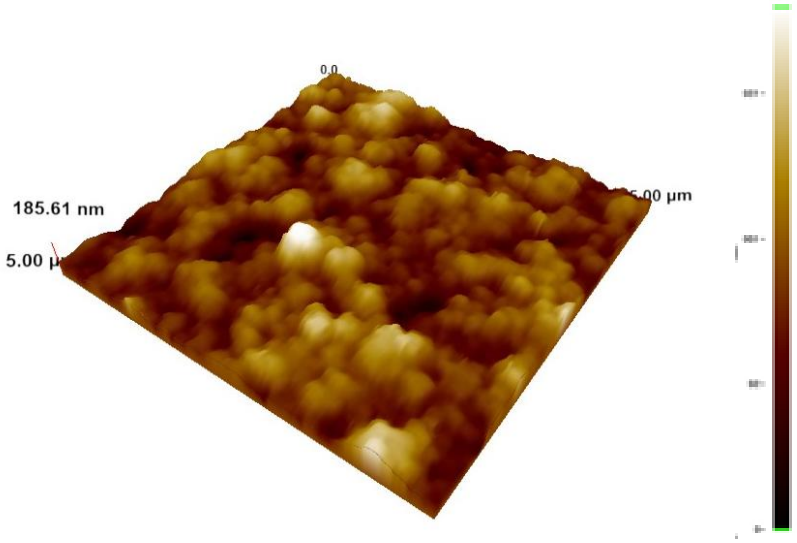

Figure 4. 45. Thickness and topography analysis of 10 bL NPC functionalized silica nanoparticles thin films by AFM

The APDMES functionalized silica nanoparticles were observed as 231 nm thickness which belonged to the highest point of the scanned area and they had 19 nm roughness.

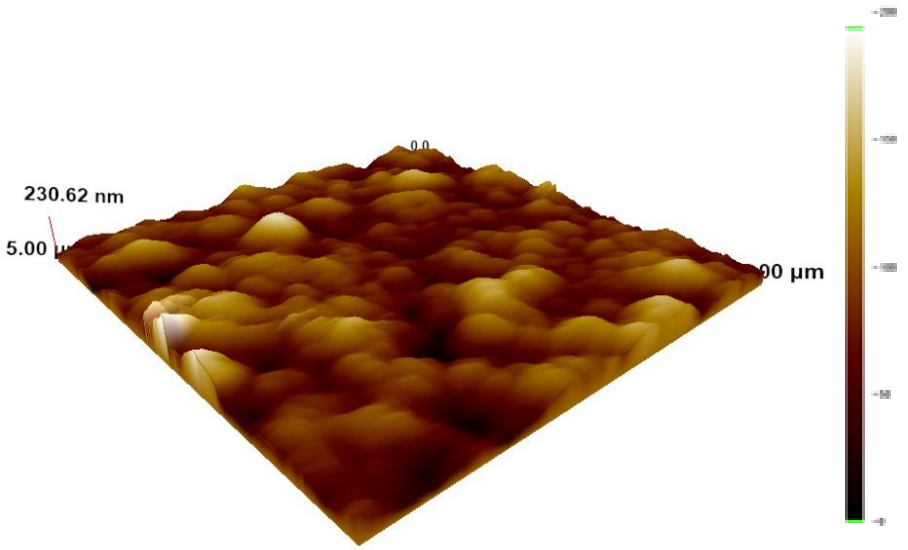

Figure 4. 46. Thickness and topography analysis of 10 bL APDMES functionalized silica nanoparticles thin films by AFM

The top point of AFM topography in AHAPS functionalized silica nanoparticles was 187 nm acquiring 16 nm roughness.

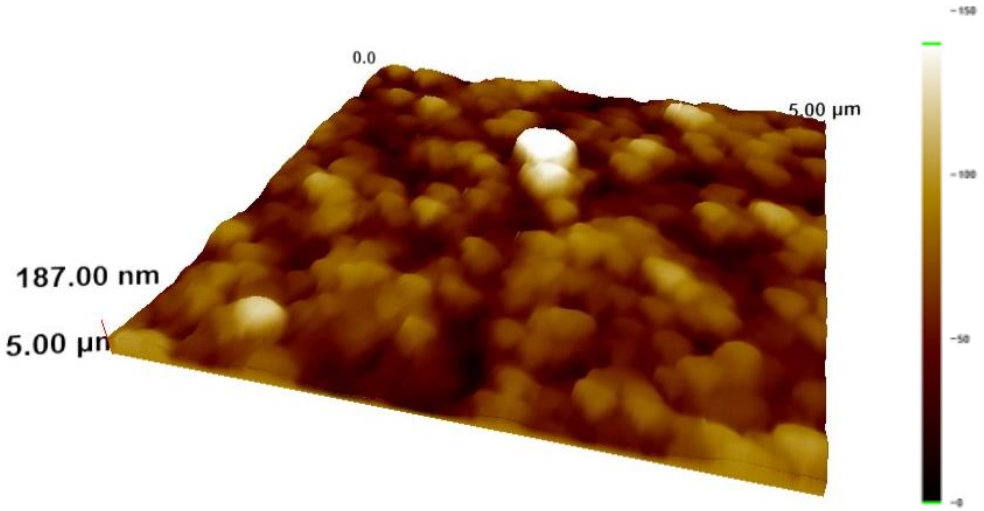

Figure 4. 47. Thickness and topography analysis of 10 bL AHAPS functionalized silica nanoparticles thin films by AFM

The maximum thickness and roughness were accomplished in AHAPS/PEG blend functionalized silica nanoparticles thin films due to the fact that two different silica nanoparticles having opposite surface charge were deposited onto wafer. The ultimate thickness was found as 298 nm possessing 37 nm roughness.

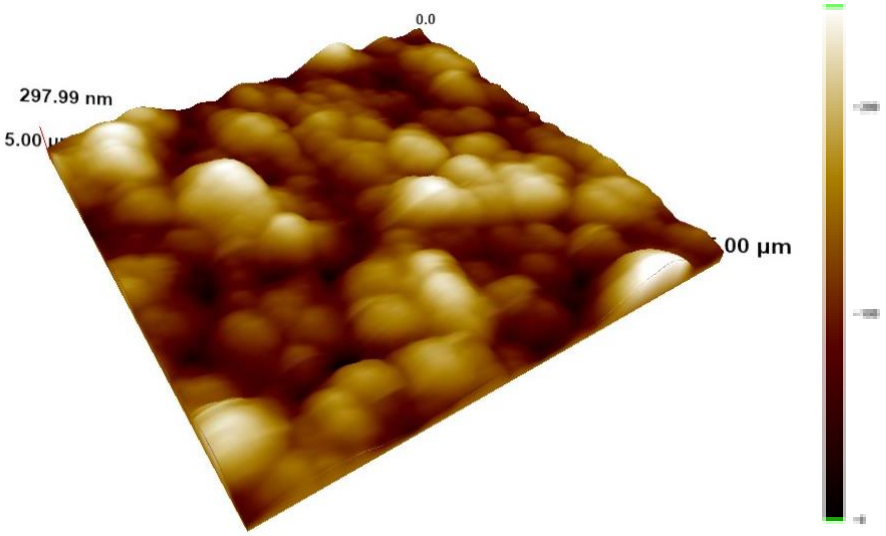

Figure 4. 48. Thickness and topography analysis of 10 bL AHAPS/PEG blend functionalized silica nanoparticles thin films by AFM

5. CONCLUSION

The silica nanoparticles were synthesized by water in oil (W/O) microemulsion ranging from 40 to 80 nm diameters. The particle size was controlled by changing surfactant, ammonia and TEOS concentration. The highest particle size was obtained in 2.02 water to surfactant ratio, 0.05 mM ammonia and 0.15 mM TEOS concentration sample, but the lowest size belonged to 0.51 water to surfactant ratio, 0.025 mM ammonia and 0.15 mM TEOS concentration sample.

The functionalization of silica nanoparticles was performed by using APS, NPC, APDMES, AHAPS, PEG-Silane and DETAS which yields the zeta potential values of the nanoparticles from negative (-40 mV) to positive (50 mV). APS functionalized silica nanoparticles indicated the excellent stability and the higher zeta potential value immediately after the pH adjustment. However, they were undergone intramolecular cyclization due to the formation of five membered cyclic intermediate and primary amine rendered unstable to silica surface during hydrolysis resulted in detachment of functional groups from. Therefore, surface, so agglomeration problem was observed when APS functionalized silica solution was applied to substrate by LbL. NPC functionalized silica nanoparticles exhibit positive surface charges arising from NH^{3+} groups. Surface charge of them was high with respect to APDMES and DETAS because of having quaternary amine moiety. Apart from all these functional groups, APDMES supported to generate vertically growth on silica nanosphere since dimethyl silyl groups were not allowed binding, so the silica was able to bound to only ethoxy sites. As a result of that, silica nanostructures cannot be functionalized all of its entire surface and positive surface charge could be lost after pH treatment even at the low pH values. AHAPS functionalized silica nanoparticles displayed excellent stability from the pH values of 3.5 to 6.0 owing to their secondary amine groups. Different from APS, detachment can be controlled by the length of alkyl because intramolecular catalysis is prevented by steric hindrance. Comparable to other functional silica nanoparticles, PEG-Silane possessed negative surface charge by reason of having non-charged functional group that was produced steric hinderance by physically interaction. Identical with AHAPS, DETAS functionalized silica had positive surface charge until pH value of 9.0, but it did not present good stability according to DLVO theory due to being below +30 mV. Zeta potential measurement was performed to determine surface charge of the particles. FT-IR and NMR spectrum gave information whether the functional group was bound or not.

The functionalized silica nanoparticles were dispersed in water to deposit onto substrate by LbL process. Silica nanoparticles including NPC, APDMES, AHAPS and AHAPS/PEG blend functional groups were coated successfully. In order to characterize thin films, SEM, ellipsometry and AFM were used to observe morphology, thickness and roughness, respectively. 100 nm thickness was obtained in each 5 bL of NPC, APDMES and AHAPS functionalized silica coated thin films. The films were generally transparent, but they could opacify with increasing thickness. The highest roughness was determined as 36 nm in AHAPS/PEG.

In this study, synthesis and functionalization of silica nanoparticle were accomplished to use in LbL application. The crosslinking was generated between the particles to enhance mechanical properties of the thin film to be used for further applications.

REFERENCES

1. Russel, W.B., et al., *Colloidal dispersions*. 1991: Cambridge university press.
2. Shinoda, K., T. Nakagawa, and B.-I. Tamamushi, *Colloidal surfactants: some physicochemical properties*. Vol. 12. 2016: Elsevier.
3. Hiemenz, P.C. and R. Rajagopalan, *Principles of Colloid and Surface Chemistry, revised and expanded*. 1997: CRC press.
4. Israelachvili, J.N., *Intermolecular and surface forces*. 2011: Academic press.
5. London, F., *The general theory of molecular forces.* Transactions of the Faraday Society, 1937. **33**: p. 8b-26.
6. Derjaguin, B., et al., *Investigations of the forces of interaction of surfaces in different media and their application to the problem of colloid stability.* Discussions of the Faraday Society, 1954. **18**: p. 24-41.
7. Ettelaie, R. and R. Buscall, *Electrical double layer interactions for spherical charge regulating colloidal particles.* Advances in colloid and interface science, 1995. **61**: p. 131-160.
8. Derjaguin, B. and L. Landau, *Theory of the stability of strongly charged lyophobic sols and of the adhesion of strongly charged particles in solutions of electrolytes.* Progress in Surface Science, 1993. **43**(1): p. 30-59.
9. Verwey, E.J.W., *Theory of the Stability of Lyophobic Colloids.* The Journal of Physical and Colloid Chemistry, 1947. **51**(3): p. 631-636.
10. Chen, Y.L., et al., *Molecular mechanisms and kinetics during the self-assembly of surfactant layers.* Journal of Colloid and Interface Science, 1992. **153**(1): p. 244-265.
11. Hassan, P.A., S. Rana, and G. Verma, *Making Sense of Brownian Motion: Colloid Characterization by Dynamic Light Scattering.* Langmuir, 2015. **31**(1): p. 3-12.
12. Bhattacharjee, S., *DLS and zeta potential – What they are and what they are not?* Journal of Controlled Release, 2016. **235**: p. 337-351.
13. Usui, S., H. Sasaki, and H. Matsukawa, *The dependence of zeta potential on bubble size as determined by the dorn effect.* Journal of Colloid and Interface Science, 1981. **81**(1): p. 80-84.
14. Hwang, H. *DLVO Theory*. 2011; Available from: http://soft-matter.seas.harvard.edu/index.php/DLVO_theory.

15. Kaszuba, M., et al., *High-concentration zeta potential measurements using light-scattering techniques.* Philosophical Transactions of the Royal Society of London A: Mathematical, Physical and Engineering Sciences, 2010. **368**(1927): p. 4439-4451.
16. Kirkwood, J., et al., *Using isoelectric point to determine the pH for initial protein crystallization trials.* Bioinformatics, 2015. **31**(9): p. 1444-1451.
17. Iler, R.K., *The Chemistry of Silica: Solubility, Polymerization, Colloid and Surface Properties and Biochemistry of Silica*. 1979: Wiley.
18. E., B.H. and R.W. O., *Colloidal Science: Fundamentals and Applications*. 2006: Taylor & Francis Group, LLC.
19. Matsoukas, T. and E. Gulari, *Dynamics of growth of silica particles from ammonia-catalyzed hydrolysis of tetra-ethyl-orthosilicate.* Journal of Colloid and Interface Science, 1988. **124**(1): p. 252-261.
20. Van Blaaderen, A. and A. Vrij, *Synthesis and characterization of monodisperse colloidal organo-silica spheres.* Journal of Colloid and Interface Science, 1993. **156**(1): p. 1-18.
21. Arriagada, F. and K. Osseo-Asare, *Synthesis of nanosize silica in a nonionic water-in-oil microemulsion: effects of the water/surfactant molar ratio and ammonia concentration.* Journal of colloid and interface science, 1999. **211**(2): p. 210-220.
22. Ebelmen, J. *Sur les produits de la décomposition des espèces minérales de la famille des silicates*. in *Annales des Mines*. 1845.
23. Cushing, B.L., V.L. Kolesnichenko, and C.J. O'Connor, *Recent Advances in the Liquid-Phase Syntheses of Inorganic Nanoparticles.* Chemical Reviews, 2004. **104**(9): p. 3893-3946.
24. Jeffrey, B.C. and S.G. W., *Sol-Gel Science: The Physics and Chemistry of Sol-Gel Processing*. 1990: Acedemic Press, Inc.
25. Hench, L.L. and J.K. West, *The sol-gel process.* Chemical Reviews, 1990. **90**(1): p. 33-72.
26. Singh, L.P., et al., *Sol-Gel processing of silica nanoparticles and their applications.* Adv Colloid Interface Sci, 2014. **214C**: p. 17-37.
27. Brinker, C., *Hydrolysis and condensation of silicates: Effects on structure*. Vol. 100. 1988. 31-50.

28. Bogush, G.H. and C.F. Zukoski, *Studies of the kinetics of the precipitation of uniform silica particles through the hydrolysis and condensation of silicon alkoxides.* Journal of Colloid and Interface Science, 1991. **142**(1): p. 1-18.
29. Stöber, W., A. Fink, and E. Bohn, *Controlled growth of monodisperse silica spheres in the micron size range.* Journal of Colloid and Interface Science, 1968. **26**(1): p. 62-69.
30. Bogush, G.H., M.A. Tracy, and C. Zukoski, *Preparation of Monodisperse Silica Particles: Control of Size and Mass Fraction*. Vol. 104. 1988. 95-106.
31. van Blaaderen, A. and A. Vrij, *Synthesis and characterization of colloidal dispersions of fluorescent, monodisperse silica spheres*. Vol. 8. 1992.
32. Van Helden, A.K., J.W. Jansen, and A. Vrij, *Preparation and characterization of spherical monodisperse silica dispersions in nonaqueous solvents.* Journal of Colloid and Interface Science, 1981. **81**(2): p. 354-368.
33. Ibrahim, I.A.M., A.A.F. Zikry, and M.A. Sharaf, *Preparation of spherical silica nanoparticles: Stober silica.* J American Sci, 2010. **6**.
34. Wang, X.D., et al., *Preparation of spherical silica particles by Stober process with high concentration of tetra-ethyl-orthosilicate.* J Colloid Interface Sci, 2010. **341**(1): p. 23-9.
35. Koch, C.C., *Nanostructured Materials: Processing, Properties, and Applications*. Second ed. 2007: Willliam Andrew Publishing.
36. Abarkan, I., T. Doussineau, and M. Smaïhi, *Tailored macro/microstructural properties of colloidal silica nanoparticles via microemulsion preparation.* Polyhedron, 2006. **25**(8): p. 1763-1770.
37. Adair, J.H., et al., *Recent developments in the preparation and properties of nanometer-size spherical and platelet-shaped particles and composite particles.* Materials Science and Engineering: R: Reports, 1998. **23**(4): p. 139-242.
38. López-Quintela, M., *Synthesis of nanomaterials in microemulsions: formation mechanisms and growth control.* Curr. Opin. Colloid Interface Sci., 2003. **8**: p. 137-144.
39. Hoar, T.P. and J.H. Schulman, *Transparent Water-in-Oil Dispersions: the Oleopathic Hydro-Micelle.* Nature, 1943. **152**: p. 102.
40. Schulman, J.H., W. Stoeckenius, and L.M. Prince, *Mechanism of Formation and Structure of Micro Emulsions by Electron Microscopy.* The Journal of Physical Chemistry, 1959. **63**(10): p. 1677-1680.

41. Malik, M.A., M.Y. Wani, and M.A. Hashim, *Microemulsion method: A novel route to synthesize organic and inorganic nanomaterials.* Arabian Journal of Chemistry, 2012. **5**(4): p. 397-417.
42. Najjar, R., *Microemulsions-a brief introduction*, in *Microemulsions-An Introduction to Properties and Applications*. 2012, InTech.
43. Holmberg, K., et al., *Surfactants and Polymers in Aqueous Solution*. Second ed. 2003: Wiley.
44. Ganguli, A.K., A. Ganguly, and S. Vaidya, *Microemulsion-based synthesis of nanocrystalline materials.* Chemical Society Reviews, 2010. **39**(2): p. 474-485.
45. Savko, N., *The Role of Inverse Nonionic Microemulsion in the Synthesis of SiO2 Nanoparticles*, in *Chemical and Pharmaceutical Sciences and Technologies*. 2010, University of Trieste. p. 125.
46. W.C., G., *Classification of Surface-Active Agents by 'HLB'.* Journal of the Society of Cosmetic Chemists, 1949. **1**(5): p. 311–326.
47. Aulton, M.E., *Pharmaceutics : the science of dosage form design*. 2002, Edinburgh; New York: Churchill Livingstone.
48. Kozlecki, T., et al., *Improved Synthesis of Nanosized Silica in Water-in-Oil Microemulsions.* Journal of Nanoparticles, 2016. **2016**: p. 9.
49. Winsor, P.A., *Hydrotropy, solubilisation and related emulsification processes.* Transactions of the Faraday Society, 1948. **44**(0): p. 376-398.
50. Schwarze, M., et al., *Microemulsion systems for catalytic reactions and processes.* Catalysis Science & Technology, 2015. **5**(1): p. 24-33.
51. USKOKOVIĆ, V. and M. DROFENIK, *SYNTHESIS OF MATERIALS WITHIN REVERSE MICELLES.* Surface Review and Letters, 2005. **12**(02): p. 239-277.
52. Boutonnet, M., et al., *The preparation of monodisperse colloidal metal particles from microemulsions.* Colloids and Surfaces, 1982. **5**(3): p. 209-225.
53. Pileni, M.P., *Structure and reactivity in reverse micelles*. 1989, Amsterdam; Oxford; New York; Tokyo: Elsevier.
54. Santra, S., et al., *Synthesis and characterization of silica-coated iron oxide nanoparticles in microemulsion: The effect of nonionic surfactants.* Langmuir, 2001. **17**(10): p. 2900-2906.
55. Fu, X. and S. Qutubuddin, *Synthesis of titania-coated silica nanoparticles using a nonionic water-in-oil microemulsion.* Colloids and Surfaces A: Physicochemical and Engineering Aspects, 2001. **179**(1): p. 65-70.

56. López-Quintela, M.A., et al., *Microemulsion dynamics and reactions in microemulsions.* Current Opinion in Colloid & Interface Science, 2004. **9**(3-4): p. 264-278.
57. Osseo-Asare, K. and F.J. Arriagada, *Preparation of SiO2 Nanoparticles in a Non-Ionic*

Reverse Micellar System. Colloids and Surfaces, 1990. **50**: p. 321-339.
58. Osseo-Asare, K. and F.J. Arriagada, *Growth Kinetics of Nanosize Silica in a Nonionic Water-in-Oil Microemulsion: A Reverse Micellar Pseudophase Reaction Model.* Journal of Colloid and Interface Science, 1999. **218**(1): p. 68-76.
59. Finnie, K.S., et al., *Formation of Silica Nanoparticles in Microemulsions.* Langmuir, 2007. **23**(6): p. 3017-3024.
60. Bagwe, R.P., et al., *Optimization of Dye-Doped Silica Nanoparticles Prepared Using a Reverse Microemulsion Method.* Langmuir, 2004. **20**(19): p. 8336-8342.
61. Pileni, M.-P., *Nanocrystals: fabrication, organization and collective properties.* Comptes Rendus Chimie, 2003. **6**(8-10): p. 965-978.
62. Pileni, M.P., *Control of the Size and Shape of Inorganic Nanocrystals at Various Scales from Nano to Macrodomains.* The Journal of Physical Chemistry C, 2007. **111**(26): p. 9019-9038.
63. Graf, C., et al., *Surface Functionalization of Silica Nanoparticles Supports Colloidal Stability in Physiological Media and Facilitates Internalization in Cells.* Langmuir, 2012. **28**(20): p. 7598-7613.
64. L. Witucki, G., *A Silane Primer: Chemistry and Applications of AIkoxy Silanes*. Vol. 65. 1993.
65. Gomes, M.C., et al., *The role of surface functionalization of silica nanoparticles for bioimaging.* Journal of Innovative Optical Health Sciences, 2016. **09**(04): p. 1630005.
66. Sperling, R.A. and W.J. Parak, *Surface modification, functionalization and bioconjugation of colloidal inorganic nanoparticles.* Philosophical Transactions of the Royal Society A: Mathematical, Physical and Engineering Sciences, 2010. **368**(1915): p. 1333-1383.
67. Ribeiro, T., C. Baleizão, and J. Farinha, *Functional Films from Silica/Polymer Nanoparticles.* Materials, 2014. **7**(5): p. 3881.

68. Liberman, A., et al., *Synthesis and surface functionalization of silica nanoparticles for nanomedicine.* Surf Sci Rep, 2014. **69**(2-3): p. 132-158.
69. Zou, H., S. Wu, and J. Shen, *Polymer/Silica Nanocomposites: Preparation, Characterization, Properties, and Applications.* Chemical Reviews, 2008. **108**(9): p. 3893-3957.
70. Montalti, M., et al., *Dye-doped silica nanoparticles as luminescent organized systems for nanomedicine.* Chemical Society Reviews, 2014. **43**(12): p. 4243-4268.
71. Plueddemann, E.P., *Silane Coupling Agents*. 1982: Springer.
72. Arkles, B., *Tailoring Surfaces with Silanes*. Vol. 7. 1977. 766-778.
73. Zisman, W.A., *Surface Chemistry of Plastics Reinforced by Strong Fibers.* Product R&D, 1969. **8**(2): p. 98-111.
74. Sterman, S. and J.G. Marsden, *SILANE COUPLING AGENTS.* Industrial & Engineering Chemistry, 1966. **58**(3): p. 33-37.
75. Knopp, D., D. Tang, and R. Niessner, *Review: Bioanalytical applications of biomolecule-functionalized nanometer-sized doped silica particles.* Analytica Chimica Acta, 2009. **647**(1): p. 14-30.
76. Qhobosheane, M., et al., *Biochemically functionalized silica nanoparticles.* Analyst, 2001. **126**(8): p. 1274-1278.
77. Wang, L., W. Zhao, and W. Tan, *Bioconjugated silica nanoparticles: Development and applications.* Nano Research, 2008. **1**(2): p. 99-115.
78. Weihong, T., et al., *Bionanotechnology based on silica nanoparticles.* Medicinal Research Reviews, 2004. **24**(5): p. 621-638.
79. Vogel, B.M., et al., *Interfacial modification of silica surfaces through γ-isocyanatopropyl triethoxy silane–amine coupling reactions.* Applied Surface Science, 2008. **254**(6): p. 1789-1796.
80. Wang, H., et al., *Amino acid-based anti-fouling functionalization of silica nanoparticles using divinyl sulfone.* Acta Biomaterialia, 2016. **40**(Supplement C): p. 273-281.
81. Haensch, C., S. Hoeppener, and U.S. Schubert, *Chemical modification of self-assembled silane based monolayers by surface reactions.* Chemical Society Reviews, 2010. **39**(6): p. 2323-2334.

82. Zhu, M., M.Z. Lerum, and W. Chen, *How To Prepare Reproducible, Homogeneous, and Hydrolytically Stable Aminosilane-Derived Layers on Silica.* Langmuir, 2012. **28**(1): p. 416-423.
83. Kanan, S.M., W.T.Y. Tze, and C.P. Tripp, *Method to Double the Surface Concentration and Control the Orientation of Adsorbed (3-Aminopropyl)dimethylethoxysilane on Silica Powders and Glass Slides.* Langmuir, 2002. **18**(17): p. 6623-6627.
84. Haller, I., *Covalently attached organic monolayers on semiconductor surfaces.* Journal of the American Chemical Society, 1978. **100**(26): p. 8050-8055.
85. An, Y., et al., *Preparation and self-assembly of carboxylic acid-functionalized silica.* J Colloid Interface Sci, 2007. **311**(2): p. 507-13.
86. Waddell, T.G., D.E. Leyden, and M.T. DeBello, *The nature of organosilane to silica-surface bonding.* Journal of the American Chemical Society, 1981. **103**(18): p. 5303-5307.
87. Pasternack, R.M., S. Rivillon Amy, and Y.J. Chabal, *Attachment of 3-(Aminopropyl)triethoxysilane on Silicon Oxide Surfaces: Dependence on Solution Temperature.* Langmuir, 2008. **24**(22): p. 12963-12971.
88. Asenath Smith, E. and W. Chen, *How To Prevent the Loss of Surface Functionality Derived from Aminosilanes.* Langmuir, 2008. **24**(21): p. 12405-12409.
89. Kumar, R., et al., *Covalently Dye-Linked, Surface-Controlled, and Bioconjugated Organically Modified Silica Nanoparticles as Targeted Probes for Optical Imaging.* ACS Nano, 2008. **2**(3): p. 449-456.
90. Santra, S., et al., *Conjugation of Biomolecules with Luminophore-Doped Silica Nanoparticles for Photostable Biomarkers.* Analytical Chemistry, 2001. **73**(20): p. 4988-4993.
91. Santra, S., et al. *Development of novel dye-doped silica nanoparticles for biomarker application*. 2001. SPIE.
92. Bagwe, R.P., L.R. Hilliard, and W. Tan, *Surface Modification of Silica Nanoparticles to Reduce Aggregation and Nonspecific Binding.* Langmuir, 2006. **22**(9): p. 4357-4362.
93. Howarter, J.A. and J.P. Youngblood, *Optimization of Silica Silanization by 3-Aminopropyltriethoxysilane.* Langmuir, 2006. **22**(26): p. 11142-11147.

94. Etienne, M. and A. Walcarius, *Analytical investigation of the chemical reactivity and stability of aminopropyl-grafted silica in aqueous medium.* Talanta, 2003. **59**(6): p. 1173-1188.
95. Fiorilli, S., et al., *Vapor-phase self-assembled monolayers of aminosilane on plasma-activated silicon substrates.* Journal of Colloid and Interface Science, 2008. **321**(1): p. 235-241.
96. Kim, J., et al., *Investigations of Chemical Modifications of Amino-Terminated Organic Films on Silicon Substrates and Controlled Protein Immobilization.* Langmuir, 2010. **26**(4): p. 2599-2608.
97. Acres, R.G., et al., *Molecular Structure of 3-Aminopropyltriethoxysilane Layers Formed on Silanol-Terminated Silicon Surfaces.* The Journal of Physical Chemistry C, 2012. **116**(10): p. 6289-6297.
98. Aissaoui, N., et al., *Silane Layers on Silicon Surfaces: Mechanism of Interaction, Stability, and Influence on Protein Adsorption.* Langmuir, 2012. **28**(1): p. 656-665.
99. Qiao, B., et al., *High density silanization of nano-silica particles using γ-aminopropyltriethoxysilane (APTES).* Applied Surface Science, 2015. **351**: p. 646-654.
100. Korzeniowska, B., et al., *Silica nanoparticles for cell imaging and intracellular sensing.* Nanotechnology, 2013. **24**(44): p. 442002.
101. Mahmoudi, M., et al., *Protein−Nanoparticle Interactions: Opportunities and Challenges.* Chemical Reviews, 2011. **111**(9): p. 5610-5637.
102. Fenoglio, I., et al., *Multiple aspects of the interaction of biomacromolecules with inorganic surfaces.* Advanced Drug Delivery Reviews, 2011. **63**(13): p. 1186-1209.
103. Branda, F., et al., *Synthesis structure and stability of amino functionalized PEGylated silica nanoparticles.* Colloids and Surfaces A: Physicochemical and Engineering Aspects, 2010. **367**(1-3): p. 12-16.
104. Xie, M., et al., *A multifunctional mesoporous silica nanocomposite for targeted delivery, controlled release of doxorubicin and bioimaging.* Colloids and Surfaces B: Biointerfaces, 2013. **110**: p. 138-147.
105. Beyer, D., et al., *Surface Modification via Reactive Polymer Interlayers.* Langmuir, 1996. **12**(10): p. 2514-2518.

106. L., B.A., J.A.P. R., and C. Frank, *Layer-By-Layer-Assembled Capsules and Films for Therapeutic Delivery.* Small, 2010. **6**(17).
107. Yan, Y., et al., *Toward Therapeutic Delivery with Layer-by-Layer Engineered Particles.* ACS Nano, 2011. **5**(6): p. 4252-4257.
108. Yanwei, T., et al., *Layer-by-layer assembly of silica nanoparticles on 3D fibrous scaffolds: Enhancement of osteoblast cell adhesion, proliferation, and differentiation.* Journal of Biomedical Materials Research Part A, 2014. **102**(11): p. 3803-3812.
109. Li, Q.-L., et al., *Mesoporous Silica Nanoparticles Coated by Layer-by-Layer Self-assembly Using Cucurbit[7]uril for in Vitro and in Vivo Anticancer Drug Release.* Chemistry of Materials, 2014. **26**(22): p. 6418-6431.
110. Richardson, J.J., et al., *Innovation in Layer-by-Layer Assembly.* Chemical Reviews, 2016. **116**(23): p. 14828-14867.
111. Blodgett, K.B., *MONOMOLECULAR FILMS OF FATTY ACIDS ON GLASS.* Journal of the American Chemical Society, 1934. **56**(2): p. 495-495.
112. Blodgett, K.B. and I. Langmuir, *Built-Up Films of Barium Stearate and Their Optical Properties.* Physical Review, 1937. **51**(11): p. 964-982.
113. Hans, K. and M. Dietmar, *Systems of Monomolecular Layers—Assembling and Physico-Chemical Behavior.* Angewandte Chemie International Edition in English, 1971. **10**(9): p. 620-637.
114. Decher, G., *Fuzzy Nanoassemblies: Toward Layered Polymeric Multicomposites.* Science, 1997. **277**(5330): p. 1232-1237.
115. Gero, D. and H. Jong-Dal, *Buildup of ultrathin multilayer films by a self-assembly process, 1 consecutive adsorption of anionic and cationic bipolar amphiphiles on charged surfaces.* Makromolekulare Chemie. Macromolecular Symposia, 1991. **46**(1): p. 321-327.
116. G., D. and H.J. D., *Buildup of Ultrathin Multilayer Films by a Self-Assembly Process: II. Consecutive Adsorption of Anionic and Cationic Bipolar Amphiphiles and Polyelectrolytes on Charged Surfaces.* Berichte der Bunsengesellschaft für physikalische Chemie, 1991. **95**(11): p. 1430-1434.
117. Decher, G., J.D. Hong, and J. Schmitt, *Buildup of ultrathin multilayer films by a self-assembly process: III. Consecutively alternating adsorption of anionic and cationic polyelectrolytes on charged surfaces.* Thin Solid Films, 1992. **210**: p. 831-835.

118. Cini, N., *Comparision of Polyelectrolyte Complex Formation in Bulk and at Interfaces*. 2010, University of Strasbourg

Technical University of Istanbul.

119. Bruening, M. and D. Dotzauer, *Just spray it.* Nature Materials, 2009. **8**: p. 449.
120. R. Farhat, T. and J. B. Schlenoff, *Corrosion Control Using Polyelectrolyte Multilayers*. Vol. 5. 2002.
121. Lee, D., M.F. Rubner, and R.E. Cohen, *All-Nanoparticle Thin-Film Coatings.* Nano Letters, 2006. **6**(10): p. 2305-2312.
122. Bravo, J., et al., *Transparent Superhydrophobic Films Based on Silica Nanoparticles.* Langmuir, 2007. **23**(13): p. 7293-7298.
123. Cebeci, F.C., et al., *Nanoporosity-driven superhydrophilicity: A means to create multifunctional antifogging coatings.* Langmuir, 2006. **22**: p. 2856-2862.
124. Lee, D., et al., *Multilayers of Oppositely Charged SiO2 Nanoparticles: Effect of Surface Charge on Multilayer Assembly.* Langmuir, 2007. **23**(17): p. 8833-8837.
125. Yoo, D., S.S. Shiratori, and M.F. Rubner, *Controlling Bilayer Composition and Surface Wettability of Sequentially Adsorbed Multilayers of Weak Polyelectrolytes.* Macromolecules, 1998. **31**(13): p. 4309-4318.
126. Srivastava, S. and N.A. Kotov, *Composite Layer-by-Layer (LBL) Assembly with Inorganic Nanoparticles and Nanowires.* Accounts of Chemical Research, 2008. **41**(12): p. 1831-1841.
127. Ariga, K., J.P. Hill, and Q.M. Ji, *Layer-by-layer assembly as a versatile bottom-up nanofabrication technique for exploratory research and realistic application.* Physical Chemistry Chemical Physics, 2007. **9**(19): p. 2319-2340.
128. Zhai, L., et al., *Stable superhydrophobic coatings from polyelectrolyte multilayers.* Nano Letters, 2004. **4**(7): p. 1349-1353.
129. Xu, P., et al., *Preparation and morphology of SiO2/PMMA nanohybrids by microemulsion polymerization*. Vol. 284. 2006. 755-762.
130. Ma, X.-k., et al., *Surface modification and characterization of highly dispersed silica nanoparticles by a cationic surfactant.* Colloids and Surfaces A: Physicochemical and Engineering Aspects, 2010. **358**(1-3): p. 172-176.
131. Metin, C.O., et al., *Stability of aqueous silica nanoparticle dispersions.* Journal of Nanoparticle Research, 2011. **13**(2): p. 839-850.

132. Morrow, B.A. and D.T. Molapo, *Infrared Studies of Chemically Modified Silica*, in *Colloidal Silica: Fundamentals and Applications*. 2006, Taylor & Francis Group.
133. Muroya, M.-a., *Correlation between the formation of silica skeleton structure and Fourier transform reflection infrared absorption spectroscopy spectra.* Colloids and Surfaces A: Physicochemical and Engineering Aspects, 1999. **157**(1): p. 147-155.
134. Lu, H.-T., *Synthesis and characterization of amino-functionalized silica nanoparticles.* Colloid Journal, 2013. **75**(3): p. 311-318.
135. Tsang, S.C., et al., *Silica-Encapsulated Nanomagnetic Particle as a New Recoverable Biocatalyst Carrier.* The Journal of Physical Chemistry B, 2006. **110**(34): p. 16914-16922.
136. Scaffaro, R., et al., *Surface modification of poly(ethylene-co-acrylic acid) with amino-functionalized silica nanoparticles.* Journal of Materials Chemistry, 2011. **21**(11): p. 3849-3857.
137. Foschiera, J.L., T.M. Pizzolato, and E.V. Benvenutti, *FTIR thermal analysis on organofunctionalized silica gel.* Journal of the Brazilian Chemical Society, 2001. **12**: p. 159-164.